# Density-Functional Theory Exchange-Correlation Functionals for Hydrogen Bonds in Water

vorgelegt von
M. Sc.
Biswajit Santra
aus Berlin

Von der Fakultät II of Mathematik und Naturwissenschaften
der Technischen Universität Berlin
zur Erlangung des akademischen Grades
DOCTOR RERUM NATURALIUM

genehmigte Dissertation

Promotionsausschuss:

Vorsitzender: Prof. Dr. Mario Dähne
Berichter: Prof. Dr. Andreas Knorr
Berichter: Prof. Dr. Matthias Scheffler
Berichter: Prof. Dr. Angelos Michaelides

Tag der wissenschaftlichen Aussprache: 31.08.2010

Berlin 2010

D 83

*To my parents ...*

# Abstract

Hydrogen bonds (HBs) involving water molecules are ubiquitous in nature. However an accurate description of HBs with simulation techniques, including even quantum mechanical approaches such as density-functional theory (DFT), is a major challenge. Mainly because of a good balance between computational cost and accuracy, DFT has been routinely applied to study water in various environments, for example, liquid water, ice, adsorbed, and confined water, yet how well DFT exchange-correlation (*xc*) functionals describe HBs between water molecules is unknown and indeed controversial. To address this issue a series of systematic studies on water from different environments (representative of gas phase clusters, liquid water, and various phases of ice) have been performed with a range of DFT *xc* functionals and, in principle, more accurate explicitly correlated quantum chemistry methods.

For small gas phase water clusters (dimer to pentamer in their global minimum configurations) several hybrid *xc* functionals (where a fraction of *exact exchange* is included) are found to be far superior to the more common and widely used pure DFT *xc* functionals. Similarly on water clusters extracted from a simulation of liquid water the hybrid functionals offer much improved performance. It is shown that the poor performance of generalized gradient approximation (GGA) *xc* functionals for liquid water is because of a poor description of the covalent O-H bond stretching of water molecules with GGA *xc* functionals. This provides a possible explanation for the predicted low diffusion coefficients obtained in many previous GGA simulations of liquid water and raises a general concern over the ability of pure GGA *xc* functionals to describe the intra-molecular deformation in other molecular liquids too, highlighting the importance of *exact exchange* in simulations of molecular liquids.

Aiming to finally understand the significance of van der Waals (vdW) dispersion forces in holding water molecules together, a systematic study of the four low-lying isomers of the gas phase water hexamer was performed. This revealed that due to the lack of vdW interactions no *xc* functional tested found the correct lowest energy structure of the water hexamers. More open structures ("cyclic" or "book") were favored over the more compact "prism" isomer which is known (from explicitly correlated calculations) to be the lowest energy isomer. This clearly indicates the importance of vdW forces in holding water molecules together and indicates a need for an improved account of vdW forces in conjunction with DFT *xc* functionals. A similar conclusion has been reached through simulations on a range of ambient and high pressure phases of ice, where it is found that vdW forces play a crucial role in determining the relative stabilities of the high density phases.

Overall, significant contributions have been made to both better understand the nature of the interactions between water molecules and to pinpoint the shortcomings in DFT *xc* functionals to describe HBs among water molecules. This will aid in the development of improved *xc* functionals and deepens our understanding of the gas and condensed phases of water and other hydrogen bonded systems too.

# Zusammenfassung

Wasserstoffbrückenbindungen (Englisch: Hydrogen Bonds, HBs) zwischen Wassermolekülen sind in der Natur allgegenwärtig. Trotzdem ist eine genau Beschreibung mit Simulationstechniken, eingeschlossen auch quantenmechanische Ansätze wie z.B. Dichtefunktionaltheorie (DFT), eine große Herausforderung. Hauptsächlich auf Grund der guten Balance zwischen Rechenzeitaufwand und Genauigkeit wurde DFT routinemäßig angewendet, um Wasser in unterschiedlichen Umgebungen, wie z.B. flüssiges Wasser, Eis, adsorbiertes und eingeschlossenes Wasser, zu untersuchen. Trotzdem ist nicht bekannt, wie gut DFT Austausch-Korrelations (Englisch: Exchange-Correlation, *xc*) Funktionale die HBs zwischen Wassermolekülen beschreiben – dies ist ein kontroverses Thema. Um diesen Aspekt zu beleuchten, wurde eine Serie von systematischen Studien von Wasser in unterschiedlichen Umgebungen (Gasphasen-Cluster, flüssiges Wasser und verschiedene Phasen von Eis) mit einer großen Bandbreite von DFT *xc* Funktionalen und vom Prinzip her genauer explizit korrelierten quantenchemischen Methoden durchgeführt.

Für kleine Gasphasen-Cluster (Dimere bis Pentamere in ihren globalen Minimum-Konfigurationen) scheinen einige Hybridfunktionale (bei denen *exakter Austausch* integriert ist) den üblicheren und weit verbreitet genutzten puren DFT *xc* Funktionalen gegenüber weit überlegen zu sein. In ähnlicher Weise gilt dies auch für Wasser-Cluster, die aus Simulationen flüssigen Wassers extrahiert wurden. Es wird gezeigt, dass die schlechten Ergebnisse der generalisierten Gradienten Approximation (Englisch: Generalized Gradient Approximation, GGA) *xc* Funktionale für flüssiges Wasser in der schlechten Beschreibung der Veränderung der kovalenten O-H Bindungslänge der Wassermoleküle begründet liegen. Dies bietet eine mögliche Erklärung für die in vielen vorhergehenden GGA Simulationen von flüssigem Wasser als zu klein vorhergesagten Diffusionskoeffizienten und macht daher die Fähigkeit purer GGA *xc* Funktionale zur Beschreibung intra-molekularer Deformation in anderen molekularen Flüssigkeiten zu einem Thema generellen Interesses, was die Bedeutung von *exaktem Austausch* für Simulationen molekularer Flüssigkeiten unterstreicht.

Um die Bedeutung von van der Waals (vdW) Dispersionskräften beim Zusammenhalten von Wassermolekülen endgültig zu verstehen, wurde eine systematische Studie der vier energetisch niedrigen Isomere des Gasphasen-Wasser-Hexamers durchgeführt. Daraus ging hervor, dass auf Grund des Fehlens von vdW Wechselwirkungen keines der getesteten *xc* Funktionale die korrekte nieder energetischste Struktur des Wasser-Hexamers gefunden hat. Offenere Strukturen ("zyklisch" oder "Buch") sind gegenüber dem kompakteren "Prisma" Isomer begünstigt – aus explizit korrelierten Rechnungen ist bekannt, dass es sich bei letzterem um das niedrigst energetische Isomer handelt. Dies zeigt deutlich die Bedeutung von vdW Kräften beim Zusammenhalten von Wassermolekülen und weist auf die Notwendigkeit einer verbesserten Berücksichtigung von vdW

Kräften im Zusammenhang mit DFT *xc* Funktionalen hin. Simulationen einer Reihe von Umgebungs- und Hochdruck-Phasen von Eis lieferten ein ähnliches Ergebnis – auch hier fand man, dass vdW Kräfte eine enscheidende Rolle bei der Ermittlung der relativen Stabilitäten der Phasen hoher Dichte spielen.

Alles in allem wurden bedeutsame Beiträge geleistet, zum einen die Natur der Wechselwirkungen zwischen Wassermolekülen besser zu verstehen und zum anderen die Schwächen von DFT *xc* Funktionalen bei der Beschreibung der HBs zwischen Wassermolekülen aufzuzeigen. Dies wird die Entwicklung verbesserter *xc* Funktionale fördern und unser Verständnis der Gas- und kondensierten Phase von Wasser und anderen Wasserstoff gebundenen Systemen vertiefen.

# Contents


**1. Introduction** **1**

**2. Theoretical Background** **7**
2.1. Electronic Structure Problem . . . . . 7
2.1.1. Born-Oppenheimer Approximation . . . . . 7
2.2. Wave Function Based Methods . . . . . 9
2.2.1. The Hartree-Fock Approximation . . . . . 9
2.2.2. Correlated Methods Beyond Hartree-Fock . . . . . 11
2.3. Density-Functional Theory . . . . . 17
2.3.1. Thomas-Fermi Model . . . . . 18
2.3.2. Hohenberg-Kohn Theorem . . . . . 18
2.3.3. The Kohn-Sham Equations . . . . . 20
2.3.4. Exchange-Correlation Functionals . . . . . 21
2.4. Basis Sets . . . . . 26
2.4.1. Atom Centered Localized Basis sets . . . . . 27
2.4.2. Plane Waves . . . . . 31
2.5. Pseudopotentials . . . . . 33
2.6. Brief Summary . . . . . 35

**3. The Accuracy of DFT xc Functionals for Water Clusters in the Gas Phase** **41**
3.1. Introduction . . . . . 41
3.2. Accurate Reference Dissociation Energy: MP2 . . . . . 42
3.3. DFT Dissociation Energy . . . . . 45
3.4. Results . . . . . 47
3.4.1. Dissociation Energy . . . . . 47
3.4.2. Cooperativity . . . . . 49
3.4.3. Geometry . . . . . 50
3.4.4. Requirement for Large Basis Sets . . . . . 51
3.4.5. Relevance to Other H-bonded Systems . . . . . 52
3.5. Summary . . . . . 53

**4. Water Hexamers: The Importance of van der Waals Interactions** **55**
4.1. Introduction . . . . . 55
4.2. Computational Details . . . . . 56
4.2.1. van der Waals Correction . . . . . 57

4.3. Results . . . 58
4.3.1. Reference Dissociation Energies: MP2 . . . 59
4.3.2. DFT Dissociation Energies . . . 60
4.3.3. Geometry . . . 61
4.3.4. Many-body Decomposition of The Dissociation Energies . . . 63
4.3.5. DFT+vdW Dissociation Energy . . . 66
4.4. Discussion and Conclusions . . . 69

**5. Water Clusters Extracted from DFT Liquid Water: The Importance of Monomer Deformations 73**
5.1. Introduction . . . 73
5.2. Methods, procedures, and definition of parameters . . . 75
5.2.1. Liquid water . . . 75
5.2.2. Clusters . . . 76
5.2.3. Definition of Parameters . . . 77
5.3. Results . . . 78
5.3.1. Monomers . . . 79
5.3.2. Dimers . . . 82
5.4. Discussion . . . 85
5.5. Summary . . . 87

**6. The Importance of van der Waals Forces in Crystalline Ice 89**
6.1. Introduction . . . 89
6.2. Methodology . . . 89
6.2.1. Ice Structures . . . 89
6.2.2. Basis Set . . . 90
6.2.3. van der Waals Correction . . . 91
6.3. Results . . . 91
6.3.1. Equilibrium volume . . . 92
6.3.2. Lattice energy . . . 94
6.4. Summary . . . 98

**7. Summary and Perspectives 99**

**Appendices 103**

**A. Extrapolation Schemes 105**

**B. NAO Basis Sets 109**

**C. Comparison of Gaussian, plane-waves, and NAO Basis Sets 111**

**D. Isotropic Change in Lattice Parameter 113**

**E. Refit of parameter $S_r$ for BLYP+vdW 115**

**Acknowledgements** **117**

**Curriculum Vitae** **118**

**Publications** **120**

**Bibliography** **123**

# List of Figures


2.1. Excited state wavefuntions . . . . . 12
2.2. "Jacob's ladder" . . . . . 22
2.3. GGA enhancement factors . . . . . 25
2.4. $H_2O$ basis set extrapolation . . . . . 32
2.5. Schematic diagram of pseudopotential . . . . . 34

3.1. Structures of water dimer to pentamer . . . . . 43
3.2. Extrapolation of $H_2O$ dimer dissociation energy . . . . . 44
3.3. Error in dissociation energy and geometry with several *xc* functionals . . 49
3.4. Mean error with MG3S basis sets. . . . . 52

4.1. Structures of water hexamers . . . . . 56
4.2. Errors in DFT dissociation energies . . . . . 62
4.3. TPSS and PBE1W structures of prism . . . . . 64
4.4. Variation in the dispersion contribution . . . . . 68

5.1. Schematic diagram of extraction of clusters from DFT liquid water . . . . 75
5.2. Distributions of O-O and O-H distances . . . . . 76
5.3. CCSD(T) and DFT one-body energies . . . . . 78
5.4. Errors in PBE and BLYP one body-energies . . . . . 79
5.5. CCSD(T) total dissociation energy and two-body energy . . . . . 81
5.6. Errors in PBE and BLYP dissociation and two-body energies . . . . . 83
5.7. Two-body energies as a function of O-$H_d$ . . . . . 84
5.8. Variation in exchange and correlation energy . . . . . 86

6.1. Phase diagram of crystalline ice . . . . . 90
6.2. Unit cells of various phases of ice . . . . . 91
6.3. Energy vs. volume of ice . . . . . 92
6.4. RDF of ice . . . . . 95
6.5. vdW contributions from H-H, O-H, and O-O atom pairs . . . . . 96

B.1. NAO basis set convergence . . . . . 110

D.1. *c/a* contour plot . . . . . 114

E.1. Damping functions . . . . . 116

# List of Tables


2.1. Brief description of electronic structure theories . . . . . 35
2.2. Summary of employed *xc* functionals . . . . . 38

3.1. MP2 and DFT dissociation energies of water dimer to pentamer . . . . . 47
3.2. Mean error in the DFT structures of the water dimer to pentamer . . . . 50

4.1. Dissociation energies of water hexamers . . . . . 59
4.2. Mean errors in the structures of hexamers with DFT . . . . . 63
4.3. Many-body contributions to the total dissociation energies . . . . . 65
4.4. DFT+vdW dissociation energies . . . . . 67

5.1. Harmonic vibrational frequencies of a water monomer . . . . . 80
5.2. Mean values of the one-body, two-body, and dissociation energies . . . . . 82
5.3. Errors in PBE and PBE0 exchange and correlation energy . . . . . 86

6.1. Equilibrium volumes of ice . . . . . 93
6.2. Lattice energies of ice . . . . . 94
6.3. Comparison of calculated $C_6$ coefficients from ice phases . . . . . 97

A.1. Comparison of extrapolation schemes . . . . . 106
A.2. Extrapolated dissociation energies . . . . . 107

B.1. NAO basis set used . . . . . 109

C.1. Comparison of Gaussian, plane wave, and NAO basis stes . . . . . 111

D.1. c/a ratio of ice VIII . . . . . 114

# List of Abbreviations

| | |
|---|---|
| BO | Born-Oppenheimer |
| BSSE | Basis Set Superposition Error |
| CBS | Complete Basis Set |
| CCSD | Coupled Cluster with Single and Double excitations |
| CCSD(T) | Coupled Cluster with Single and Double excitations plus a perturbative correction for connected Triples |
| CI | Configuration Interaction |
| DFT | Density-Functional Theory |
| DMC | Diffusion quantum Monte Carlo |
| GGA | Generalized Gradient Approximation |
| GTO | Gaussian Type Orbitals |
| HBs | Hydrogen Bonds |
| HF | Hartree-Fock |
| LDA | Local-Density Approximation |
| MP2 | $2^{\text{nd}}$ order Møller-Plesset perturbation theory |
| NAO | Numeric Atom-centered Orbitals |
| QMC | Quantum Monte Carlo |
| STO | Slater Type Orbitals |
| vdW | van der Waals |
| XAS | X-ray Absorption Spectroscopy |
| $xc$ | Exchange-Correlation |

# 1. Introduction

> *It is the hydrogen bond that determines the magnitude and nature of the mutual interactions of water molecules and that is consequently responsible for the striking physical properties of this uniquely important substance.*
>
> – Linus Pauling

Water is the most important substance on earth and considered to be one of the fundamental ingredients for the source of life. Historically, water has been one of the most investigated objects. Water possesses a special place in mythologies[1] and for centuries it was thought to be one of the "five elements" which the universe was assumed to be made of[2]. The modern picture of water that it is a compound and comprised of the elements hydrogen (H) and oxygen (O) was discovered only in the $19^{\text{th}}$ century. In 1826, J. J. Berzelius proposed the structure of water which is known today as $H_2O$[3].

The water molecule has one of the simplest structures, yet collections of water molecules exhibit various unique and important properties. To mention a few, water exists in the liquid state at room temperature[4], the density of liquid water decreases when solid water (ice) melts, water under pressure flows faster, etc. Key to many of those properties are the network of hydrogen bonds (HBs) that hold water molecules together. The hydrogen bond in water comes about as a result of an attractive interaction between the H atom attached to a water molecule and the O atom of an adjacent water molecule. The strength of HBs between water molecules are of a similar magnitude to thermal energy (in the order of 15–30 kJ/mol), which are suitable to play important roles in reactions occurring at normal temperature. The Uniqueness of the HBs in water also stems from the ability of one water molecule to participate in as much as four HBs (in some cases five). Also the strength of HBs highly depends on the orientation of water molecules and they are cooperative[5] in nature, which brings in more complexity with growing numbers of interacting water molecules. Hydrogen bonds are not only limited within water molecules but also important when water interacts with other materials. This capability

[1] Even today a dip in the holy water of the river Ganges is believed to remove all sin and paves a way towards the heaven.

[2] According to the Greek philosopher Aristotle (384 B.C - 322 B.C.) the universe consisted of fire, earth, air, aether, and water. A review can be found in the book *A Biography of Water* [1].

[3] More than 99% of water on earth is $H_2O$ (more precisely $^{1}H_2{}^{16}O$), whereas, few fractions of percent are present with various isotopes of H and O (e.g., $^{2}H$, $^{3}H$, $^{17}O$). They exhibit different properties than $H_2O$. For example, melting temperature of $^{2}H_2{}^{16}O$ (277 K), also known as $D_2O$, is 4 K higher than $H_2O$ (273.4 K). This thesis will deal mostly with $H_2O$ and in few cases $D_2O$.

[4] The molecular weight of water (18 a.m.u.) is too small and compared to other molecules of similar weight water should boil well below 273 K.

[5] The strength of an individual hydrogen bond gets enhanced as the number of HBs increases.

makes water an excellent solvent and also helps to nucleate water on surfaces, playing an important role, for instance, in cloud formation and many catalytic reactions. Interactions of water with biologically relevant molecules, such as, proteins and DNA is also obviously important to living entities [2, 3]. All these features have brought water in to the center of attention in interdisciplinary fields of research and for many years now it has been one of the major challenges of the physical sciences to understand the nature of HBs associated with water.

For decades sophisticated experimental tools were the only techniques used to answer various fundamental questions concerning HBs in water. One of the fundamental properties which anyone would be interested in is how water molecules are arranged in natural ice and liquid water. In this regard diffraction experiments with X-rays or neutrons have provided significant insights. In 1935, Linus Pauling proposed the basic structure of natural ice that each water molecule is attached with four others via HBs with a tetrahedral arrangement [4, 5]. A definitive confirmation of this model came through a neutron diffraction experiment in 1957 [6]. Even though the structure of ice seems to be well accepted, the basic structure of liquid water is still ambiguous. Especially, recent X-ray absorption spectroscopy (XAS) measurements which have led to the suggestion that in ambient liquid one water molecule is connected with only two other water molecules via strong HBs [7]. This contradicts perceived wisdom that each water molecule has four tetrahedrally coordinated HBs [8, 9]. Consequently, several studies have been performed to clarify the issue but no definite conclusions have been reached yet and the issue remains controversial (see, e.g., Refs. [10–32]).

Nowadays atomic scale simulations using computers (with efficient algorithms) have evolved as an equally promising and alternative tool to experiments for understanding materials. Computational techniques have been used to successfully verify experimental observations and they are able to bring new insights and clarifications to the experimental findings at the atomic level. Today this can be regarded as a parallel field to laboratory experiments and quite regularly knowledge obtained from computers and experiments are complimentary to each other. The rapid improvements in computer power together with more efficient computer algorithms provides a huge scope to perform simulations of high enough accuracy so that answers to questions like what the structure of liquid water is or how ice particles form on certain dust particles can be obtained. Moreover, accessing extreme physical conditions computationally is much simpler than to achieve this in real experiments. For example, geophysical pressures of millions of atmospheres representative of planetary cores require considerable effort to reach in a laboratory experiment, yet for theory can be computed without any particular difficulty [33, 34].

The success of the computer simulations of materials rests upon an accurate modeling of how atoms interact with each other. On the one hand there are pre-parameterized empirical potentials which have been applied with considerable success in the past and still nowadays represent the state-of-the-art to model large systems, such as biomolecules with tens of thousands of atoms. The potential parameters are usually fitted to reproduce some gas phase properties (e.g., the dipole moment, the dimer dissociation energy) or to recover some liquid state properties at ambient conditions (e.g., heat of vaporization,

density). Interestingly, the first such simple potential for water was made in 1933 [35] and since then due to huge general interest more than a hundred other water potentials have been proposed. But applications of empirical potentials are very much limited to capture the properties of systems they are parameterized for and in most cases they fail for other properties[6]. On the other hand there are techniques that are based on a quantum mechanical description of the atoms, which are computationally much more demanding but much more rigorous than empirical potentials. These methods do not require any input from experiments, thus, they are often termed as *ab initio* methods. Nowadays quite often the parameters for the empirical potentials are obtained from the knowledge of the *ab initio* methods. In this thesis a variety of *ab initio* methods have been employed aimed at achieving very high accuracy.

The essence of *ab initio* methods is to solve the Schrödinger equation or some analogous quantum mechanical equation. The solutions of the Schrödinger equation describe the quantum state of a system, possessing the information from which other physical properties of the system can be derived. In practice it is extremely difficult to solve the Schrödinger equation exactly for systems containing more than a few electrons. Thus various approximate methods have been proposed and developed over the years and they each have their own advantages and disadvantages. These methods are often categorized in to wave function based and density-functional based approaches. Many of the wave function based methods (e.g., quantum chemical approaches, quantum Monte Carlo) are often more accurate than the methods based on density-functional theory (DFT). In particular, coupled cluster is often considered as the "theoretical gold standard" and routinely used for benchmark purposes. Unfortunately, with coupled cluster and other wave function based methods the computational cost increases severely with the system size and treating just a few tens of electrons becomes a bottleneck even with the world's largest computers and most efficient algorithms. In this respect DFT has emerged as a very useful technique because it is capable of dealing with systems with hundreds or thousands or even more electrons. Undoubtedly, DFT is the most popular *ab initio* method nowadays, especially for condensed phase simulations and currently the only practical method available for understanding the unique properties of HBs in the condensed phases of water. Since the first DFT simulation of liquid water was performed in 1993 [38], DFT has continued to bring new insights to various properties of liquid water [38, 39], ice [40–44], interfacial water [45–48], confined water [49], solvation [50], adsorbed water [51–55], proton transfer [56], etc. However, as with all electronic structure methods, DFT has shortcomings. These shortcomings are mostly concerned with accuracy.

DFT is exact in principle but in practice it requires an approximation for the treatment of the so called electron *exchange* and *correlation* interactions. The exchange-correlation ($xc$) energy contributes a small fraction to the total energy of a system but for the accurate description of binding between atoms this turns out to be extremely crucial. Two standard ways to calculate the $xc$ energy are the local-density approximation (LDA)

[6]Recent review articles from Finney [36] and Guillot [37] briefly summarize some of the well known limitations of several popular empirical potentials.

and the generalized gradient approximation (GGA)[7]. These two *xc* functionals have been extremely successful in various fields but they often fail for the treatment of weakly bound systems (e.g., HBs and van der Waals bond). For purely van der Waals (vdW) bonded systems both LDA and GGA are known to be inadequate. However, for H-bonded systems or mixed H-bonded vdW bonded systems it is somewhat unclear how these functionals perform. There are more sophisticated *xc* functionals than LDA and GGA (as will be discussed in chapter 2) but how these perform and how to systematically improve the performance of DFT *xc* functionals for weakly bonded systems remain open questions. Some of these questions will be addressed in this thesis.

Regarding the treatment of HBs in the condensed phases of water with standard *xc* functionals there exist numerous outstanding problems. In comparison to experiments some of the well documented shortcomings are the following: (i) with standard *xc* functionals the melting temperature of $H_2O$ ice is found to be 415 K [31] at ambient pressure[8]; (ii) at ambient temperature the density of liquid water is found to be about 0.75-0.85 gm/cm$^3$ [32] (experimental value is $\sim$0.99 gm/cm$^3$); (iii) many *xc* functionals produce much less diffusive and too higly structured liquid water at room temperature [10–32]; and (iv) the density and lattice energy of ice can be either too large or too small depending on the choice of *xc* functional [41, 57]. So far it has not been possible to find a single *xc* functional which can be used regularly for simulations involving water molecules in gas, solid, and liquid phase with satisfactory results and, in general, a much better description of water and ice with DFT is highly desired.

As a first step towards this, knowledge of how various *xc* functionals perform for individual HBs between water molecules is essential and in this respect studies on small gas phase water clusters are expected to bring new insights. Through a series of systematic studies some of the key points addressed in this thesis are: (i) how accurate *xc* functionals are in describing the absolute and relative strength of HBs in small water clusters; (ii) what the shortcomings are and ways to systematically improve the description with standard *xc* functionals; and (iii) if the performance of *xc* functionals on clusters can explain their behavior in the condensed phase. These questions are tackled by comparing the DFT data to that from accurate reference data, obtained from explicitly correlated wave function based methods, e.g., coupled cluster[9], second order Møller-Plesset perturbation theory (MP2), and quantum Monte Carlo (QMC).

The first specific issue addressed in this thesis is a systematic study on the global

[7] Description of LDA and GGA can be found in chapter 2.

[8] To date this is the only prediction of the melting temperature of $H_2O$ ice at an *ab initio* level. The simulation was performed by treating the nuclei as classical particles, i.e., the quantum nature of the nuclei was neglected. It is established that the experimentally observed properties of water are significantly influenced by the quantum nature of H and a classical treatment will induce errors in the simulations, however, the magnitude of the effect is still not quantified precisely. Studies made with empirical potentials have suggested that quantum effects induce structural and dynamical changes in the order of 25 to 50 K, i.e., quantum water can approximately be described by classical water at elevated temperatures. Considering a difference of 50 K the estimated melting temperature is lowered to 365 K, which is still $\sim$90 K above the experimental value.

[9] Specifically, coupled cluster with single and double excitations plus a perturbative correction for connected triples [CCSD(T)] is employed here (see chapter 2 for more details).

minimum conformers of the water dimer to pentamer. A variety of *xc* functionals are considered and clear evaluations of each obtained. It is found that knowing how the *xc* functionals behave for the water dimer does not clarify how it will behave for the larger clusters. Consistently accurate binding energies (within 10 meV/H-bond) are achieved only from a few hybrid GGA *xc* functionals considered, and good but slightly inferior performance (within 20 meV/H-bond) for several GGAs tested.

A general perception is that if a functional produces HBs that are too weak within water clusters, very likely it will predict understructured and too diffusive liquid water. However, certain popular functionals display the opposite behavior in this respect and this has remained without a satisfactory explanation for some time now. A close investigation to understand this issue has revealed quite intriguing shortcomings with GGA *xc* functionals regarding the description of the structural deformations of the water monomers inside liquid water. Specifically, upon going from the gas phase to the liquid phase the covalent O-H bonds of the water monomers are elongated and with the GGAs this process is found to be energetically much too easy. As a result the performance of pure GGAs for water clusters within liquid water is generally inferior to their performance in the gas phase. A few hybrid functionals are again found to be more accurate in this regard. This implies that one should be cautious when simulating liquid water with GGA *xc* functionals.

van der Waals interactions are present everywhere, especially for weak bonded systems vdW contributions can contribute significantly to the total binding. Exactly how important vdW interactions are for the interaction between water molecules is not known conclusively neither at a quantitative nor a qualitative level. This knowledge is crucial in conjunction with DFT since standard functionals are unable to capture vdW interactions appropriately. In this respect a study of the low-lying isomers of water hexamers has brought new insights. The four low-lying isomers of the water hexamer (commonly known as "prism", "cage", "book", and "cyclic") provide a critical test for *xc* functionals because energetically they differ from each other by only 10-20 meV/$H_2O$. Surprisingly, all the *xc* functionals are neither able to find the correct low-energy structure, (i.e., "prism") nor they can produce the correct energetic ordering among the isomers. Moreover, it is found that this deficiency is attributed to the inaccurate description of vdW interactions between water molecules. Indeed the correct energetic ordering was obtained upon including vdW interactions explicitly with regular DFT energies. This is one important illustration that vdW interactions are crucial for the interaction between water molecules and special care needs to be taken when treating water with standard DFT *xc* functionals.

Finally, knowing the importance of vdW forces in water clusters an attempt has been made here to understand the influence of vdW forces in the condensed phases of water. Various high and low pressure phases of crystalline ice are studied and their densities, lattice energies, and bulk moduli are compared with regular DFT *xc* functionals and vdW corrected versions of those. It is observed that the proportion of the lattice energy coming from vdW interactions monotonously increases with the density of the ice phases. As a consequence, vdW interactions play a crucial role in stabilizing the high density

phases of ice. In addition, calculations predict that the effective volume of the water molecules is reduced when vdW forces are accounted for.

The rest of this thesis is organized as follows. Chapter 2 provides a brief description of the theoretical background of the computational methods used. How accurately various DFT *xc* functionals can describe HBs among small gas phase clusters is illustrated in chapter 3. The importance of vdW forces in gas phase water hexamers is discussed in chapter 4. Chapter 5 describes the importance of monomer deformations for liquid water simulations with GGA *xc* functionals. The importance of vdW forces in various phases of crystalline ice is discussed in chapter 6. Finally, a summary and possible perspectives for future research directions are presented in chapter 7.

# 2. Theoretical Background

## 2.1. Electronic Structure Problem

A key aim of most electronic structure theory is to solve the non-relativistic time independent many-body Schrödinger equation

$$\hat{H}\Psi(\{\mathbf{R}_A\},\{\mathbf{r}_i,\sigma_i\}) = E\Psi(\{\mathbf{R}_A\},\{\mathbf{r}_i,\sigma_i\}) \quad . \tag{2.1}$$

For a system containing $M$ nuclei and $N$ electrons the many-body wavefunction ($\Psi$) is a function of all the spatial coordinates of nuclei ($\{\mathbf{R}_A\}, A = 1, ..., M$) and spatial and spin coordinates of electrons ($\{\mathbf{r}_i, \sigma_i\}, i = 1, ..., N$). The Hamiltonian ($\hat{H}$) is a sum of all possible interactions between electrons and nuclei. In atomic units (energy in Hartree and length in Bohr), $\hat{H}$ can be expanded as:

$$\hat{H} = -\sum_{i=1}^{N}\frac{\nabla_i^2}{2} - \sum_{A=1}^{M}\frac{\nabla_A^2}{2M_A} + \sum_{i=1}^{N}\sum_{j>i}^{N}\frac{1}{|\mathbf{r}_i-\mathbf{r}_j|} + \sum_{A=1}^{M}\sum_{B>A}^{M}\frac{Z_A Z_B}{|\mathbf{R}_A-\mathbf{R}_B|} - \sum_{i=1}^{N}\sum_{A=1}^{M}\frac{Z_A}{|\mathbf{r}_i-\mathbf{R}_A|} \tag{2.2}$$

In the above equation, $M_A$ is the ratio of the mass of nucleus $A$ to the mass of an electron and $Z_A$ is the atomic number of nucleus $A$. The $\nabla_i^2$ and $\nabla_A^2$ are the Laplacian operators. The first two terms in Eq. (2.2) represent the kinetic energies of all the electrons and nuclei, respectively. The third and fourth term, respectively, correspond to the Coulomb repulsion between electrons and between nuclei. The fifth term is the Coulomb attraction between electrons and nuclei. Eq. (2.1) is deceptively simple by its form but enormously complex to solve. Ever since it was discovered it is a dream of researchers to find reasonable approximations to reduce the complexity. The first important approximation is obtained by decoupling the dynamics of the electrons and the nuclei, which is known as Born-Oppenheimer approximation [58].

### 2.1.1. Born-Oppenheimer Approximation

The very essence of the Born-Oppenheimer approximation comes from the fact that the nuclei are much heavier than the electrons. Even for the lightest nucleus, a proton, its mass is approximately 2000 times larger than the electrons. So, in most cases the timescale of the response of the electrons is a few orders of magnitude faster than that of the nuclei, which allows the dynamics of the electrons and nuclei to be decoupled. Through this simple approximation, nuclei can be treated as classical particles and can be considered as static with respect to quantum particle electrons. Then for any given nuclear configurations the electrons are assumed to remain in their instantaneous ground

state. As a result, the second term in Eq. (2.2) can be neglected and the fourth term, the repulsion between nuclei, can be treated as a constant for a fixed configuration of the nuclei. The remaining terms in Eq. (2.2) are called the electronic Hamiltonian ($\hat{H}_e$),

$$\hat{H}_e = -\sum_{i=1}^{N} \frac{\nabla_i^2}{2} + \sum_{i=1}^{N}\sum_{j>i}^{N} \frac{1}{|\mathbf{r}_i - \mathbf{r}_j|} - \sum_{i=1}^{N}\sum_{A=1}^{M} \frac{Z_A}{|\mathbf{r}_i - \mathbf{R}_A|} \quad . \tag{2.3}$$

The solution to a Schrödinger equation involving the electronic Hamiltonian ($\hat{H}_e$) becomes

$$\hat{H}_e \Psi_e(\{\mathbf{R}_A\}, \{\mathbf{r}_i, \sigma_i\}) = E_e \Psi_e(\{\mathbf{R}_A\}, \{\mathbf{r}_i, \sigma_i\}) \quad . \tag{2.4}$$

The electronic wavefunction ($\Psi_e$) depends on nuclear coordinates ($\{\mathbf{R}_A\}$) only parametrically now, thus for fixed configuration of nuclei we suppress $\{\mathbf{R}_A\}$. Furthermore, for simplicity we put together electronic spatial and spin coordinates ($\{\mathbf{r}_i, \sigma_i\}$) in to one variable $\{\mathbf{x}_i\}$ (*i.e.*, $\{\mathbf{x}_i\} = \{\mathbf{r}_i, \sigma_i\}$) and rewrite Eq. (2.4) as

$$\hat{H}_e \Psi_e(\{\mathbf{x}_i\}) = E_e \Psi_e(\{\mathbf{x}_i\}) \quad . \tag{2.5}$$

The total energy for some fixed configurations of the nuclei will also include the constant nuclear repulsion term leading to,

$$E_{total} = E_e + \sum_{A=1}^{M}\sum_{B>A}^{M} \frac{Z_A Z_B}{|\mathbf{R}_A - \mathbf{R}_B|} \quad . \tag{2.6}$$

In general under the Born-Oppenheimer approximation the electronic structure problem reduces to solving Eq. (2.5) and throughout this thesis equations resembling (2.5) and (2.6) are solved and total energies are obtained.

However, one should bear in mind that the Born-Oppenheimer approximation is certainly not universally valid. It is well known that the Born-Oppenheimer approximation will break down when there are multiple potential energy surfaces close to each other in energy or crossing each other. Dissociative adsorption of molecules on metal surfaces is a famous contemporary example. Similarly, reactions involving hydrogen and proton transfer may be susceptible to breakdowns in the Born-Oppenheimer approximation. More caution must be exerted when dealing with systems such as those (see, e.g., Refs. [59–62]).

The major difficulty in solving Eq. (2.5) is the interaction between electrons, where all the many-body quantum effects are hidden. Since the motion of the electrons is correlated one should know the instantaneous coordinates of each electron, which essentially requires the treatment of $3^N$ variables for an $N$-electron system. Despite the almost intractable nature of these interactions, many approximate methods have been developed to solve Schrödinger or Schrödinger-like equations by mapping the $N$-electron Schrödinger equation in to effective one-electron Schrödinger-like equations, which are easier to tackle. Some of these approximate solutions, the ones made use of in this thesis, will be introduced in the following. The different approximate schemes employed here

can be divided in to two major categories: (i) the wave function based methods, where the many-electron wave function is the key; and (ii) density-functional theory (DFT), in which electron density is the central quantity. Here, the wave function based methods will be introduced first.

## 2.2. Wave Function Based Methods

As mentioned above the fundamental quantity for the wave function based methods is the many-electron wave function, $\Psi$, whose correct functional form is far from simple. The first step in the determination of $\Psi$ is often simply an educated guess and then reliance on the variational principle. The variational principle tells that the expectation value of the electronic Hamiltonian ($\hat{H}_e$) for any guessed or trial wave function is always larger (upper bound) than the electronic ground state energy $E_0[\Psi_0]$ and the equality will hold only when the wavefunction is in the true ground state ($\Psi_0$), *i.e.*, ($E[\Psi] \geq E_0[\Psi_0]$). The advantage of the variational principle is that starting with a trial wave function one can approach towards the ground state energy $E_0[\Psi_0]$ by variationally improving the quality of the wave function. In the following, the variational principle will be applied to minimize the approximated Hartree-Fock wave function.

### 2.2.1. The Hartree-Fock Approximation

The Hartree-Fock (HF) approach is regarded as the fundamental first step in much of quantum chemistry[1]. In the HF approach the wave function of interacting $N$-electrons, $\Psi(\{\mathbf{x}_i\})$, can be approximately described with a single Slater determinant. A Slater determinant is nothing but a linear combination of the product of independent electron wave functions ($\{\phi_i(\mathbf{x}_i)\}$) (also known as spin orbitals) with all possible combinations of the permutations of their coordinates. Also the Slater determinant satisfies the antisymmetric property of the electronic wave function, which is essential because electrons are fermions and obey Pauli's exclusion principle. For an $N$-electron system the HF wave function looks like

$$\Psi(\{\mathbf{x}_i\}) \approx \Psi^{\mathrm{HF}}(\{\mathbf{x}_i\}) = \frac{1}{\sqrt{N!}} \begin{vmatrix} \phi_i(\mathbf{x}_i) & \phi_j(\mathbf{x}_i) & \dots & \phi_N(\mathbf{x}_i) \\ \phi_i(\mathbf{x}_j) & \phi_j(\mathbf{x}_j) & \dots & \phi_N(\mathbf{x}_j) \\ \vdots & \vdots & \ddots & \vdots \\ \phi_i(\mathbf{x}_N) & \phi_j(\mathbf{x}_N) & \dots & \phi_N(\mathbf{x}_N) \end{vmatrix}. \tag{2.7}$$

In the Slater determinant each of the columns are labeled by spin orbitals and exchange of two electron coordinates will interchange the two columns inside the determinant, thus

[1] In 1928, D. R. Hartree proposed a simplest possible ansatz [63] in which the total wave function of interacting $N$-electrons [$\Psi(\{\mathbf{x}_i\})$] is approximately taken as a product of $N$ independent electrons $\{\phi_i(\mathbf{x}_i)\}$. But the Hartree wave function does not satisfy the antisymmetric property of the total electronic wave function, which needs to be fulfilled since electrons are fermions. In 1930, V. Fock proposed to use a Slater determinant instead of Hartree products to represent total electronic wave function [64].

satisfying the antisymmetric requirement. The antisymmetric property of the Slater determinant can be simply realized considering a two-electron system:

$$\Psi(\mathbf{x}_1,\mathbf{x}_2)=\frac{1}{\sqrt{2!}}\big[\phi_1(\mathbf{x}_1)\phi_2(\mathbf{x}_2)-\phi_2(\mathbf{x}_1)\phi_1(\mathbf{x}_2)\big]=-\Psi(\mathbf{x}_2,\mathbf{x}_1) \quad . \tag{2.8}$$

Now using the HF wave function the electronic energy can be written as,

$$\begin{aligned} E^{\mathrm{HF}} &= \langle\Psi^{\mathrm{HF}}|\hat{H}_e|\Psi^{\mathrm{HF}}\rangle \\ &= \sum_{i=1}^{N}\int\phi_i^*(\mathbf{x}_i)\Big[-\frac{\nabla_i^2}{2}+V^{\mathrm{ext}}(\mathbf{x}_i)\Big]\phi_i(\mathbf{x}_i)d\mathbf{x}_i \\ &\quad +\frac{1}{2}\sum_{i=1}^{N}\sum_{j=1}^{N}\iint\phi_i^*(\mathbf{x}_i)\phi_j^*(\mathbf{x}_j)\frac{1}{|\mathbf{r}_i-\mathbf{r}_j|}\phi_j(\mathbf{x}_j)\phi_i(\mathbf{x}_i)\,d\mathbf{x}_i\,d\mathbf{x}_j \\ &\quad -\frac{1}{2}\sum_{i=1}^{N}\sum_{j=1}^{N}\iint\phi_i^*(\mathbf{x}_i)\phi_j^*(\mathbf{x}_j)\frac{1}{|\mathbf{r}_i-\mathbf{r}_j|}\phi_j(\mathbf{x}_i)\phi_i(\mathbf{x}_j)\,d\mathbf{x}_i\,d\mathbf{x}_j \quad . \end{aligned} \tag{2.9}$$

The above equation can be treated as an energy functional, $E^{\mathrm{HF}}[\{\phi_i^*(\mathbf{x}_i)\},\{\phi_i(\mathbf{x}_i)\}]$, and can be minimized variationally by applying Lagrange undetermined multiplier subject to the constraints that the independent electron wave function $\{\phi_i(\mathbf{x}_i)\}$ are orthonormal, *i.e.*, $\langle\phi_i(\mathbf{x}_i)|\phi_j(\mathbf{x}_j)\rangle=\delta_{ij}$. This leads to a mapping from a complex $N$-electron Schrödinger equation in to effective one-electron Schrödinger-like equations

$$\hat{F}_i\phi_i(\mathbf{x}_i)=\epsilon_i\phi_i(\mathbf{x}_i),\qquad \hat{F}_i=-\frac{\nabla^2}{2}+V^{\mathrm{ext}}(\mathbf{x}_i)+V^{\mathrm{Hartree}}(\mathbf{x}_i)+V_i^{\mathrm{Exchange}}(\mathbf{x}_i) \quad . \tag{2.10}$$

$\hat{F}_i$ represents a one-electron Hamiltonian, known as the Fock operator. $\epsilon_i$ and $\phi_i$ are the corresponding eigenvalues and eigenvectors, respectively. The first two terms in $\hat{F}_i$ are, respectively, the kinetic energy of $N$ independent electron and the external potential. The external potential, $V^{\mathrm{ext}}(\mathbf{x}_i)$, is the Coulomb attraction on $i^{\mathrm{th}}$ electron due to all the nuclei. The third and fourth terms approximately account for the many body electron-electron interactions. $V^{\mathrm{Hartree}}(\mathbf{x}_i)$ is the Hartree potential, which is the Coulomb repulsion between $i^{\mathrm{th}}$ electron and the electron density produced by all electrons

$$V^{\mathrm{Hartree}}(\mathbf{x}_i)=\int\frac{n(\mathbf{x}_j)}{|\mathbf{r}_i-\mathbf{r}_j|}\,d\mathbf{x}_j,\qquad n(\mathbf{x}_j)=\sum_{j=1}^{N}|\phi_j(\mathbf{x}_j)|^2 \quad . \tag{2.11}$$

The fourth term solely appears from the antisymmetric nature of the wave function and is known as *exchange* potential ($V_i^{\mathrm{Exchange}}(\mathbf{x}_i)$). Unlike $V^{\mathrm{ext}}(\mathbf{x}_i)$ and $V^{\mathrm{Hartree}}(\mathbf{x}_i)$, $V_i^{\mathrm{Exchange}}(\mathbf{x}_i)$ does not have any classical analogy, and it can only be written as an integral operator

$$V_i^{\mathrm{Exchange}}(\mathbf{x}_i)\phi_i(\mathbf{x}_i)=\left[\sum_{j=1}^{N}\int\phi_j^*(\mathbf{x}_j)\frac{1}{|\mathbf{r}_i-\mathbf{r}_j|}\phi_j(\mathbf{x}_i)d\mathbf{x}_j\right]\phi_i(\mathbf{x}_j) \tag{2.12}$$

As evident from the above equation, $V_i^{\text{Exchange}}(\mathbf{x}_i)$ leads to an exchange of the variable in the two spin orbitals. Furthermore, the exchange operator, $V_i^{\text{Exchange}}(\mathbf{x}_i)$ is said to be a nonlocal operator, as the results of $V_i^{\text{Exchange}}(\mathbf{x}_i)$ operating on the spin orbital $\phi_i(\mathbf{x}_i)$ will depend on the value of $\phi_i(\mathbf{x}_i)$ throughout all space. Also worth to mention is that when $i$=$j$ the last two terms in Eq. (2.9) cancel each other, and so by construction the HF method is self interaction free. Eq. (2.10) is the usual form of the HF equation, which is a linear eigenvalue problem and must be solved self consistently. The HF method treats the exchange interaction between electrons with the same spin exactly and often in the literature is described as an *exact exchange* approach[2]. The HF method is used extensively to study various materials science problems, such as adsorption [65], defects in solids [66], and electronic structure of insulators [67].

A major drawback though lies in the effective mean field treatment of the Coulomb repulsion between electrons, which provides a inaccurate description of the spatial separation of the electrons as it would be in a complete many-electron interaction. This missing part is widely designated as electron *correlation* [68]. Indeed, the difference between the ground state HF energy and the exact ground state energy is used as a standard definition of the *correlation* energy in quantum chemistry. The *correlation* energy is typically a small fraction of the total energy. However, it can be a very important contribution to many systems of physical and chemical interest. For example, the restricted HF method cannot describe the dissociation of $H_2$ into two open-shell H atoms. Or, at least one quarter of the strength of hydrogen bonds between water molecules comes from correlations beyond HF (see chapter 3). In the following we will briefly describe some of the methods which explicitly calculate the electron *correlation* and are employed in this thesis.

### 2.2.2. Correlated Methods Beyond Hartree-Fock

In quantum chemistry, methods beyond HF aim to improve on HF by taking account of electron correlation. Most of these methods require more flexible wave functions than that of a single determinant HF and usually it is obtained by means of excitations of electrons from occupied to virtual orbitals. A schematic diagram (Fig. 2.1) shows examples of selected single ($\Phi_i^a$), double ($\Phi_{ij}^{ab}$), and triple ($\Phi_{ijk}^{abc}$) excitations. These methods include configuration interaction (CI), Møller-Plesset perturbation theory, and coupled cluster. For CI methods, a linear combination of ground-state and excited-state Slater determinants is used rather than one single Slater determinant in HF to approximate the wave function. However, CI was not been used in this thesis[3], so it

[2]This nomenclature is popular in quantum chemistry community, however, in other popular method like DFT, the definition of exchange is little different. Therefore, in the following it will be always referred as Hartree-Fock exchange.

[3]It is well-known that truncated CI like CISD (truncated at double excitation level) is not size extensive and that full CI calculations which are prohibitively expensive are limited to the smallest systems like $H_2$. In contrast, CCSD or CCSD(T) are size extensive and can be applied to larger systems. Out of interest, corrections to truncated CI to recover size extensiveness have been proposed (J. Chem. Phys. **101**, 8908 (1994)). Nonetheless, in this thesis coupled cluster will be used for the high accuracy

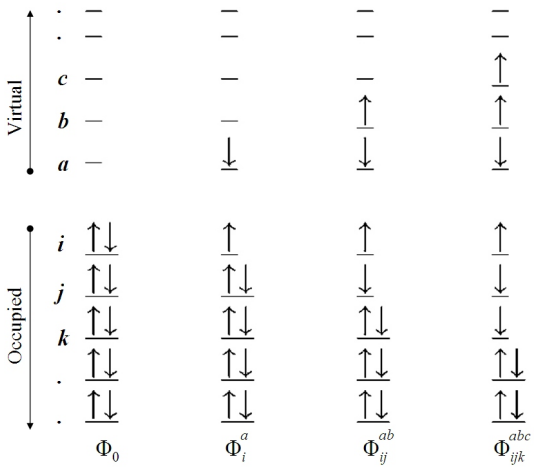


**Figure 2.1.:** A schematic diagram showing examples of selected single ($\Phi_i^a$), double ($\Phi_{ij}^{ab}$), and triple ($\Phi_{ijk}^{abc}$) excitations. $\Phi_0$ refers to HF wave function. The figure is adapted from Ref. [69].

will not be further discussed. Møller-Plesset perturbation theory, as the name suggests, treats electron correlation in a perturbative manner. And in the coupled cluster method, the electron correlation is handled through use of a so-called cluster operator. Both Møller-Plesset perturbation theory and coupled cluster will be briefly introduced.

### Møller-Plesset Perturbation Theory

The principle of perturbation theory in general is to start from a simple model which has been solved exactly or approximately and gradually add a small "perturbation" to this simple model. If the disturbance is not so large, the various physical quantities of interest can be obtained from the starting model.

Suppose we wish to solve the eigenvalue problem,

$$\hat{H}|\Psi_k\rangle = (\hat{H}_0 + \lambda\hat{H}')|\Psi_k\rangle = \xi_k|\Psi_k\rangle \quad , \tag{2.13}$$

where $\hat{H}_0$ is the reference Hamiltonian whose solutions are known and form a complete orthonormal set

$$\hat{H}_0|\Phi_i\rangle = E_i|\Phi_i\rangle,\ i = 0, 1, 2, \ldots, \infty \quad . \tag{2.14}$$

$\hat{H}'$ is a small perturbative Hamiltonian ($\hat{H}' \ll \hat{H}_0$) and $\lambda$ is a perturbation parameter such that expanding in series of $\lambda$ we can systematically improve the solutions of $\hat{H}_0$ so that they become closer and closer to the solutions of the total Hamiltonian $\hat{H}$. Expanding exact solutions in a Taylor series in $\lambda$,

$$|\Psi_k\rangle = |\Psi_k^{(0)}\rangle + \lambda|\Psi_k^{(1)}\rangle + \lambda^2|\Psi_k^{(2)}\rangle + \cdots \tag{2.15}$$

$$\xi_k = \xi_k^{(0)} + \lambda\xi_k^{(1)} + \lambda^2\xi_k^{(2)} + \cdots \tag{2.16}$$

calculations.

Here the $0^{th}$ order terms are known solutions of Eq. (2.14), i.e., $|\Psi_k^{(0)}\rangle$=$|\Phi_0\rangle$ and $\xi_k^{(0)}$=$E_0$. $|\Psi_k^{(1)}\rangle, |\Psi_k^{(2)}\rangle, ...$ and $\xi_k^{(1)}, \xi_k^{(2)}, ...$ are the first-, second-, etc. order corrections and the goal here is to represent these unknown quantities in terms of known quantities, $\{\Phi_i\}$ and $\{E_i\}$.

Using the intermediate normalization, i.e., for all $k$ $\langle\Psi_k|\Phi_0\rangle$=1, it can be shown that all $\langle\Psi_k^{(i)}|\Phi_0\rangle$=0 for $i$=$1, 2, ....$ Substituting Eq. (2.15) and Eq. (2.16) to Eq. (2.13) and equating the coefficients of equal power of $\lambda$, the general expression for the $n^{th}$ order perturbation becomes

$$\hat{H}_0\Psi_k^{(n)} + \hat{H}'\Psi_k^{(n-1)} = \sum_{i=0}^{n} \xi_k^{(i)}\Psi_k^{(n-i)} \quad . \tag{2.17}$$

Multiplying the above equation by $\langle\Phi_0|$ from left we get,

$$\xi_k^{(n)} \quad = \quad \langle\Phi_0|\hat{H}'|\Psi_k^{(n-1)}\rangle \quad . \tag{2.18}$$

So, the $n^{th}$ order correction to the energy can be obtained from the $(n\text{-}1)^{th}$ order wave function. Now to obtain $\xi_k^{(2)}$ we expand the unknown first-order correction to the wave function ($\Psi_k^{(1)}$) as a linear combination of the solutions of Eq. (2.14)

$$\Psi_k^{(1)} = \sum_{i\neq 0}^{\infty} |\Phi_i\rangle\langle\Phi_i|\Psi_k^{(1)}\rangle \quad . \tag{2.19}$$

From Eq. (2.17) we take the first order correction ($n$=1) and multiply with $\langle\Phi_i|$ from left and obtain the expansion coefficient

$$\langle\Phi_i|\Psi_k^{(1)}\rangle = \frac{\langle\Phi_i|\hat{H}'|\Phi_0\rangle}{E_i - E_0} \quad . \tag{2.20}$$

So the second order correction to the energy becomes,

$$\begin{aligned} \xi_k^{(2)} &= \langle\Phi_0|\hat{H}'|\Psi_k^{(1)}\rangle \\ &= \sum_{i\neq 0}^{\infty} \langle\Phi_0|\hat{H}'|\Phi_i\rangle\langle\Phi_i|\Psi_k^{(1)}\rangle \\ &= \sum_{i\neq 0}^{\infty} \frac{\langle\Phi_0|\hat{H}'|\Phi_i\rangle\langle\Phi_i|\hat{H}'|\Phi_0\rangle}{E_i - E_0} \quad , \end{aligned} \tag{2.21}$$

which is the sum of matrix elements of the perturbed Hamiltonian ($\hat{H}'$) over all the known solutions of the reference Hamiltonian ($\hat{H}_0$).

So far the theory has been completely general. To apply perturbation theory to electron correlation calculations, the unperturbed Hamiltonian ($\hat{H}_0$) must be selected.

The most common choice is to take this as a sum over Fock operators which is defined in Eq. (2.10), leading to the Møller-Plesset (MP) perturbative theory [70]:

$$\hat{H}_0 = \sum_{i=1}^{N} \hat{F}_i \quad , \tag{2.22}$$

and the perturbative Hamiltonian is

$$\hat{H}' = \hat{H} - \hat{H}_0 = \sum_{i<j}^{N} \frac{1}{|\mathbf{r}_i - \mathbf{r}_j|} - \sum_i V_i^{\mathrm{HF}} \quad . \tag{2.23}$$

$V_i^{\mathrm{HF}}$ is the sum of Hartree and exchange potentials defined in Eqs. (2.11) and (2.12), respectively. Now we start to derive the electron correlation energy by using MP theory, especially, we focus on the second-order energy which is the MP2 method. First, the HF wave function $\Phi_0$ is an eigenfunction of $\hat{H}_0$,

$$\hat{H}_0|\Phi_0\rangle = E_0|\Phi_0\rangle \tag{2.24}$$

and the second order correction to the energy can be obtained from Eq. (2.21), where $\Phi_0$ is the HF reference wave function and $\Phi_i$ are all possible excited states. Since the perturbation operator is a two-electron operator the matrix element involving triples, quadruples, etc. excitations are zero. Among the single and double excitations, single excitations do not contribute as shown below,

$$\begin{aligned} \langle\Phi_0|\hat{H}'|\Phi_i^a\rangle &= \langle\Phi_0|\big(\hat{H} - \sum_{j=1}^{N} \hat{F}_j\big)|\Phi_i^a\rangle \\ &= \langle\Phi_0|\hat{H}|\Phi_i^a\rangle - \sum_{j=1}^{N}\langle\Phi_0|\hat{F}_j|\Phi_i^a\rangle \\ &= \langle\Phi_0|\hat{H}|\Phi_i^a\rangle - E_a\langle\Phi_0|\Phi_i^a\rangle \quad . \end{aligned} \tag{2.25}$$

The first term in the above equation is zero due to the Brillouin theorem [71] and the second one is also zero because of the orthogonality of the eigenvectors of the Fock operator. Therefore, the only term which contributes to the energy correction is the double excitation. Denoting the occupied and virtual orbitals by $(i, j, k, ...)$ and $(a, b, c, ...)$, respectively, $\Phi_{ij}^{ab}$ represents doubly excited states, where two electrons from $i$ and $j$ orbitals are promoted to $a$ and $b$ orbitals.

$$\xi_k^{(2)} = \sum_{i<j}^{occ}\sum_{a<b}^{vir} \frac{\langle\Phi_0|\hat{H}'|\Phi_{ij}^{ab}\rangle\langle\Phi_{ij}^{ab}|\hat{H}'|\Phi_0\rangle}{E_0 - E_{ij}^{ab}} \tag{2.26}$$

The matrix elements between the HF and the doubly excited state are given by two-electron integrals over molecular orbitals. The difference in total energy between two

Slater determinants becomes a difference in molecular orbital energies. Thus the explicit expression for MP2 becomes,

$$E^{\mathrm{MP2}} = \xi_k^{(2)} = \sum_{i<j}^{occ} \sum_{a<b}^{vir} \frac{\left[\langle\phi_i\phi_j|\phi_a\phi_b\rangle - \langle\phi_i\phi_j|\phi_b\phi_a\rangle\right]^2}{\epsilon_i + \epsilon_j - \epsilon_a - \epsilon_b} \tag{2.27}$$

In the above equation, the $\phi_i$, $\phi_j$ are the occupied orbitals and $\phi_a$, $\phi_b$ are the virtual (unoccupied) orbitals. The $\epsilon_i$, $\epsilon_j$, $\epsilon_a$, and $\epsilon_b$ are the corresponding orbital energies.

MP2 shows improvements over HF in many respects in electronic structure calculations [72, 73]. For example, MP2 can capture (at least approximately) the weak non-covalent interactions like dispersion for which HF completely fails. Also the geometry (G3 test set [74]) predicted from MP2 shows much improvement over HF compared with experimental measurements [75]. It is worth cautioning, however, that Møller-Plesset perturbation theory is far from a panacea. For example, it is not appropriate for metallic systems and for some molecular properties like spectroscopic constants which are not necessarily converged when going to high orders, or the convergence is slow or oscillatory [76]. Thus higher order corrections, e.g., MP3 ($3^{\mathrm{rd}}$ order) or MP25 ($25^{\mathrm{th}}$ order) will not definitely bring better results than MP2! Despite this, MP2 is a very powerful and useful post-HF method considering its accuracy and scaling ($N^5$) and widely used in electronic structure calculations of gas phase or molecular systems.

### Coupled Cluster Methods

The coupled cluster method was introduced into quantum chemistry by Čížek and Pauldus [77, 78] in the 1960's and emerged as perhaps the most reliable, yet computationally affordable method for the approximate solution of the electronic Schrödinger equation and the prediction of molecular properties [69, 79, 80]. A short account of this method is given now.

The coupled cluster wave function can be written as

$$\Psi_{cc} = e^T \Phi_0 = (1 + T + \frac{1}{2!}T^2 + \frac{1}{3!}T^3 + \cdots)\Phi_0 \quad . \tag{2.28}$$

Here $\Phi_0$ is a Slater determinant and the cluster operator $T$ is composed of a series of connected operators

$$T = T_1 + T_2 + T_3 + \cdots + T_n \quad , \tag{2.29}$$

which can be expanded in terms of its components that introduce single ($\Phi_i^a$), double ($\Phi_{ij}^{ab}$), triple ($\Phi_{ijk}^{abc}$), etc. excitations into the wave function,

$$\begin{aligned} T_1\Phi_0 &= \sum_{i}^{occ}\sum_{a}^{vir} t_i^a \Phi_i^a \quad , \\ T_2\Phi_0 &= \sum_{i<j}^{occ}\sum_{a<b}^{vir} t_{ij}^{ab} \Phi_{ij}^{ab} \quad . \\ &\vdots \end{aligned} \tag{2.30}$$

These $T_n$ contributions are referred to as connected since they can not be reduced further. However, by virtue of nonlinear terms in the exponential expansion, we have, in addition, the disconnected (but linked) higher order excitations like, $T_1^2$, $T_1T_2$, $T_2^2$, etc. The exponential operator $e^T$ can be written as

$$\begin{aligned} e^T &= 1 + T_1 + (T_2 + \frac{1}{2}T_1^2) + (T_3 + T_1T_2 + \frac{1}{3!}T_1^3) \\ &\quad + (T_4 + T_3T_1 + \frac{1}{2}T_2^2 + \frac{1}{2}T_2T_1^2 + \frac{1}{4!}T_1^4) + \cdots \end{aligned} \tag{2.31}$$

The first term generates the reference HF and the second all singly excited states. The terms in the first set of parenthesis generate all doubly excited states, and so on.

With the coupled cluster wave function in Eq. (2.28), the Schrödinger equation becomes

$$\hat{H}e^T\Phi_0 = Ee^T\Phi_0 \quad . \tag{2.32}$$

Multiplying from left by $\langle\Phi_0|$ and integrating gives

$$\begin{aligned} E &= \langle\Phi_0|\hat{H}e^T|\Phi_0\rangle \\ &= \langle\Phi_0|\hat{H}(1 + T + \frac{1}{2!}T^2 + \frac{1}{3!}T^3 + \cdots)|\Phi_0\rangle \quad . \end{aligned} \tag{2.33}$$

Note that $\hat{H}$ is at most a two-particle operator and then $T$ is at least a one-particle excitation operator. We can simplify the above equation to

$$E = \langle\Phi_0|\hat{H}(1 + T + \frac{1}{2!}T^2)|\Phi_0\rangle \quad . \tag{2.34}$$

This is the natural truncation of the coupled cluster energy equation and it only depends on the form of $\hat{H}$ not on that of $T$ or on the number of electrons.

Till now, everything is exact. Expansion of the cluster operator $T$ up to $T_N$ would mean all possible excited determinants are included and the coupled cluster results would equal those obtained from full CI calculations. However, in practice a truncation of $T$ must be performed. Only including $T_1$ does not improve anything upon Hartree-Fock because of Brillouin's theorem. So the lowest approximation starts from $T_2$. If $T$ is expanded as $T_1$+$T_2$, this will be referred to as CCSD, which is the coupled cluster method with single and double excitations. Now we focus on CCSD to get $E$ in Eq. (2.34). If $T = T_1 + T_2$, then Eq. (2.34) becomes,

$$\begin{aligned} E &= \langle\Phi_0|\hat{H}|\Phi_0\rangle + \langle\Phi_0|\hat{H}|T_1\Phi_0\rangle + \langle\Phi_0|\hat{H}|T_2\Phi_0\rangle + \frac{1}{2}\langle\Phi_0|\hat{H}|T_1^2\Phi_0\rangle \\ &= E_0 + \sum_i^{occ}\sum_a^{vir} t_i^a\langle\Phi_0|\hat{H}|\Phi_i^a\rangle + \sum_{i<j}^{occ}\sum_{a<b}^{vir}(t_{ij}^{ab} + t_i^at_j^b - t_i^bt_j^a)\langle\Phi_0|\hat{H}|\Phi_{ij}^{ab}\rangle \quad , \end{aligned} \tag{2.35}$$

and the first matrix elements are zero (Brillouins theorem) and the second matrix elements are just two-electron integrals over molecular orbitals. The energy can be written

as,

$$E = E_0 + \sum_{i<j}^{occ} \sum_{a<b}^{vir} (t_{ij}^{ab} + t_i^a t_j^b - t_i^b t_j^a)(\langle \phi_i \phi_j | \phi_a \phi_b \rangle - \langle \phi_i \phi_j | \phi_b \phi_a \rangle) \quad . \tag{2.36}$$

The above equation is the expression of the energy obtained from CCSD, with the coefficients of single and double excitation generally obtained iteratively. Once these coefficients are known, the energy and wave functions can be calculated.

CCSD calculations are already very expensive, scaling as $N^6$ where $N$ is the number of basis functions in the calculation, and to go beyond CCSD makes the calculations extremely demanding. For example, CCSDT which iteratively treats the third-order excitations, scales as $N^8$ which makes it practically unfeasible for anything but the smallest of systems. To avoid this demanding scaling, the triple excitations can be obtained in a perturbative manner, with an approach widely known as CCSD(T) [81]. Starting from the energy at the CCSD level and following the procedure outlined in Eq. (2.18), the triple excitation energy can be expressed as [82]

$$E_{\mathrm{CCSD}}^{\mathrm{T}} = \sum_{i<j<k}^{occ} \sum_{a<b<c}^{vir} \frac{\langle \Phi_0 | (1 + \Lambda_1 + \Lambda_2) \bar{H}_{\mathrm{CCSD}} | \Phi_{ijk}^{abc} \rangle}{\epsilon_i + \epsilon_j + \epsilon_k + \epsilon_a - \epsilon_b - \epsilon_c} \quad , \tag{2.37}$$

where $\bar{H}_{\mathrm{CCSD}} = e^{-(T_1+T_2)} \hat{H} e^{(T_1+T_2)}$ and $\Lambda$ is the deexcitation operator and expressed in second quantization as,

$$\begin{aligned} \Lambda_1 &= \sum_{i,a} \lambda_a^i \; i^\dagger \, a \\ \Lambda_2 &= \frac{1}{4} \sum_{i,j,a,b} \lambda_{ab}^{ij} \; i^\dagger \, a \, j^\dagger \, b \quad , \end{aligned} \tag{2.38}$$

where $i^\dagger$, $j^\dagger$ are *creation* operators and $a$, $b$ are *annihilation* operators. CCSD(T) is often considered as the "gold standard" method of quantum chemistry due to its very high accuracy. For example, CCSD(T) predicts the binding energy of the water dimer to be 217.6 meV [83] which is in a good agreement with the experimental value of 216.8 meV [84]. In general, the results from CCSD(T) calculations are often used to benchmark other theoretical methods like MP2 and DFT [85, 86].

## 2.3. Density-Functional Theory

Density-functional theory (DFT) differs from the wave function based methods by using the electron density $n(\mathbf{r})$ as the central quantity. An important advantage of using the electron density over the wave function is the much reduced dimensionality. Regardless of how many electrons one has in the system, the density is always 3 dimensional. This enables DFT to readily be applied to much larger systems, hundreds or even thousands of atoms become possible. Partly for this reason, DFT has become the most widely

used electronic structure approach today, particularly in the condensed matter physics community. In this section, a basic introduction to DFT will be given. Authoritative and comprehensive discussions of DFT can be found in a range of excellent review articles [87–90] and textbooks [91, 92].

First, the electron density is defined as

$$n(\mathbf{r}) \quad = \quad N \int \cdots \int |\Psi(\mathbf{x}_1, \mathbf{x}_2, \ldots, \mathbf{x}_N)|^2 d\sigma_1 d\mathbf{x}_2 \cdots d\mathbf{x}_N \tag{2.39}$$

where $\{\mathbf{x}_i\}$ represents both spatial and spin coordinates. $n(\mathbf{r})$ determines the probability of finding any of the $N$ electrons within the volume $\mathbf{r}$ but with arbitrary spin while the other $N$-1 electrons have arbitrary positions and spin in the state represented by $\Psi$. This is a nonnegative simple function of three variables, $x$, $y$, and $z$, integrating to the total number of electrons,

$$N = \int n(\mathbf{r})\, d\mathbf{r} \tag{2.40}$$

### 2.3.1. Thomas-Fermi Model

That the electronic energy can be expressed in terms of the electronic density was first exploited back in 1920s by Thomas and Fermi [93, 94]. In Thomas-Fermi model, the kinetic energy of the electrons is derived from the quantum statistical theory based on the uniform electron gas, but the electron-nucleus and electron-electron interactions are treated classically. Within this model, the kinetic energy of the electrons is defined as,

$$T[n] = C_F \int n^{5/3}(\mathbf{r})\, d\mathbf{r} \quad \text{, with } C_F = \frac{3}{10}(2\pi^2)^{2/3} = 2.871 \quad . \tag{2.41}$$

From the above equation, the approximation is made that the kinetic energy of the electrons depends exclusively on the electron density. By adding the interaction between electron-nucleus and electron-electron, a total energy in terms of electron density is obtained,

$$E[n] = C_F \int n^{5/3}(\mathbf{r})\, d\mathbf{r} - Z \int \frac{n(\mathbf{r})}{r}\, d\mathbf{r} + \frac{1}{2} \int \int \frac{n(\mathbf{r}_1) n(\mathbf{r}_2)}{|\mathbf{r}_1 - \mathbf{r}_2|}\, d\mathbf{r}_1\, d\mathbf{r}_2 \tag{2.42}$$

The second and third terms are the electron-nucleus and electron-electron interactions, respectively.

The importance of this simple Thomas-Fermi model is not how well it performs in computing the ground state energy and density but more as an illustration that the energy can be determined purely using the electron density.

### 2.3.2. Hohenberg-Kohn Theorem

In 1964, Hohenberg and Kohn first derived the fundamentals of density-functional theory which allows to express electronic Hamiltonian as a functional of $n(\mathbf{r})$ [95][4]. This formally

[4] Also this was realized much earlier through Hellmann-Feynman theorem [96, 97].

relies on two key theorems: (i) there exists a on-to-one correspondence between external potential $v(\mathbf{r})$ and electron density $n(\mathbf{r})$; and (ii) the ground state electron density can be found by using a variational principle.

In the electronic Hamiltonian only $v(\mathbf{r})$ depends explicitly on the configuration of the nuclei. If the first theorem is proven, then from $n(\mathbf{r})$ one can obtain $v(\mathbf{r})$ within a trivial additive constant and the whole electronic Hamiltonian can be expressed as a functional of $n(\mathbf{r})$. This makes DFT a formal theory and more systematic over Thomas-Fermi model. The proof is done in a simple and extremely elegant manner using the principle of *reductio ad absurdum*, and this is derived for a non-degenerate system[5]. Suppose there is a collection of electrons enclosed into a box influenced by an external potential $v(\mathbf{r})$. Assuming the electron density of this system is known and it also determines $v(\mathbf{r})$ and thus all properties. If there is another external potential $v'(\mathbf{r})$ which differs from $v(\mathbf{r})$ by more than a constant that can also give the same electron density $n(\mathbf{r})$ for the ground state, then we will have two different Hamiltonians $\hat{H}$ and $\hat{H}'$ whose ground state electron density is the same but the normalized wave function $\Psi$ and $\Psi'$ would be different. Then we will have

$$\begin{aligned} E_0 < \langle \Psi' | \hat{H} | \Psi' \rangle &= \langle \Psi' | \hat{H}' | \Psi' \rangle + \langle \Psi' | \hat{H} - \hat{H}' | \Psi' \rangle \\ &= E_0' + \int n(\mathbf{r})[v(\mathbf{r}) - v'(\mathbf{r})]\, d\mathbf{r} \end{aligned} \tag{2.43}$$

where $E_0$ and $E_0'$ are the ground-state energies for $\hat{H}$ and $\hat{H}'$, respectively. Similarly, we can get

$$\begin{aligned} E_0' < \langle \Psi | \hat{H}' | \Psi \rangle &= \langle \Psi | \hat{H}' | \Psi \rangle + \langle \Psi | \hat{H}' - \hat{H} | \Psi \rangle \\ &= E_0 - \int n(\mathbf{r})[v(\mathbf{r}) - v'(\mathbf{r})]\, d\mathbf{r} \end{aligned} \tag{2.44}$$

Adding Eq. (2.43) and Eq. (2.44) we get, $E_0 + E_0' < E_0' + E_0$, which is an obvious contradiction. So there are no two different external potentials that can give the same $n(\mathbf{r})$. Thus $n(\mathbf{r})$ uniquely determines $v(\mathbf{r})$ (to within a constant) and all ground-state properties.

Now for a given $v(\mathbf{r})$ we can write the energy $E_v$ explicitly as a function of the electron density $n(\mathbf{r})$:

$$\begin{aligned} E_v[n] &= T[n] + V_{ne}[n] + V_{ee}[n] \\ &= \int n(\mathbf{r}) v(\mathbf{r})\, d\mathbf{r} + F_{HK}[n] \quad , \end{aligned} \tag{2.45}$$

where

$$F_{HK}[n] = T[n] + V_{ee}[n] \tag{2.46}$$

Here note that $F_{HK}[n]$ is only dependent on $n(\mathbf{r})$ and independent from any external potential $v(\mathbf{r})$. Thus $F_{HK}[n]$ is a universal functional of $n(\mathbf{r})$.

[5]For degenerate systems see the article from M. Levy, Phys. Rev. A **26**, 1200 (1982).

The second Hohenberg-Kohn theorem demonstrates that the ground state energy can be obtained variationally, with the density that minimizes the total energy being the exact ground state density. This is expressed as:

$$E_0[n_0] \leq E_v[n] \tag{2.47}$$

Following from the first part of the theorem, suppose the ground state wave function is $\Psi$ and its related electron density is $n(\mathbf{r})$. Thus the $n(\mathbf{r})$ uniquely determines the external potential $v(\mathbf{r})$. If there is another wave function $\Psi'$ with a arbitrary variation from $\Psi$ and its electron density is $n'(\mathbf{r})$, then we can obtain,

$$\langle \Psi' | \hat{H} | \Psi' \rangle = \int n'(\mathbf{r}) v(\mathbf{r})\, d\mathbf{r} + F_{HK}[n'] = E[n'] \geq E[n] \tag{2.48}$$

So the energy will reach the minimum only when the electron density is the ground-state electron density.

If $F_{HK}[n]$ were a known and sufficiently simple functional of $n(\mathbf{r})$, the problem of determining the ground-state energy and density in a given external potential would be rather easy since it requires merely minimization of a functional of the three-dimensional density function. However, it is not and the major part of the complexities of the many-electron problem are associated with the determination of the universal functional $F_{HK}[n]$.

### 2.3.3. The Kohn-Sham Equations

In 1965, Kohn and Sham published a paper which transformed density-functional theory into a practical electronic structure theory [98]. Kohn and Sham recognized that the failure of Thomas-Fermi theory mainly resulted from the bad description of the kinetic energy. To address this problem (similar to the Hartree-Fock approach) they re-introduced the idea of non-interacting electrons moving in an effective field.

The functional form of $F_{HK}[n(\mathbf{r})]$ is written as a sum of the kinetic energy of non-interacting electrons ($T_s$), the Hartree energy ($E^{\text{Hartree}}$), and all the many-body quantum effects are put together in to the exchange and correlation energy ($E_{xc}$). So the energy functional obtained in the previous section now becomes,

$$\begin{aligned} E[n] &= \int n(\mathbf{r}) v(\mathbf{r})\, d\mathbf{r} + F_{HK}[n(\mathbf{r})] \\ &= \int n(\mathbf{r}) v(\mathbf{r})\, d\mathbf{r} + T_s[n(\mathbf{r})] + E^{\text{Hartree}}[n(\mathbf{r})] + E_{xc}[n(\mathbf{r})] \quad . \end{aligned} \tag{2.49}$$

The next step in this electronic structure problem is to define an effective potential,

$$\begin{aligned} V^{\text{eff}} &= \frac{\delta\{\int n(\mathbf{r}) v(\mathbf{r})\, d\mathbf{r} + E^{\text{Hartree}}[n(\mathbf{r})] + E_{xc}[n(\mathbf{r})]\}}{\delta n(\mathbf{r})} \\ &= v(\mathbf{r}) + \int \frac{n(\mathbf{r}')}{|\mathbf{r} - \mathbf{r}'|}\, d\mathbf{r}' + v_{xc}(\mathbf{r}) \quad , \end{aligned} \tag{2.50}$$

where $v_{xc}(\mathbf{r})$ is the exchange-correlation potential defined as:

$$v_{xc}(\mathbf{r}) = \frac{\delta E_{xc}[n(\mathbf{r})]}{\delta n(\mathbf{r})} \quad . \tag{2.51}$$

This leads to the central equation in Kohn-Sham DFT which is the one-electron Schrödinger-like equation expressed as:

$$\Big[ -\frac{1}{2}\nabla^2 + V^{\text{eff}} \Big] \phi_i = \epsilon_i \phi_i \tag{2.52}$$

Here $\{\phi_i\}$ are the Kohn-Sham one-electron orbitals and the electron density is defined as,

$$n(\mathbf{r}) = \sum_{i=1}^{N} |\phi_i|^2 \quad . \tag{2.53}$$

The $\epsilon_i$'s are the energies of the Kohn-Sham one-electron orbitals. Clearly this is a Hartree-Fock-like single particle equation which needs to be solved iteratively. Finally, the total energy can be determined from the resulting density through

$$E = \sum_{i=1}^{N} \epsilon_i - \frac{1}{2} \int \int \frac{n(\mathbf{r}) n(\mathbf{r}')}{|\mathbf{r} - \mathbf{r}'|} + E_{xc}[n] - \int v_{xc}(r) n(\mathbf{r})\, d\mathbf{r} \tag{2.54}$$

Equations (2.50), (2.52), and (2.53) are the celebrated Kohn-Sham equations. Note that the $V^{\text{eff}}$ depends on $n(\mathbf{r})$ through Eq. (2.53). So the Kohn-Sham equation must be solved self-consistently. The general procedure is to begin with an initial guess of the electron density, construct the $V^{\text{eff}}$ from Eq. (2.50), and then get the Kohn-Sham orbitals. Based on these orbitals, a new density is obtained from Eq. (2.53) and the process repeated until convergence is achieved. Finally, the total energy will be calculated from Eq. (2.54) with the final electron density. If each term in the Kohn-Sham energy functional was known, we would be able to obtain the exact ground state density and total energy. Unfortunately, there is one unknown term, the exchange-correlation (xc) functional ($E_{xc}$). $E_{xc}$ includes the non-classical aspects of the electron-electron interaction along with the component of the kinetic energy of the real system different from the fictitious non-interacting system. Since $E_{xc}$ is not known exactly, it is necessary to approximate it, which is the focus of the next section.

### 2.3.4. Exchange-Correlation Functionals

For practical use of the Kohn-Sham equations we must know what the form of the exchange-correlation energy functional is. However, the exact form of $E_{xc}$ is not known and may never be known (in a closed mathematical form). Thus since the birth of DFT some sort of approximations for $E_{xc}$ have been used. By now there is an almost endless list of approximated functionals with varying levels of complexity. Rather recently

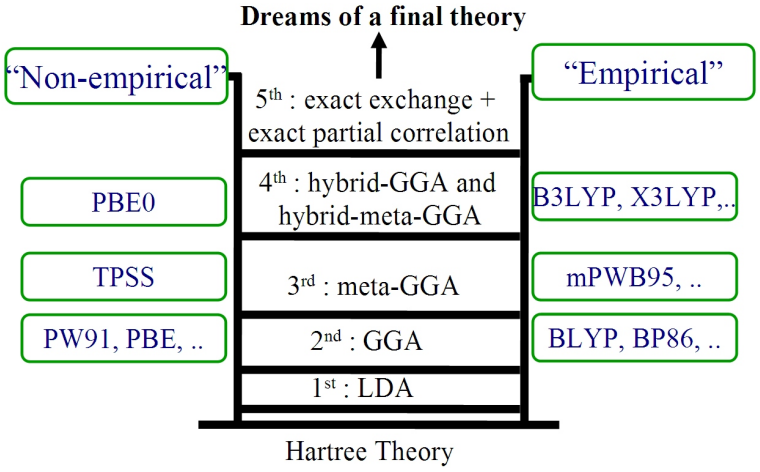


**Figure 2.2.:** Schematic diagram of "Jacob's ladder" of exchange-correlation functionals proposed by J. P. Perdew.

a useful way for categorizing the many and varied $E_{xc}$ functionals that exist has been proposed by Perdew and is known as "Jacob's ladder" (Fig. 2.2) [99]. In this scheme functionals are grouped according to their complexity on rungs of a ladder which lead from the Hartree approximation on "earth" to the exact exchange-correlation functional in "heaven". Furthermore, functionals can be categorized into *non-empirical* (formulated only by satisfying some physical rules) and *empirical* (made by fitting to the known results of atomic or molecular properties). The first few rungs of this ladder are now briefly discussed as a means to introduce some of the most common types of exchange-correlation functionals in widespread use (many of which have been tested in this thesis):

(a) The local-density approximation (LDA):

In this approach a real inhomogeneous system is divided into infinitesimal volumes, and the electron density in each of the volumes is taken to be constant. The exchange-correlation energy for the density within each volume is then assumed to be the exchange-correlation energy obtained from the uniform electron gas for that density. Thus, the total exchange-correlation energy of the system can be written as

$$E_{\mathrm{xc}}^{\mathrm{LDA}}[n] = \int n(\mathbf{r})\epsilon_{\mathrm{xc}}^{\mathrm{unif}}\left(n(\mathbf{r})\right)\, d\mathbf{r} \quad , \tag{2.55}$$

where $\epsilon_{\mathrm{xc}}^{\mathrm{unif}}$ is the exchange-correlation energy per particle of the interacting uniform electron gas of density $n(\mathbf{r})$. In practice, exchange and correlation are calculated separately.

The analytical expression for the exchange energy is known exactly[6]:

$$E_{\mathrm{x}}^{\mathrm{LDA}}[n] = -\frac{3}{4}\left(\frac{3}{\pi}\right)^{1/3}\int n^{4/3}(\mathbf{r})\,d\mathbf{r} \quad . \tag{2.56}$$

The correlation energy is more complicated and generally obtained by fitting to the many-body studies of Gell-Man and Brueckner and Ceperly and Alder [100, 101]. Modern LDA functionals tend to be exceedingly similar, differing only in how their correlation contributions have been fitted to the many-body free electron gas data. The Perdew-Zunger (PZ) [102], Perdew-Wang (PW) [103] and Vosko-Wilk-Nusair (VWN) [104] functionals are all common LDA functionals.

Strictly, the LDA is valid only for slowly varying densities. Experience with calculations of atoms, molecules, and solids shows that Eq. (2.55) can in general also be applied to these systems. Indeed LDA works surprisingly well, especially for metals. A partial explanation for this success of the LDA is systematic error cancelation: Typically, in inhomogeneous systems LDA underestimates correlation but overestimates exchange, resulting in unexpectedly good values of $E_{\mathrm{xc}}^{\mathrm{LDA}}$. This error cancelation is not accidental, but systematic, and caused by the fact that for any density the LDA satisfies a number of so-called sum rules [105–108].

However, recent studies have shown that LDA tends to overestimate cohesive energies by ∼15-20% and underestimates lattice constants by ∼2-3% for metals and insulators [109–111]. Problem with LDA becomes more severe for weakly bonded systems, such as vdW and H-bonded systems. For example, the binding energy of the water dimer and the cohesive energy of bulk ice are both >50% too large with LDA compared to the experimental values [40, 41, 57]. Also long range vdW interactions are completely missing in LDA. For this reason LDA has not been used in any of the work reported in this thesis.

(b) The generalised gradient approximation (GGA):

It was realized very early that only the local uniform density at each given point is not a reasonable approximation for the rapidly varying electron densities of many materials, and that the gradient of the density ($\nabla n(\mathbf{r})$) needs to be included. A first attempt was the so-called gradient-expansion approximations (GEA), where one tries to systematically calculate gradient corrections of the form $|\nabla n(\mathbf{r})|$, $|\nabla n(\mathbf{r})|^2$, $|\nabla^2 n(\mathbf{r})|$, etc., to the LDA. In practice, the inclusion of low-order gradient corrections almost never improves on the LDA, and often even worsens it [112]. Higher-order corrections are exceedingly difficult to calculate.

Eventually it was found that instead of power-series-like gradient expansions one could apply more general functions of $n(\mathbf{r})$ and $\nabla n(\mathbf{r})$. Such functionals, of the general form

$$E_{\mathrm{xc}}^{\mathrm{GGA}}[n] = \int f^{\mathrm{GGA}}\left(n(\mathbf{r}), \nabla n(\mathbf{r})\right)\,d\mathbf{r} \quad , \tag{2.57}$$

[6]Note that this definition differs from the average over the HF exchange energy.

are the second generation functionals (sitting on the second rung of Jacob's ladder) known as GGAs.

GGAs are often called "semi-local" functionals due to their dependence on $\nabla n(\mathbf{r})$. For many properties, for example geometries and ground state energies of molecules and solids, GGAs can yield better results than the LDAs. Especially for covalent bonds and weakly bonded systems many GGAs are far superior to LDA. Overall though because of flexibility in the choice of $f^{\mathrm{GGA}}$ a zoo of GGA functionals have been developed and depending on the system under study a wide variety of results can be obtained.

The functional form of $f^{\mathrm{GGA}}$ is taken as a correction to the LDA exchange and correlation while (again) ensuring consistency with known sum rules. Within GGA the exchange energy takes the form

$$E_{\mathrm{x}}^{\mathrm{GGA}}[n] = \int n(\mathbf{r})\epsilon_{\mathrm{x}}^{\mathrm{unif}}\left(n(\mathbf{r})\right)\, F_{\mathrm{x}}^{\mathrm{GGA}}(s)\, d\mathbf{r} \quad . \tag{2.58}$$

$F_{\mathrm{x}}^{\mathrm{GGA}}(s)$ is the exchange enhancement factor and tells how much exchange energy is enhanced over its LDA value for a given $n(\mathbf{r})$. The choice of $F_{\mathrm{x}}$ makes one GGA differ from another. Here $s$ is a dimensionless reduced gradient

$$s = \frac{|\nabla n(\mathbf{r})|}{2(3\pi^2)^{1/3} n(\mathbf{r})^{4/3}} \quad . \tag{2.59}$$

So as to illustrate what $F_{\mathrm{x}}(s)$ is like two very popular GGA exchange functionals applied in this thesis are now briefly discussed. They are Perdew-Burke-Ernzerhof (PBE [113]) and Becke88 (B88 [114]) functionals, which have the following forms:

$$F_{\mathrm{x}}^{\mathrm{PBE}}(s) = 1 + \kappa - \frac{\kappa}{(1 + \mu s^2/\kappa)} \tag{2.60}$$

$$F_{\mathrm{x}}^{\mathrm{B88}}(s) = 1 + \frac{\beta x(s)^2}{C\left[1 + 6\beta x(s)\, \sinh^{-1}(x(s))\right]} \quad , \quad x(s) = 2(6\pi^2)^{1/3} s \tag{2.61}$$

In PBE, $\kappa$ and $\mu$ are parameters obtained from physical constraints (non-empirical). In B88, $C$ and $\beta$ are parameters obtained from empirical fitting (empirical). When the density gradient is zero, $F_{\mathrm{x}}^{\mathrm{GGA}}(s) = 1$ and so we return to the LDA exchange. Fig. 2.3 shows the behavior of these two enhancement factors as a function of $s$. For slowly varying densities (small $s$) they coincide but differ when the density change is rapid (large $s$).

The functional form to the gradient corrected correlation energy ($E_c^{\mathrm{GGA}}$) is also expressed as complex function of $s$. A few of the most popular gradient corrected correlation functionals are PBE [113], PW91 [115] Lee-Yang-Parr (LYP [116]), and Perdew86 (P86 [117]). Usually LYP and P86 correlation are applied together with B88 exchange. GGAs are always necessary for a reasonable description of HBs [118–120] and some of the popular GGAs for treating HBs are PBE, BLYP, PW91, BP86, etc.

(c) *The meta-GGAs*:

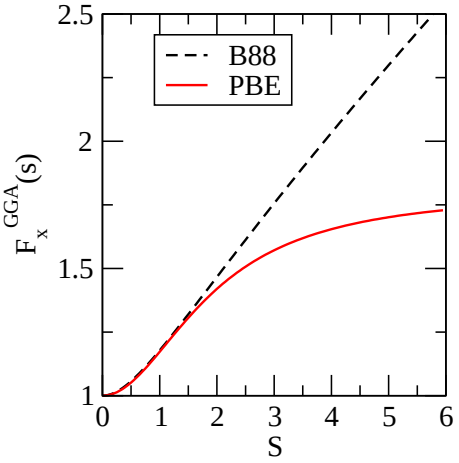


**Figure 2.3.:** GGA enhancement factors of PBE [113] and B88 [114] exhange funtionals.

These are the third generation functionals (third rung of Jacob's ladder) and use the second derivative of the density, $\nabla^2 n(\mathbf{r})$, and/or kinetic energy densities, $\tau_\sigma(n) = 1/2\Sigma_i|\nabla\varphi_i(n)|^2$, as additional degrees of freedom. In gas phase studies of molecular properties meta-GGAs such as the TPSS [121] functional have been shown to offer improved performance over LDAs and GGAs [110, 122–124].

(d) The hybrid functionals:

These fourth generation functionals add "exact exchange" calculated from the HF functional to some conventional treatment of DFT exchange and correlation. The philosophy behind the hybrid functional is simple and rooted in the "adiabatic connection" formula, which is a rigorous *ab initio* formula for the exchange-correlation energy of DFT [125]. One conventional expression of this formula is:

$$E_{xc} = \int_0^1 U_{xc}^\lambda d\lambda \quad , \tag{2.62}$$

where $\lambda$ is an interelectronic coupling strength parameter that switches on the $\frac{1}{|\mathbf{r}_i - \mathbf{r}_j|}$ Coulomb repulsion between electrons and $U_{xc}^\lambda$ is the potential energy of exchange and correlation at $\lambda$. This formula connects the non-interacting reference system with the fully interacting one at density $n(\mathbf{r})$. Recognizing that the non-interacting $\lambda = 0$ limit is nothing more than HF exchange, it is expected that exact exchange must play a role in "better" of exchange-correlation functionals and thus LDA and GGA exchange and correlation functionals are mixed with a fraction of HF exchange.

The most widely used, particularly in the quantum chemistry community, is the B3LYP [126–128] functional which employs three parameters, $a_{1-3}$ (determined through fitting to experiment) to control the mixing of the HF exchange and density functional

exchange and correlation. It has the following form:

$$E_{\mathrm{xc}} = E_{\mathrm{xc}}^{\mathrm{LDA}} + a_1(E_{\mathrm{x}}^{\mathrm{HF}} - E_{\mathrm{x}}^{\mathrm{LDA}}) + a_2\Delta E_{\mathrm{x}}^{\mathrm{GGA}} + a_3\Delta E_{\mathrm{c}}^{\mathrm{GGA}} \quad . \tag{2.63}$$

Here B88 and LYP are used as GGA exchange and correlation. Reformulating this to eliminate two parameters leads to an equation of the form

$$E_{\mathrm{xc}} = E_{\mathrm{x}}^{\mathrm{GGA}} + a(E_{\mathrm{x}}^{\mathrm{HF}} - E_{\mathrm{x}}^{\mathrm{GGA}}) \tag{2.64}$$

and setting $a$=1/4 (based on the grounds of perturbation theory [68]) leads to a class of functionals with only as many parameters as their underlying GGAs. If PBE is the GGA used in Eq. (2.64) we arrive at the hybrid PBE0 functional [129]. Another popular hybrid functional worth mentioning here is BH&HLYP [125], which has 50% HF exchange. Such functionals have been shown to offer noticeably improved performance over LDA and GGA functionals for the calculation of gas phase properties of molecules and solids [123, 124, 130–132].

In the fourth rung another class of functionals exists and they are known as hybrid meta-GGA functionals. As the name suggests it is combination of meta-GGA and hybrid functionals with suitable parameters fitted to various molecular databases. Among many, MPWB1K [133] and PW6B95 [124] have been used in this thesis.

Beyond these few rungs of Jacob's ladder, there are other $xc$ functionals of increasing complexity. However, adding complexity by climbing higher on Jacob's ladder or by obeying more and more constraints [109] does not necessarily bring improved performance in total energies. This will become more apparent in chapter 3, where it is shown that H-bond energies do not necessarily improve upon going from GGAs to meta-GGAs to hybrids and beyond.

With growing number of $xc$ functionals (and their acronyms) tailored to improve molecular or solid state properties it is difficult to remember which functional is good for what. In the following chapters more than 10 different functionals are used and brief descriptions of those are summarized in Table 2.2.

## 2.4. Basis Sets

In this section, the concept of the basis set will be introduced. Basis sets are almost always necessary to practically solve the electronic Schrödinger equation. Essentially, almost all electronic structure methods today rely on an expansion on the unknown wave function in terms of a set of basis functions. Any type of basis function may in principle be used like exponential, Gaussian, polynomial, plane-wave, spline, Slater type orbitals, and numeric atomic orbitals, etc. However, some issues are useful to consider when selecting basis functions:

- The basis functions should allow for the wave function/density to be accurately described with as low a computational cost as possible.

- The behavior of the basis functions will ideally capture some of the physics of the problem. For example, for bound atomic or molecular systems this means functions should go to zero when the distance between the nucleus and the electron becomes large. Or in a condensed matter system basis functions with a periodicity matching the crystal lattice can be useful.

For these and other reasons atom centered orbitals like Gaussian functions have become very popular in the calculations of chemical problems. Gaussian orbital basis sets have been used in this thesis and also numeric atom-centered basis sets. These basis sets will be now discussed and later plane wave basis sets will be introduced, which are very popular for electronic structure calculations of condensed matter systems.

### 2.4.1. Atom Centered Localized Basis sets

Two most popular atom centered localized basis sets have been employed in the thesis and those are briefly discussed in the following.

#### I. Gaussian Functions

Early in quantum chemistry, Slater type orbitals (STO) were used as basis functions because of their similarity with the solutions of the hydrogen atom. The Slater type orbitals have the form in spherical coordinates,

$$\phi_i(\zeta, n, l, m, r, \theta, \varphi) = N r^{n-1} e^{-\zeta r} Y_{lm}(\theta\varphi) \quad , \tag{2.65}$$

where $N$ is the normalization constant, and $Y_{lm}$ are the spherical harmonic functions. $n$, $l$, and $m$ are the quantum numbers: principal, angular momentum, magnetic, respectively. $\zeta$ is called the "exponent". The exponential dependence on distance reflects the exact form of the hydrogenic orbitals. However, the calculation of the three- and four-center two-electron integrals with Slater orbitals is extremely slow and has no analytical form. Thus in modern quantum chemistry calculations, the Slater orbitals are generally restricted to atomic and diatomic systems.

In contrast, it is much faster to work with Gaussian functions in the evaluation of the two-electron integrals than STO functions. Thus for this pragmatic reason, Gaussian functions have become the most popular basis functions in quantum chemistry. Numerous quantum chemistry codes employ Gaussian functions as basis sets. The Gaussian function type orbital (GTO) has the following form in Cartesian coordinates:

$$g(\zeta, l_x, l_y, l_z, x, y, z) = N e^{-\zeta r^2} x^{l_x} y^{l_y} z^{l_z} \quad . \tag{2.66}$$

Note that the $l_x$, $l_y$, $l_z$ in Cartesian coordinates are not the quantum numbers but instead parameters. However, the sum of them, $L = l_x + l_y + l_z$ is analogous to the angular momentum for atoms, to mark function as s-type ($L = 0$), p-type ($L = 1$), d-type ($L = 2$), and f -type ($L = 3$), etc. The Gaussian function described in Eq. (2.66) is generally known as a primitive Gaussian function. It is very common to group several

primitive Gaussian functions into one Gaussian function and this new Gaussian function is known as a contracted Gaussian function,

$$g(c) = \sum_i a_i g_i(p) \quad , \tag{2.67}$$

where $c$ and $p$ designate contracted and primitive, respectively. By contracting, several primitive Gaussians into one, the computational effort can be reduced through the optimization of several coefficients in one go. When using Gaussian function basis sets it is far from trivial to decide what set of (contracted) Gaussian functions are appropriate for the system under investigation. Generally some experience is required. However, the minimum basis set which must be used corresponds to the number of atomic orbitals in the system. For example, the minimum basis set for hydrogen is just a single s-function. For the first row elements in the periodic table, this means two s-functions and one set of p-functions ($2p_x$, $2p_y$, $2p_z$). For almost all practical problems the minimum basis set description is inadequate. The next improvement is to double all the basis functions (but with different exponent $\zeta$) which produce the double zeta (DZ) type basis. For hydrogen, a DZ basis set will use two s-functions ($1s$, $1s'$). For the first row elements in the periodic table, this means four s-function ($1s$, $1s'$, $2s$, $2s'$) and two sets of $p$-functions ($2p$, $2p'$). When the basis set has three sets of basis functions for each orbital, you will get the tripe zeta (TZ) basis and so on. As we will see below, it is common to make a distinction between core and valence electrons, with more sets of basis functions (larger zeta) allocated to the valence electrons compared to the core electrons.

Further improvements can be achieved by adding so-called polarization or diffuse functions. Although a free isolated atom will have spherical symmetry, the atoms in a molecule or some other chemical environment will exhibit some distortions in their electron density. To take account of this effect through the basis set, we need to augment basis sets with additional functions of larger angular momentum. For example, hydrogen will be augmented by adding a $p$ orbital into its minimum basis set. In a similar spirit, so-called diffuse functions are sometimes also included in the basis set. The purpose of adding diffuse functions is to improve the description at large distances from the nuclei. This is especially important for anions as the additional electrons are loosely bound to nuclei. In general, diffuse functions have a very small exponent, $\zeta$, typically from 0.01 to 0.1, so it will extend far from the nucleus.

### Pople and Dunning Basis Sets

Many and various Gaussian basis sets exist. Here we focus on the two different classes of Gaussian basis sets used in this thesis: Pople style basis sets and the correlation consistent basis sets of Dunning and co-workers [134–136]. For the Pople style basis sets, it is better to take an example to explain the meaning of the notation. For example, a 6-31G basis set is a double split valence basis set. This notation means that the core orbitals are described by one contracted Gaussian function comprised of six primitive Gaussians. The valence orbital has been split into two contracted Gaussians, one comprised of three primitive Gaussians and the other just one primitive Gaussian. As another example a

6-311G basis set is a triple split valence basis set. The core orbital is still a contraction of six primitive Gaussians. However the valence is now split into three parts which are contractions of three, one, and one primitive Gaussians, respectively.

Normally, the basis sets are obtained from the HF atomic calculations [137]. When coming to molecular calculations, the basis functions are augmented with polarization functions accounting for the distortion from the atomic state in the molecular environment. However, there is not a clear way to achieve systematic improvements with increasing number of basis functions. Thus the convergence is not easy to guarantee and the choice of the basis set is sometimes drawn from the researcher's own experience. In contrast, the correlation consistent basis sets, from Dunning's group, are designed to systematically recover the correlation energy with the increasing size of the basis sets. The name "correlation consistent" refers to the fact that the basis sets are designed so that the functions which contribute similar amount of correlation energy are included at the same stage, independent of the function type. For example, the contributions from $2d$ and $1f$ function are similar, so they belong to the same group and will be added together. By this way, Dunning proposed a series of correlation consistent basis sets, cc-pVDZ ($3s2p1d$), cc-pVTZ ($4s3p2d1f$), cc-pVQZ ($5s4p3d2f1g$), and cc-pV5Z ($6s5p4d3f2g1h$) where the number of contracted Gaussian functions are indicated in brackets. These basis sets can also be augmented with additional diffuse functions, which have smaller exponents for every angular momentum channel. This is denoted by the new prefix "aug" and their inclusion is crucial for describing weakly bound systems. As the key feature of the correlation consistent basis set is to systematically improve with basis set size, there are several different ways to extrapolate the results to the CBS limit, which will be discussed below.

### II. Numerical Atom-Centered Basis Sets

Another type of atom centered basis set employed in this thesis is the numeric atom-centered orbitals (NAO). NAOs have the following functional form:

$$\phi_i(\mathbf{r}) = \frac{u_i(r)}{r} Y_{lm}(\theta\varphi) \quad , \tag{2.68}$$

where $Y_{lm}$ are spherical harmonics and the radial function $u_i(r)$ is numerically tabulated and fully flexible to achieve any desired shape. As with GTOs, $u_i(r)$ is taken as localized function but the choice of the functional form depends on the researcher's experience. Here, in particular we describe the functional form implemented in the FHI-aims [138] computer code. $u_i(r)$ is taken from the solution of the Schrödinger-like equation:

$$\Big[ -\frac{1}{2}\frac{d^2}{dr^2} + \frac{l(l+1)}{r^2} + v_i(r) + v_{cut}(r) \Big] \phi_i = \epsilon_i \phi_i \tag{2.69}$$

$v_i(r)$ is the potential which defines the main behavior of $u_i(r)$ and $v_{cut}(r)$ is a steeply increasing confining potential, which ensures a smooth decay of each radial function to be strictly zero outside a confining radius. For each species the *minimal* basis consists of a number of atomic orbitals, constructed by choosing $v_i(r)$ as the corresponding

self-consistent free-atom radial potential. Like GTOs the *minimal* basis are further augmented with higher angular momentum polarization functions, which are suitably chosen from various hydrogen-like, cation-like, or atom-like radial functions with a variable confinement potential $v_{cut}(r)$. The polarization basis functions typically arise in groups of different angular momenta, *spd* or *spdf*, and are thus organized in so-called *tiers*. The number of the *tier* thereby denotes the accuracy of the basis set. The different basis sets used in the present work are given in detail in Appendix B.

### Basis Set Superposition Error

Localized basis functions, such as GTOs or NAOs, are prone to a problem known as basis set superposition error (BSSE) [139]. When two fragments $A$ and $B$ approach each other to form the new species, fragment $A$ feels the basis functions of fragment $B$ and fragment $B$ also feels the basis functions of fragment $A$. Effectively each fragment feels a larger basis set than what it has as an isolated fragment and in so doing artificially stabilizing the cluster. One widely used method to assess the BSSE is the Counterpoise correction scheme of Boys and Bernardi [140]. To illustrate how this method works, consider the binding energy of the dimer ($AB$). The binding energy ($E_{\text{bind}}$) can be expressed as,

$$E_{\text{bind}} = E(AB)_{ab} - E(A)_a - E(B)_b \tag{2.70}$$

where $E(AB)_{ab}$, $E(A)_a$, and $E(B)_b$ are the energy of $AB$, monomer $A$, and monomer $B$, respectively. The subscript indicates the corresponding basis set for $AB$, $A$, and $B$. Because of the incompleteness of the basis set for A and B, there exists a BSSE in $E_{\text{bind}}$. When using the Counterpoise method, the BSSE can be evaluated with,

$$\Delta E_{\text{BSSE}} = E(\tilde{A})_{ab} + E(\tilde{B})_{ab} - E(\tilde{A})_a - E(\tilde{B})_b \tag{2.71}$$

where $E(\tilde{A})_{ab}$ and $E(\tilde{A})_{ab}$, respectively represents the energy of monomer $A$ and $B$ in the structure it adopts in the dimer ($AB$) and with the full basis set of the dimer available. $E(\tilde{A})_a$ and $E(\tilde{A})_b$ are then the energies of A and B, respectively, with only their own basis functions but again in the structure they adopt in the dimer. Thus Eq. (2.71) gives the difference between the energies of each fragment with the corresponding monomer and the full dimer basis sets. Obviously, the artificial enhancements each monomer gains in the dimer can be established and eliminated if desired by obtaining a corrected binding energy: $E_{\text{bind}} - \Delta E_{\text{BSSE}}$.

If high accuracy is desired, BSSE should be removed. However, removal of BSSE is not sufficient to guarantee high accuracy in, e.g., binding energies because of the incompleteness of the basis sets. Fortunately, there are well established extrapolation schemes that can alleviate basis set incompleteness errors, which will be introduced in the following section.

### Extrapolation to the Complete Basis Set Limit

As we have emphasized, one particular feature of Dunning's correlation consistent basis sets is that they systematically allow the correlation energy to be improved with increasing basis set size. This systematic convergence provides opportunities to extrapolate

to the CBS, which could remove the errors from the incompleteness of the basis set. Quite often the first step of the extrapolation is to separate the extrapolation of the Hartree-Fock energy and the electron correlation energy [141].

Many extrapolation schemes have been developed for obtaining estimated CBS energy with Dunning's basis sets [135, 141–144]. For the extrapolation of the Hartree-Fock energy, the extrapolation is mostly done with expressions like,

$$E^{\mathrm{HF}}(X) = E^{\mathrm{HF}}_{\mathrm{CBS}} + Ae^{-BX} \quad , \tag{2.72}$$

where $X$ is the highest angular momentum quantum number in a basis set, i.e., 2 for aug-cc-pVDZ, 3 for aug-cc-pVTZ, 4 for aug-cc-pVQZ, 5 for aug-cc-pV5Z, etc. $E^{\mathrm{HF}}_X$ is the corresponding HF energy and $E^{\mathrm{HF}}_{\mathrm{CBS}}$ CBS is the HF energy at the CBS. $A$ and $B$ are the fitting parameters. For electron correlation extrapolation, there are yet more options. For example, one of the popular three-parameter extrapolations schemes is,

$$E^{\mathrm{corr}}(X) = E^{\mathrm{corr}}_{\mathrm{CBS}} + \frac{C}{X^3} + \frac{D}{X^5} \tag{2.73}$$

where $E^{\mathrm{corr}}_X$ is the corresponding electron correlation energy for a given cardinal number $(X)$ and $E^{\mathrm{corr}}_{\mathrm{CBS}}$ is the electron correlation energy at the CBS. $C$ and $D$ are again the fitting parameters.

Later in this thesis extrapolation methods are used. To illustrate how the extrapolation schemes work the variation of the HF energy and electron correlation energy of a water molecule is shown in Fig. 2.4. The energy of a single molecule has been calculated with aug-cc-pVTZ, aug-cc-pVQZ, and aug-cc-pV5Z basis sets and the extrapolations were done for the HF energy and correlation energy by using Eq. (2.72) and Eq. (2.73), respectively. Two features of Fig. 2.4 are apparent and worth very briefly commenting upon. First, $E^{\mathrm{HF}}$ and $E^{\mathrm{corr}}$ exhibit uniform convergence to the CBS limit upon increasing basis set size. Second, the variation in $E^{\mathrm{HF}}$ with basis set size in considerably (about 3 times) smaller than $E^{\mathrm{corr}}$ and $E^{\mathrm{HF}}$ is much faster in approaching the CBS limit than $E^{\mathrm{corr}}$.

### 2.4.2. Plane Waves

The majority of the calculations in this thesis are performed with atom centered localized basis sets. However, some calculations (in chapter 5) for periodic systems are carried out with plane wave basis sets and pseudopotentials. Also the approach of combining plane wave basis sets and pseudopotentials is the workhorse of the present day DFT calculations for periodic systems, so, such methods are briefly described here.

For the treatment of periodic systems, like solids, plane wave basis sets have become the natural choice because of Bloch's theorem. In a periodic potential, $U(\mathbf{r})$, where $U(\mathbf{r}+\mathbf{R}) = \mathbf{U}(\mathbf{r})$ and $\mathbf{R}$ is the Bravais lattice vector, Bloch's theorem says that the eigenfunctions of the one-electron Hamiltonian $H = -\frac{1}{2}\nabla^2 + U(\mathbf{r})$ can be written as a product of a plane wave ($e^{i\mathbf{k}\cdot\mathbf{r}}$) and a function, $\mu_{n,k}(\mathbf{r})$, having the same periodicity as the potential $U(\mathbf{r})$ :

$$\phi_{n,k}(\mathbf{r}) = e^{i\mathbf{k}\cdot\mathbf{r}}\mu_{n,k}(\mathbf{r}) \quad , \tag{2.74}$$

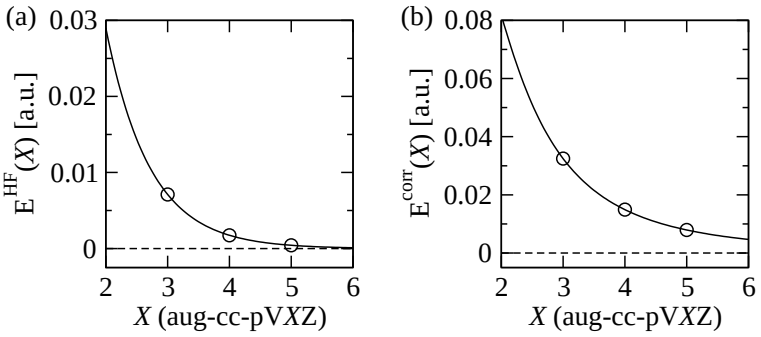


**Figure 2.4.:** Extrapolation of (a) the Hartree-Fock energy ($E^{\mathrm{HF}}(X)$) and (b) electron correlation energy ($E^{\mathrm{corr}}(X)$) of a water molecule using Eq. (2.72) and Eq. (2.73), respectively. The electron correlation calculations are done at the MP2 level. The energy zero in both plots is the extrapolated CBS limit.

where $\mu_{n,k}(\mathbf{r}+\mathbf{R}) = \mu_{n,k}(\mathbf{r})$. Here the index $k$ represents a set of plane waves within each primitive unit cell and for each $k$ the index $n$ is a second quantum number, the so called "band index".

Bloch's theorem allows to expand the electronic wave function in terms of a discrete set of plane waves. But for a periodic solid which has electrons in the order of Avogadro's number the spacing of the **k** points goes to zero and **k** can be considered as a continuous variable. So far the infinite number of electrons in the solid are accounted for by an infinite number of **k** points, and only a finite number of electronic states are occupied at each **k** point. The occupied states at each **k** point contribute to physical quantities such as the electronic potential, electron density, and total energy of the solid. However, the electronic wave functions at **k** points that are very close together will be almost identical. Hence it is possible to represent them over a region of **k** space only by that at a single **k** point. Efficient methods have been devised to choose special finite sets of **k** points, for obtaining an accurate electronic potential, electron density, and total energy. In this thesis, the method proposed by Monkhorst and Pack [145] has been used, in which a uniform mesh of **k** points is generated along the three lattice vectors in reciprocal space. The magnitude of any error in the total energy or the total energy difference due to inadequacy of the **k** point sampling can always be reduced to zero by using a denser set of **k** points. Therefore, it is crucial to test the convergence of the results with respect to the number of **k** points in general.

Now expanding the periodic function $\mu_{n,k}(\mathbf{r})$ with plane waves whose wave vectors are reciprocal lattice vectors (**G**) of the periodic crystal:

$$\mu_{n,k}(\mathbf{r}) = \sum_{\mathbf{G}} C_{n,\mathbf{G}}\, e^{i\mathbf{G}\cdot\mathbf{r}} \quad , \tag{2.75}$$

so the electronic wave function can be rewritten as

$$\phi_{n,k}(\mathbf{r}) = \sum_{\mathbf{G}} C_{n,\mathbf{k}+\mathbf{G}}\, e^{i(\mathbf{k}+\mathbf{G})\cdot\mathbf{r}} \quad . \tag{2.76}$$

While solving one electron Schrödinger-like equation with an effective periodic potential, e.g., the Kohn-Sham potential defined in Eq. (2.50), Kohn-Sham wave function can be expanded with plane wave basis sets as described in Eq. (2.76). As a result Eq. (2.52) can be rewritten as

$$\sum_{\mathbf{G}'} \Big[\frac{1}{2}|\mathbf{k}+\mathbf{G}'|^2\delta_{\mathbf{G},\mathbf{G}'} + V^{\text{eff}}(\mathbf{G}-\mathbf{G}')\Big] C_{n,\mathbf{k}+\mathbf{G}'} = \epsilon_n \, C_{n,\mathbf{k}+\mathbf{G}} \quad , \tag{2.77}$$

where $\delta_{\mathbf{G},\mathbf{G}'}$ is the Kronecker $\delta$ and reflects that the kinetic energy is diagonal and $\epsilon_n$ are the electronic energies. The above equation is the basic Schrödinger-like equations of a periodic crystal with a plane wave basis set.

Here the sum over $\mathbf{G}'$ tells that one needs an infinite number of plane waves to solve Eq. (2.77). However, the coefficient $C_{n,\mathbf{k}+\mathbf{G}}$ for the plane waves with small kinetic energy are typically more important than those with large kinetic energy. Thus the plane wave basis set can be truncated to include only plane waves that have kinetic energies less than a particular energy cutoff $E_{cut}$,

$$\frac{1}{2}|\mathbf{k}+\mathbf{G}|^2 \leq E_{cut} \quad . \tag{2.78}$$

Employing a finite basis set introduces a new source of inaccuracy, which can be reduced by increasing the number of plane waves or $E_{cut}$. Therefore, appropriate convergence tests have to be performed in order to find an $E_{cut}$ that is sufficiently converged to compute the property of interest with the required accuracy.

## 2.5. Pseudopotentials

It is well established that most physically interesting properties of solids are largely determined by the valence electrons rather than the core electrons. Meanwhile, the deeply bound core electrons within plane-wave basis sets, require a huge amount of basis functions for their description. Thus this leads to a contradiction that the less important core electrons will consume a lot of the computational cost. To alleviate this problem, the pseudopotential approximation replaces the strong ionic potential with a weaker pseudopotential. In general, there are two main purposes of the pseudopotential formalism. First, to use a much weaker pseudopotential to get rid of core electrons which due to their deep potential would need to be described by many plane-wave basis functions. Second, to eliminate the rapid oscillations of the valence electron wave functions in the core region. These issues are shown in Fig. 2.5(a), where it can be seen that the pseudopoential is much weaker than the all-electron one and that the pseudo wave function has no radial node inside the core region. It is essential within the pseudopotential scheme that outside the core region, the pseudo potential and wave function becomes the same with the corresponding all-electron ones (Fig. 2.5(a)).

The most common general form of a pseudopotential is,

$$V_{ps} = \sum_{lm} |Y_{lm}\rangle V_l(r) \langle Y_{lm}| \quad . \tag{2.79}$$

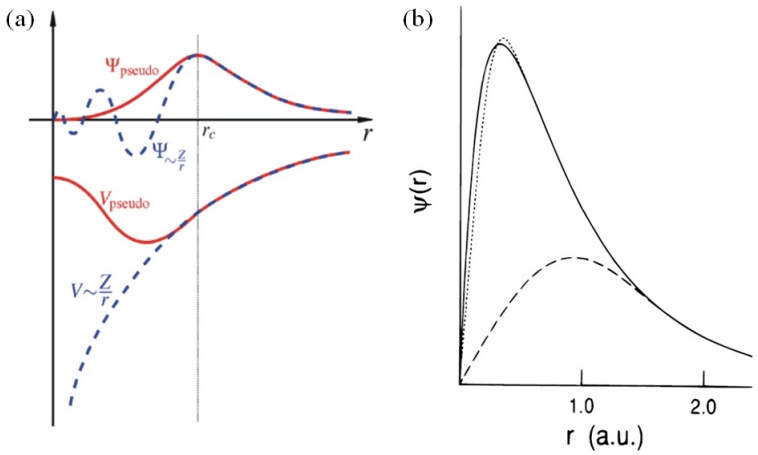


**Figure 2.5.:** (a) Schematic illustration of all-electron (dashed lines) and pseudopotential (solid lines) and their corresponding wave functions. The radius at which the all-electron and pseudo-electron values match is designated as $r_c$. (b) Oxygen $2p$ radial wave function (solid line) and corresponding pseudo wave function by using the norm-conserving HSC [148] (dotted line) and Vanderbilt ultrasoft [151] methods (dashed line). The figure is taken from Ref. [151].

One important class of pseudopotentials are so called norm-conserving pseudopotentials. Norm conserving pseudopotentials require that the all-electron and pseudo wave function agree beyond a chosen radius ($r_c$) and that the integrated density inside $r_c$ for the all-electron wave function and pseudo wave function are the same ("norm conservation"). There are many types of norm-conserving pseudopotentials from different authors such as Troullier and Martins [146], Kerker [147], Hamann, Schlüter, and Chiang [148], Vanderbilt [149], Goedecker-Teter-Hutter [150].

One issue with the norm-conserving pseudopotentials is that they can not generate smoother pseudo wave functions than the all-electron one when coming to the first row elements like O and the localized transition metals like Ni due to the "norm conservation" rule. This situation can be seen in Fig. 2.5(b) for the oxygen $2p$ orbital. There is hardly any improvement for the norm-conserving pseudopotential over the all-electron counterpart. To circumvent this difficulty, Vanderbilt [151] made a radical modification to break the norm conservation rule and relax the condition that the pseudo wave function inside the core region must have the same charge (or integrated density) as the all-electron wave function. By this way, $r_c$ can be chosen to a larger value and the the pseudo wave function can be made much softer than the all-electron wave function (Fig. 2.5(b)). Clearly, this introduces a deficit in the charge inside the core region and it is compensated with additional localized atom-centered charges. The additional charges are defined as the charge difference between the all-electron and pseudo wave functions and for convenience they are also pseudized. This kind of pseudopotential is called an ultrasoft pseudopotential, which enables much lower plane-wave cut-offs to be used in the calculations. The combination of DFT, plane-wave basis set, and pseudopotentials has

become a well-established methodology in electronic structure calculations of condensed matter.

## 2.6. Brief Summary

As already stated that a variety of methods have been employed in this thesis. In this section a few acronyms associated with electronic structure theory, which will appear often in the following chapters are briefly summarized in Table 2.1 and 2.2.

**Table 2.1.:** This table summarizes various acronyms related to electronic structure theory, which are described in this chapter and often will be referred to in the following chapters. Columns from the left are read as: (i) Acronym; (ii) Brief description of the theory; (iii) Typical scaling with number of basis functions ($N$); (iv) General performance with advantages and limitations.

| Name | Description | Scale | Performance |
|---|---|---|---|
| | Wave function based methods | | |
| HF | Hartree-Fock. In the HF many electron wavefunction is approximately taken as a single Slater determinant. This allows to simplify the interacting $N$-electron system into $N$ independent electron system. The many-body effect is captured via Coulomb repulsion with the mean all-electron density and the exchange interaction due to antisymmetric nature of the wavefunction. | $N^4$ | HF is self interaction free and applied to molecules and solids. But it has no electron correlation and thus, insufficient for metals and underestimates van der Waals and hydrogen bonded systems. |
| MP2 | Møller-Plesset perturbation theory. MP theory is in the same spirit of the Rayleigh-Schrödinger perturbation theory. Here the reference Hamiltonian is taken to be the HF Hamiltonian and the perturbative Hamiltonian is a two-electron operator. The first significant contribution of electron correlation comes from $2^{nd}$ order energy correction (referred as MP2). MP2 only involves sum over doubly excited determinants. | $N^5$ | MP2 is the cheapest (beyond HF) wave function based method to capture correlation. It shows improvement over HF in many cases, especially, hydrogen bonded systems but overestimates pure vdW interactions. The success of MP2 relies on error compensations and the results do not necessarily improve while going for higher order corrections. (e.g., MP3, MP4,$\cdots$ MP10,$\cdots$) |

Continued to Next Page...

Table 2.1 – Continued

| Name | Description | Scale | Performance |
|---|---|---|---|
| CCSD | Coupled cluster theory with single and double excitations. Electron correlation is calculated with single and doubles excitations up to *infinite order*, which allows to incorporate correlations of the *disconnected* higher order excitations as products of the amplitudes of single and double excitations. It is a big advantage over MP2 theory. | $N^6$ | So far CCSD is applied only for molecules (with few hundreds of electrons). CCSD results in many cases are inferior to MP2 and in general underestimates hydrogen bond energies and weak bonds. |
| CCSD(T) | Coupled cluster theory with single and double excitations and perturbative corrections for *connected* triples excitations. Here the CCSD Hamiltonian is taken as the reference Hamiltonian. Connected triples are found to be extremely crucial for dispersion bonded systems. | $N^7$ | It gives almost exact answers for a variety of molecular systems and often referred as the "gold standard" method in quantum chemistry. It captures vdW interactions accurately. But as the computational cost increases rapidly it is applied to systems with few tens of electrons only. |
| | Density function based methods | | |
| DFT | Density-functional theory. In DFT the ground state energy of a system is obtained from the ground state electron density. In principle DFT is exact method but in practice approximations are needed to capture many-electron exchange-correlation ($xc$) interactions. The performance of DFT depends on the choice of $xc$ functional. | $N^3$ | The most popular *ab initio* approach for simulations of condensed phases and molecules. With some $xc$ functionals it can reproduce experimental cohesive energies of a wide variety solids within 10% and lattice constants within 3%. It can be applied for systems with several thousands of electrons. It suffers from self interaction problem and poor description of long range der Waals interactions with most standard $xc$ functionals. |

Continued to Next Page...

Table 2.1 – Continued

| Name | Description | Scale | Performance |
|---|---|---|---|
| LDA | Local-density approximation. In LDA the electronic exchange-correlation ($xc$) energy is a functional of the local density [$n(\mathbf{r})$] only and the corresponding $xc$ energy is obtained from the uniform electron gas having the same density. | $N^3$ | It is valid only for systems with slowly varying densities. Overestimates cohesive energies of metals and insulators by ∼10%-20% and H bond energies by >50%. Long range vdW interactions are are not captured. |
| GGA | Generalized gradient approximation. In GGA the electronic exchange-correlation ($xc$) energy is taken to be a functional of the local density [$n(\mathbf{r})$] and the gradient of the density [$\nabla n(\mathbf{r})$]. In practice the gradient correction to the $xc$ energy is introduced by enhancing LDA $xc$ energy as a function of reduced gradient ($\lvert\nabla n(\mathbf{r})\rvert/n(\mathbf{r})^{4/3}$). | $N^3$ | GGAs describe hydrogen bonded and other weakly bound systems much better than LDA. Generally underestimates cohesive energies of metals and insulators. For system with larger density gradient performance of functionals depends strongly on the choice of the enhancement function. Long range vdW interactions are poorly described. |
| meta-GGA | The electronic exchange-correlation energy is taken to be a functional of the local density [$n(\mathbf{r})$], the gradient of the density [$\nabla n(\mathbf{r})$], and the kinetic energy density [$\nabla\psi(n(\mathbf{r}))$]. | $N^3$ | It does not improve much over the GGAs. It provides better surface energies and in some cases describes weakly bound systems better than GGAs. |
| hybrid-GGA | It is hybrid mixture of GGA $xc$ functionals with some fraction of Hartree-Fock exchange. | $N^4$ | It remedies self interaction error some extent and gives much better band gaps and reaction barrier heights than LDA and GGAs. Description of metals are worse than GGAs. It is more expensive than GGAs and technically hard to apply for periodic systems. |

**Table 2.2.:** This table briefly summarizes descriptions of several DFT exchange-correlation *xc* functionals employed in the thesis. Columns from the left are read as: (i) Exchange-Correlation functionals (*XC*) (ii) Generalized-gradient approximation (GGA) exchange (top) and correlation (bottom) (iii) Percentage of Hartree-Fock exchange; (iv) Empirical (E) or non-empirical (NE); (v) Brief description; and (vi) References.

| XC | X/C | HF | E/NE | Description | Ref. |
|---|---|---|---|---|---|
| | | | | GGA[$n(\mathbf{r})$, $\nabla n(\mathbf{r})$] | |
| BLYP | B88<br>LYP | 0% | E | Becke'88 with Lee-Yang-Parr correlation. It underestimates hydrogen bond energies but is very popular for the simulation of liquid water. | [114, 116] |
| BP86 | B88<br>P86 | 0% | E | Becke'88 exchange and Perdew'86 correlation. It has been shown to improve descriptions of weak interactions and hydrogen bonds. | [114, 117] |
| mPWLYP | mPW<br>LYP | 0% | E | Modified ("m") Perdew-Wang'91 exchange and Lee-Yang-Parr correlation. It has only been tested for weakly bound systems and typically underestimates hydrogen bond energies. | [116, 152] |
| PBE | PBE<br>PBE | 0% | NE | Perdew-Burcke-Ernzerhof '96. It is the most popular functionals for solids and also condensed phase water simulations. PBE tends to overestimate hydrogen bond energies. | [113] |
| PBE1W | PBE<br>PBE | 0% | E | A modified version of PBE with "1" optimized parameter (74%) in PBE correlation. It is especially designed to improve interactions among water ("W") molecules. | [113, 153] |
| PW91 | PW91<br>PW91 | 0% | NE | Perdew-Wang'91. It is very popular for simulations of ice and also applied to other solids It typically overestimates hydrogen bond energies. | [115] |

Continued to Next Page...

Table 2.2 – Continued

| *XC* | *X/C* | HF | E/NE | Description | Ref. |
|---|---|---|---|---|---|
| revPBE | revPBE<br>PBE | 0% | E | A revised ("rev") version of PBE exchange with $\kappa = 1.245$ in Eq. 2.60. It improves molecular atomization energies but underestimates cohesive energies of solids and hydrogen bond energies. | [113, 154] |
| XLYP | X<br>LYP | 0% | E | Here the exchange ("X") is a linear combination of Becke'88 and Perdew-Wang'91 exchange and the parameters are obtained by fitting to certain molecular databases. For hydrogen bond energies it is weaker than PW91 but stronger than BLYP. | [155] |
| meta-GGA[$n(\mathbf{r})$, $\nabla n(\mathbf{r})$, $\nabla\psi(n(\mathbf{r}))$] | | | | | |
| TPSS | TPSS<br>TPSS | 0% | NE | Tao-Perdew-Staroverov-Scuseria functional derived by following PBE with kinetic energy density as an additional parameter in the enhancement factor. It provides improved performance especially for surface energies and produces weaker hydrogen bonds than PBE. | [121] |
| hybrid-GGA[$n(\mathbf{r})$, $\nabla n(\mathbf{r})$, HF] | | | | | |
| BH&HLYP | B88<br>LYP | 50% | E | "H&H" stands for half & half, which means 50% contribution comes from HF exchange and other 50% from GGA exchange, Becke'88. It gives better thermochemical properties and hydrogen bond energies than BLYP. | [125] |
| B3LYP | B88<br>LYP | 20% | E | 3-parameter hybrid functional with Becke'88 exchange Lee-Yang-Parr correlation. Formulation of this functional is given in Eq. 2.63. The parameters are $a_1 = 0.2$, $a_2 = 0.72$, and $a_3 = 0.81$. It provides poor description of metals but it is the most popular functional to obtain thermochemical properties, reaction barrier heights, etc. | [126–128] |

Continued to Next Page...

Table 2.2 – Continued

| *XC* | *X/C* | HF | E/NE | Description | Ref. |
|---|---|---|---|---|---|
| B3P86 | B88<br>P86 | 20% | E | Same as B3LYP but with different GGA correlation, i.e., Perdew'86. It tends to improve non bonded weak interactions over B3LYP. | [114, 117] |
| B98 | B98<br>B98 | 21.9% | E | Becke'98 functional optimized on molecular databases to obtain better thermochemical properties. | [156] |
| PBE0 | PBE<br>PBE | 25% | NE | Hybrid functional based on GGA PBE. Here "0" refers to zero empirical parameter. 1/4 contribution from Hartree-Fock exchange is based on the grounds of perturbation theory. It provides much weaker cohesive energy for solids than PBE and reduces the overbinding trend in PBE for hydrogen bond energies. | [113, 129] |
| X3LYP | X<br>LYP | 21.8% | E | With the same spirit as B3LYP having different exchange (linear combination of Becke'88 and Perdew-Wang'91 exchange) and modified mixing parameters ($a_1$, $a_2$, and $a_3$). It improves over B3LYP for non-bonded interactions, especially, hydrogen bond energies. | [155] |
| hybrid-meta-GGA[$n(\mathbf{r})$, $\nabla n(\mathbf{r})$, $\nabla\psi(n(\mathbf{r}))$, HF] | | | | | |
| MPWB1K | mPW<br>B88 | 44% | E | Based on modified Perdew-Wang'91 exchange and Becke'95 correlation. It was optimized to provide improved results for thermochemistry, thermochemical kinetics, hydrogen bonding, and weak interactions. | [133] |
| PW6B95 | PW91<br>B95 | 28% | E | 6-parameter functional based on Perdew-Wang'91 exchange and Becke'95 correlation. It has been shown to provide improved results for thermochemistry and non bonded interactions. | [124] |

# 3. The Accuracy of DFT xc Functionals for Water Clusters in the Gas Phase

## 3.1. Introduction

As has been said, density-functional theory (DFT) is the most popular theoretical approach for determining the electronic structures of polyatomic systems. It has been extensively and successfully used to tackle all sorts of problems in materials science, condensed matter physics, molecular biology, and countless other areas. Many of these studies have involved the treatment of systems containing hydrogen bonds (HBs). HBs are weak (10-30 kJ/mol $\approx$ 100-300 meV/H-bond) bonds of immense widespread importance, being the intermolecular force responsible for holding water molecules together in the condensed phase, the two strands of DNA in the double helix, and the three dimensional structure of proteins [2].

Despite enormous success, questions like how good DFT is for HBs or what the best exchange-correlation (xc) functional is for treating HBs are far from uncommon for developers and practitioners of Kohn-Sham DFT. Clearly imprecise and vague questions it is nonetheless important to answer them, once, of course, terms like "good" and "best" have been defined and consideration made to the properties of interest (energetic, structural, dynamical, electronic). Indeed considerable effort has been expended in an attempt to answer questions like these [119, 120, 153, 157–169].

One particularly important class of H-bonded systems, arguably the most important, are small water clusters. Small water clusters have been implicated in a wide range of phenomena (for example, environmental chemistry and ice nucleation [52, 170, 171]). Moreover, they are thought to provide clues as to the properties of liquid water, ice and water under various conditions and environments. Along with this widespread application there have also been various benchmark studies specifically aimed at accessing the performance of various *xc* functionals in treating gas phase water clusters [153, 157–159, 161, 162], adsorbed clusters [51, 55, 171–176], and liquid water [10–32]. However, the ability of DFT to quantitatively describe HBs between $H_2O$ molecules in either small water clusters or the liquid state remains unclear. This is particularly true in light of recent experimental and theoretical studies which have raised concerns over the ability of DFT to reliably describe the structure and properties of liquid water [10–32].

It is now well established that the simplest approximation to the electron *xc* potential, the local-density approximation (LDA), is inappropriate for treating HBs. For example, the dissociation energies of small water clusters and the cohesive energy of ice are overestimated by >50% with the LDA [40, 41, 57, 177, 178]. However, despite widespread practical application and several recent benchmark studies it remains unclear precisely

how well the many popular post-LDA functionals perform at describing HBs between water clusters. Generalized gradient approximation (GGA) functionals such as PBE [113], PW91 [115], and BLYP [114, 116], for example, are widely used to examine liquid water [12, 19, 179–181], ice [41, 182–184] and adsorbed water [182, 185], yet ask three experts which one is "best" and one is likely to receive three different answers. Likewise unanimity has not been reached on the performance of the many meta-GGA or hybrid functionals that are available, such as TPSS [121], PBE0 [129], and B3LYP [116, 126–128]. Part of the reason for the lack of clarity stems from the fact that in previous benchmark studies insufficiently complete basis sets were employed and that comparisons were restricted to the simplest H-bonded systems involving $H_2O$, namely the $H_2O$ dimer and trimer. Basis set incompleteness effects can, of course, mask the true performance of a given functional and, as will be shown below, the ability of a given functional to accurately predict the strength of the HBs in the dimer or even the trimer does not necessarily reveal how well that functional will perform even for the next largest clusters, tetramers and pentamers.

In this chapter the ability of several GGA, meta-GGA, and hybrid *xc* functionals to compute the energy and structure of HBs between $H_2O$ molecules is evaluated. This study is restricted to the established lowest energy conformer of four smallest $H_2O$ clusters (dimer, trimer, tetramer, and pentamer), [186–188], which, for orientation purposes, are shown in Fig. 3.1. Section 3.2 and 3.3 demonstrate the generation of the benchmark data and the DFT data itself. In section 3.4 details of the results and analysis are provided together with a summary in section 3.5.

## 3.2. Accurate Reference Dissociation Energy: MP2

For a systematic benchmark study such as this, reliable reference data is essential. Experiment is, in principle, one source of this data. However, experimental dissociation energies are simply not available or do not come with sufficiently small error bars for all the $H_2O$ clusters examined here. Further, with the aim to systematically evaluate the performance of many DFT *xc* functionals it becomes impractical to compute all the small contributions to the experimental dissociation energy that come on top of the total electronic dissociation energy - an easily accessible total energy difference - such as zero point vibrations, relativistic contributions[1], etc. The obvious alternative source of reference data are the results obtained from correlated quantum chemistry methods such as second order Møller Plesset perturbation theory (MP2) [70] or coupled-cluster theory [190]. Indeed such methods have been widely applied to examine H-bonded systems [119, 120, 123, 164, 186, 189, 191–197]. In particular coupled-cluster with single and double excitations plus a perturbative correction for connected triples (CCSD(T)) produces essentially "exact" answers if sufficiently accurate basis sets are used. For example, the best CCSD(T) value for the dissociation energy (defined in Eq. 3.3) of the water dimer is at 217.6±2 meV [83] in good agreement with the appropriate experimental number

[1] At CCSD(T) level the relativistic effects are estimated to reduce the magnitude of the dissociation energy of the water dimer by <0.5 meV/$H_2O$ [83, 189].

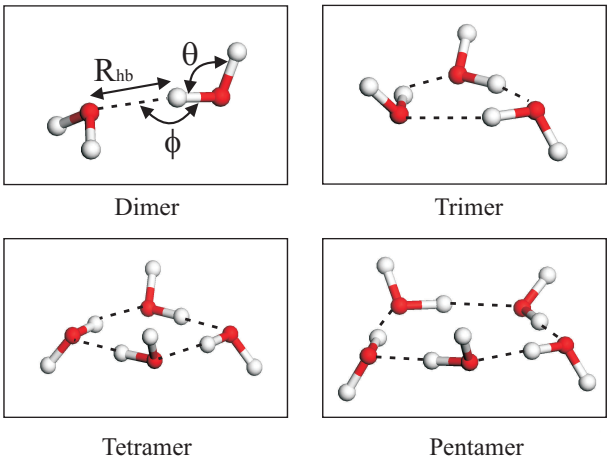


**Figure 3.1.:** Structures of the four water clusters examined here in their global minimum energy configurations. The dashed lines indicate HBs. Some of the structural parameters of the H-bond are indicated alongside the dimer. In the trimer, tetramer, and pentamer there is one H-bond per water molecule.

of 216.8±30 meV [84, 198]. However, since the computational cost of CCSD(T) scales as $N^7$, where $N$ is the number of basis functions, the most extravagant use of computational power is required for CCSD(T) calculations with large basis sets. MP2, on the other hand, scales as $N^5$ and when compared to CCSD(T) for water dimers and trimers at the CBS limit, yields dissociation energies that differ by no more than 2 meV/H-bond [189, 194]. In addition, a recent study of water hexamers using CCSD(T) with an aug-cc-pVTZ basis set revealed that the MP2 and CCSD(T) dissociation energies of various hexamer structures differ by <3 meV/$H_2O$ [199]. Thus MP2 is a suitable method for obtaining reference data with an accuracy to within a few meV/H-bond. Such accuracy, which is well beyond so-called chemical accuracy (1kcal ≈ 43 meV), is essential in studies of H-bonded systems. Since MP2 geometries are not available for all four clusters examined here new MP2 structures are computed for each one. All calculations have been performed with the Gaussian03 [200] and NWChem [201] codes[2] and all geometries were optimized with an aug-cc-pVTZ basis set within the "frozen core" approximation, i.e., correlations of the oxygen 1$s$ orbital were not considered. Although the aug-cc-pVTZ basis set is moderately large (92 basis functions/$H_2O$), this finite basis set will introduce errors in predicted MP2 structures. However, a test with the $H_2O$ dimer reveals that the aug-cc-pVTZ and aug-cc-pVQZ MP2 structures differ by only 0.004 Å in the O-O bond length and 0.16° in the H-bond angle ($\phi$, Fig. 3.1). Likewise, Nielsen and co-workers have shown that the MP2 O-O distances in the cyclic trimer differ by 0.006 Å between the aug-cc-pVTZ and aug-cc-pVQZ basis sets with all other bonds differing by <0.003 Å [197]. For present purposes these basis set incompleteness errors on the structures are

[2]Here Gaussian03 [200] and NWChem [201] codes are used interchangeably, since total energies of the water clusters obtained from the two codes differ by no more than 0.4 meV per water molecule.

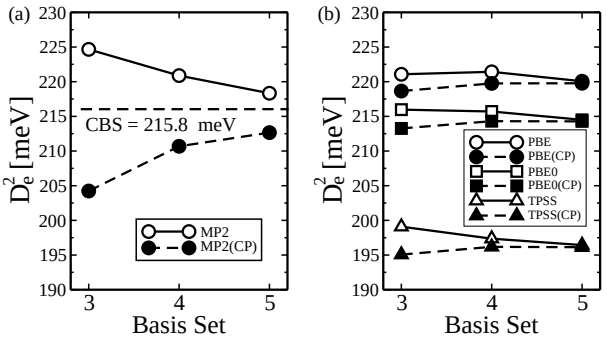


**Figure 3.2.:** (a) Variation in the MP2 dissociation energy for the $H_2O$ dimer without a counterpoise correction for basis set superposition error (BSSE) (labeled MP2) and with a counterpoise correction for BSSE (labeled MP2(CP)) as a function of basis set size. The extrapolated complete basis set (CBS) dissociation energy for the $H_2O$ dimer with MP2 is also indicated. (b) Variation in the dissociation energy for the $H_2O$ dimer with and without a counterpoise BSSE correction as a function of basis set size for three different DFT functionals. The basis set labels on the X axis of (a) and (b) indicate aug-cc-pVXZ basis sets, where X=3, 4, and 5. Lines are drawn to guide the eye only. All structures were optimized with an aug-cc-pVTZ basis set consistently with MP2 and with each DFT functional.

acceptable and it seems reasonable to assume that the aug-cc-pVTZ structures reported here come with error bars of $\pm 0.01$ Å for bond lengths and $\pm 0.5°$ for bond angles.

Total energies and dissociation energies are known to be more sensitive to basis set incompleteness effects than the geometries are. To obtain reliable MP2 total energies and dissociation energies the aug-cc-pVTZ, aug-cc-pVQZ (172 basis functions/$H_2O$) and aug-cc-pV5Z (287 basis functions/$H_2O$) basis sets are employed in conjunction with the well-established methods for extrapolating to the CBS limit. Usually the extrapolation schemes rely on extrapolating separately the Hartree-Fock (HF) and correlation contributions to the MP2 total energy. For extrapolation of the HF part Feller's exponential fit [202] is used:

$$E^{\mathrm{HF}}(X) = E^{\mathrm{HF}}_{\mathrm{CBS}} + Ae^{-BX} \quad , \tag{3.1}$$

where $X$ is the cardinal number corresponding to the basis set ($X$=3, 4, and 5 for the aug-cc-pVTZ, aug-cc-pVQZ, and aug-cc-pV5Z basis sets, respectively). $E^{\mathrm{HF}}(X)$ is the corresponding HF energy, $E^{\mathrm{HF}}_{\mathrm{CBS}}$ is the extrapolated HF energy at the CBS limit, and $A$ and $B$ are fitting parameters. For the correlation part of the MP2 total energy an inverse power of highest angular momentum equation is followed [203–205]:

$$E^{\mathrm{corr}}(X) = E^{\mathrm{corr}}_{\mathrm{CBS}} + \frac{C}{X^3} + \frac{D}{X^5} \quad , \tag{3.2}$$

where $E^{\mathrm{corr}}(X)$ is the correlation energy corresponding to $X$, $E^{\mathrm{corr}}_{\mathrm{CBS}}$ is the extrapolated CBS correlation energy, and $C$ and $D$ are fitting parameters. Various extrapolation schemes available in the literature [144, 202–207] are tested and differences between all the predicted CBS values are found to be no more than 1.2 meV/H-bond. The scheme

provided by Eqns. (3.1) and (3.2) is opted here because it is found that with input from triple-, quadruple-, and pentuple-$\zeta$ basis sets this method was best able to predict the total energy of a water monomer and dimer explicitly calculated with an aug-cc-pV6Z basis set (443 basis functions/$H_2O$). Having obtained MP2 CBS total energies for the $H_2O$ monomer and each of the $H_2O$ clusters, the MP2 CBS dissociation energies ($D_e^n$) per H-bond are calculated as,

$$D_e^n = (E^{nH_2O} - nE^{H_2O})/n_{H-bond} \quad , \tag{3.3}$$

where $E^{nH_2O}$ is the total energy of each cluster with $n$ $H_2O$ molecules, $E^{H_2O}$ is the total energy of a $H_2O$ monomer, and $n_{H-bond}$ is the number of HBs in the cluster. The CBS MP2 dissociation energies found here for the dimer, trimer, tetramer, and pentamer are 215.8, 228.5, 299.9, and 314.4 meV/H-bond, respectively[3]. These values are all within 0.5 meV/H-bond of the previous MP2 CBS dissociation energies reported by Xantheas *et al.* [192]. The various errors accepted in producing these values (MP2 (valence only) treatment of correlation, aug-cc-pVTZ structures, extrapolation to reach the CBS, etc.) will lead to errors in the reference data from the exact electronic dissociation energies on the order of $\pm$5.0 meV/H-bond at most. With the present aim to evaluate the performance of various DFT *xc* functionals such errors are acceptable.

## 3.3. DFT Dissociation Energy

In a study such as this there is an essentially endless list of functionals that one could consider evaluating. Here 16 different functionals are examined. They are chosen because either they are widely used or have been reported to perform particularly well for H-bonded systems in predicting dissociation energies and structures of the above mentioned clusters. Specifically the following *xc* functionals are chosen to optimize structures of each cluster: **(I)** PW91 [115] - an extremely popular non-empirical GGA widely used in calculations of bulk ice [41, 208, 209] and other H-bonded systems [119]; **(II)** PBE [113] - the twin of PW91 that has again been widely used and tested for H-bonded systems [120, 123, 191]; **(III)** PBE1W - a parameterized empirical variant of PBE specifically designed to yield improved energetics of HBs [191]. **(IV)** TPSS [121] - the meta-GGA variant of PBE, recently used in simulations of liquid water and evaluated for small water clusters [19, 123, 191, 191, 210]; **(V)** PBE0 [129] - a so-called parameter free hybrid variant of PBE, also recently tested for water [19, 123, 196, 211]; **(VI)** BLYP - Becke88 [114] exchange combined with LYP [116] correlation, a popular functional for liquid water simulations [12, 19, 179–181]; **(VII)** B3LYP [116, 126–128] - the extremely popular Becke three parameter hybrid functional combined with LYP non-local correlation, which has, of course, been widely used to examine H-bonded systems [19, 123, 195, 196]; **(VIII)** mPWLYP - a combination of a modified PW91 exchange functional (mPW) [152] with the LYP correlation functional, found to be the most accurate pure GGA for the energetics of HBs in water dimers and trimers [191]. **(IX)** BP86

[3]The corresponding CBS HF dissociation energies at the MP2 structures are 148.0, 140.8, 187.6, and 200.8 meV/H-bond for the dimer, trimer, tetramer, and pentamer, respectively.

- an empirical GGA combining Becke88 [114] exchange and Perdew86 [117] correlation that is well-tested for hydrogen bonded systems [196, 211]; **(X)** X3LYP [155] - another empirical hybrid functional designed to describe weak (non-covalent) interactions that is becoming a familiar name for calculations of water [19, 123, 161]; **(XI)** XLYP [155] - the non-hybrid GGA version of X3LYP, also tested for H-bonded systems [123]; **(XII)** B98 [156] - another hybrid functional, said to perform extremely well for water clusters [123, 191]; **(XIII)** MPWB1K [133] - a one parameter hybrid meta-GGA using mPW [152] exchange and Becke95 [212] correlation, said to be the joint-best for HBs between water molecules [123, 191]; **(XIV)** PW6B95 [124] - another hybrid meta-GGA combining PW91 [115] exchange and Becke95 [212] correlation, found to be the other joint-best functional for the HBs between water molecules [191]; **(XV)** B3P86 - Becke 3 parameter hybrid functional combined with Perdew86 nonlocal correlation, found to be best functional for H-bonded systems in a recent benchmark study [123]; and **(XVI)** BH&HLYP [114, 116, 125] - said to offer similar performance to B3P86 for H-bonded systems [123].

As with MP2, the question arises as to what basis sets to use in order to ensure that the DFT results reported here are not subject to significant basis set incompleteness errors, which would cloud evaluations of the various functionals. There are no established extrapolation schemes for DFT. However, it is well-known that DFT total energies are less sensitive to basis set size than explicitly correlated methods such as MP2[4] [79, 213, 214]. Indeed from the plot in Fig. 3.2 it can be seen that the computed DFT dissociation energies converge much more rapidly with respect to basis set size than MP2 does (*c.f.* Figs. 2(a) and 2(b)). Specifically, upon going from aug-cc-pVTZ to aug-cc-pV5Z the dissociation energy of the $H_2O$ dimer changes by only 1.0, 2.7, and 1.5 meV for the PBE, TPSS, and PBE0 functionals, respectively. Further, with the aug-cc-pV5Z basis set the counterpoise corrected and uncorrected dissociation energies essentially fall on top of each other, with the largest difference for the dimers and trimers being 0.45 meV/H-bond with the TPSS functional. In addition, upon going beyond aug-cc-pV5Z to aug-cc-pV6Z the dimer dissociation energies change by only 0.24, 0.11, 0.19, 0.25 meV for the PBE, TPSS, PBE0 and BLYP functionals, respectively. Thus the DFT dissociation energies reported in the following will all come from those obtained with the aug-cc-pV5Z basis set, which is sufficiently large to reflect the true performance of each functional at a level of accuracy that is reasonably expected to approach the basis set limit to within about 0.5 meV/H-bond or better.

[4] In LDA, GGA, and standard hybrid DFT *xc* functionals (and HF) the motion of a given electron is unaffected by the instantaneous position of the other electrons, whereas in the wavefunction-based approaches such as MP2 this is not the case and the short range electronic interactions which inevitably occur give rise to cusp conditions, notably the (electronic) Coulomb cusp. Such cusp conditions, which standard DFT *xc* functionals are free of, yield wavefunctions that are exceedingly difficult to describe exactly with finite basis sets. See Helgaker *et al.* for more details [79]. Since the importance of using large basis sets for MP2 is clear from Fig. 3.2, it is cautioned that even the largest Pople-style basis set, 6-311++G(3df,3pd), yields an MP2 dissociation energy for the water dimer of 230 meV/H-bond, which at ∼15 meV from the MP2/CBS number, is not necessarily of sufficient accuracy to serve as a reliable benchmark.

**Table 3.1.:** Comparison of the MP2 complete basis set dissociation energies to those obtained with various DFT functionals computed with an aug-cc-pV5Z basis set for four different water clusters. DFT dissociation energies that come within ±5.0 meV of the corresponding MP2 value are indicated in bold. The numbers in parenthesis indicate the percentage cooperative enhancement in the H-bond strength compared to the dissociation energy of the dimer. Averages of the signed and unsigned errors in the dissociation energies of all DFT functionals from the corresponding MP2 numbers over all four clusters are also provided as ME (mean error) and MAE (mean absolute error). The DFT functionals are ordered in terms of increasing MAE. All structures were optimized consistently with MP2 and with each DFT functional with an aug-cc-pVTZ basis set and all values are in meV/H-bond (1Kcal/mol = 43.3641 meV).

| | Dimer | Trimer | Tetramer | Pentamer | ME | MAE |
|---|---|---|---|---|---|---|
| MP2 | 215.8 | 228.5 (5.9) | 299.9 (38.9) | 314.4 (45.7) | — | — |
| X3LYP | **213.8** | 221.9 (3.8) | **298.3** (39.5) | **316.0** (47.8) | -2.2 | 2.9 |
| PBE0 | **214.5** | **224.6** (4.7) | **302.7** (41.1) | 320.9 (49.6) | 1.0 | 3.6 |
| mPWLYP | **218.5** | **226.0** (3.4) | 305.4 (39.8) | 323.7 (48.1) | 3.8 | 5.0 |
| B3P86 | 203.5 | 220.0 (8.1) | **299.4** (47.1) | **316.5** (55.5) | -4.8 | 5.9 |
| PBE1W | 207.9 | 216.6 (4.0) | **294.9** (41.8) | **312.7** (50.4) | -6.6 | 6.6 |
| BH&HLYP | **213.2** | 219.5 (2.9) | 291.3 (36.6) | 308.3 (44.6) | -6.6 | 6.6 |
| PBE | **220.1** | **233.5** (6.1) | 316.4 (43.8) | 334.8 (52.1) | 11.6 | 11.6 |
| B98 | 205.6 | 211.4 (2.8) | 285.9 (39.1) | 303.1 (47.4) | -13.2 | 13.2 |
| TPSS | 196.4 | 209.4 (6.6) | 288.8 (47.0) | 307.5 (56.6) | -14.1 | 14.1 |
| B3LYP | 197.4 | 206.3 (4.5) | 280.1 (41.9) | 297.2 (50.6) | -19.4 | 19.4 |
| PW6B95 | 200.9 | 210.5 (4.8) | 276.8 (37.8) | 292.7 (45.7) | -19.4 | 19.4 |
| MPWB1K | 199.1 | 210.6 (5.5) | 276.3 (38.8) | 292.3 (46.8) | -20.1 | 20.1 |
| BP86 | 184.4 | 205.7 (11.6) | 282.5 (53.2) | 300.8 (63.1) | -21.3 | 21.3 |
| PW91 | 232.5 | 244.9 (5.1) | 330.8 (42.3) | 350.5 (50.8) | 25.0 | 25.0 |
| XLYP | 191.4 | 198.6 (3.8) | 272.2 (42.2) | 288.9 (50.9) | -26.9 | 26.9 |
| BLYP | 180.7 | 191.7 (6.1) | 264.9 (46.6) | 281.2 (55.6) | -35.0 | 35.0 |

## 3.4. Results

### 3.4.1. Dissociation Energy

In Table 3.1 the computed dissociation energies obtained with MP2 and with each of the DFT functionals are reported. To allow for a more convenient comparison of the performance of the various functionals in Fig. 3.3(a) the difference between the DFT and MP2 dissociation energies ($\Delta D_e^n$) are plotted as a function of water cluster size. In this figure positive values correspond to an overestimate of the dissociation energy by a given DFT functional compared to MP2. So, what do we learn from Table 3.1 and Fig. 3.3(a)? First, the functionals which offer the best performance for the clusters examined are the hybrid X3LYP and PBE0 functionals, coming within 7 meV/H-bond for all four clusters.

Of the non-hybrid functionals the pure GGAs mPWLYP and PBE1W perform best, coming within 12 meV/H-bond for all four clusters. Second, the very popular BLYP and B3LYP functionals consistently underbind: B3LYP predicts HBs that are ∼20 meV too weak; and BLYP predicts HBs that are ∼35 meV too weak. Third, PBE overestimates the binding in the dimer and trimer ever so slightly, coming within 5 meV/H-bond, but for the tetramer and pentamer drifts away to yield errors of ∼20 meV/H-bond. Fourth, PBE and PW91 exhibit a non-negligible difference. Although it is often assumed that identical numerical results should be obtained from these two functionals this is not the case here; PW91 is consistently 12-14 meV/H-bond worse than PBE. Both functionals, however, exhibit a similar tendency towards increased overbinding as the cluster size grows. Indeed it is clear from Fig. 3.3 that all PBE-related functionals (PBE, PW91, PBE1W, TPSS, and PBE0) show this trend, which in the case of TPSS means that it gets within ∼7 meV/H-bond for the pentamer starting from an error of ∼20 meV/H-bond for the dimer. Likewise PBE1W gets closer to the reference value as the cluster size grows. Finally, despite previous suggestions to the contrary [123, 191, 211], none of the other functionals particularly stand out: B98 underbinds by just over 13 meV/H-bond, and BP86 exhibits a rather strong variation in performance with cluster size, ranging from a 30 to 14 meV/H-bond error. B3P86 shows similar behavior to BP86, although the magnitude of the error is much less and indeed for the tetramer and pentamer B3P86 gives values close (within 3 meV/H-bond) to MP2. MPWB1K and PW6B95 both underbind by ≥20 meV/H-bond.

Another interesting aspect of the results of the present study is that the performance of some functionals differs appreciably from one cluster to another. For example, PBE is only ∼4-5 meV/H-bond away from MP2 for the dimer and trimer but >15 meV/H-bond away from MP2 for the tetramer and pentamer. Conversely, TPSS is ∼20 meV/H-bond off MP2 for the dimer but within 7 meV/H-bond of MP2 for the pentamer. Other functionals which show strong variation in performance with cluster size are PW91, BP86, and B3P86, and the functional in the admirable position of showing the least variation, consistently predicting HBs that are ∼35 meV too weak, is BLYP. The general conclusion of this analysis, however, is that it is not necessarily sufficient to use the performance of a given functional for a single system, such as for example the $H_2O$ dimer, as a guide to how that functional will perform for HBs between $H_2O$ molecules in general. Indeed the results reported here indicate that H-bond test sets such as the "W7" test set [191] for water would benefit from the inclusion of structures other than dimers and trimers.

Also to note an interesting conclusion of the present study is the non-negligible difference between the H-bond energies predicted by PBE and PW91; with PW91 consistently being 12-14 meV/H-bond worse than PBE. A similar discrepancy, although in a rather different area of application - surface and defect formation energies of metals - has been identified by Mattsson and co-workers [215]. Specifically they found that the PW91 and PBE monovacancy formation energies of Al differed by ∼30-40 meV. Evidences from this study together with the findings of Mattson and co-workers it does not seem wise to expect identical numerical results from PBE and PW91.

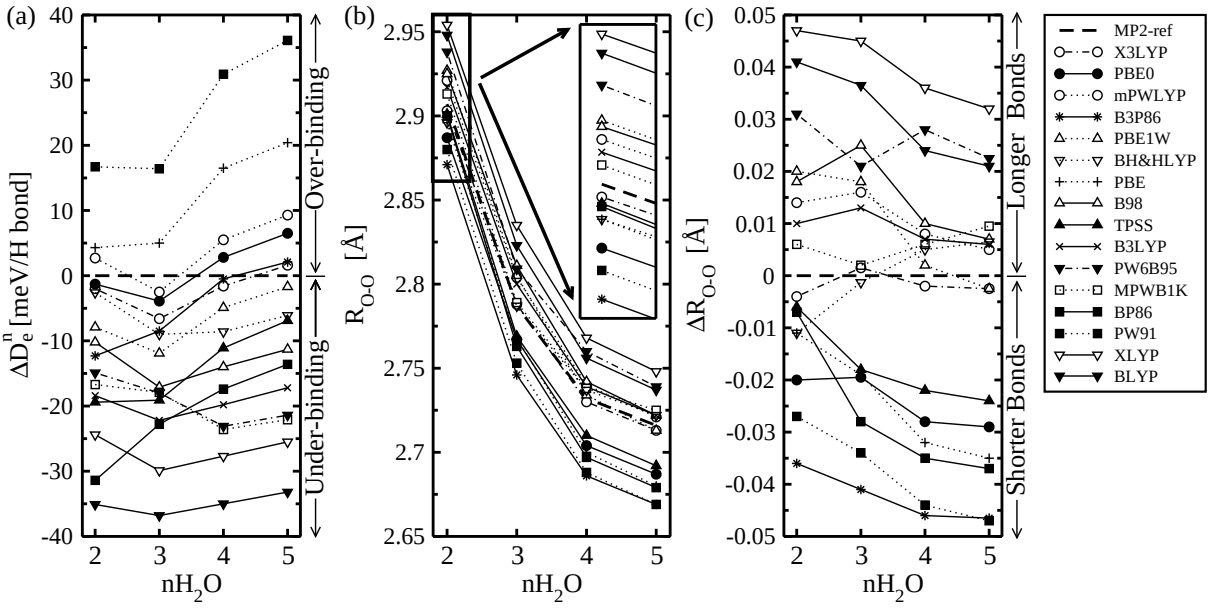


**Figure 3.3.:** (a) Difference in the dissociation energy ($\Delta D_e^n$) in meV/H-bond of the various DFT functionals compared to MP2, plotted as a function of cluster size. Positive values correspond to an overestimate of the dissociation energy by a given DFT functional. (b) Average value of the MP2 and DFT O-O distances ($R_{O-O}$) as a function of cluster size. The inset zooms in on the dimer region. (c) Difference in the average O-O distance ($\Delta R_{O-O}$) between MP2 and DFT. Positive values correspond to an overestimate of the average O-O distances by a given DFT functional. (a)-(c) All DFT energies are calculated with an aug-cc-pV5Z basis set on geometries optimized consistently with each functional with an aug-cc-pVTZ basis set. Lines are drawn to guide the eye only.

### 3.4.2. Cooperativity

An important aspect of the energetics of HBs is that they tend to undergo cooperative enhancements, which for the present systems implies that the average strengths of the HBs between the water molecules increases as the number of HBs increases. The fact that the HBs in water clusters undergo cooperative enhancements is now well established [2, 170, 216], as is the importance of cooperativity in many other types of H-bonded systems [2, 185, 217]. The ability of each functional is evaluated to correctly capture the computed MP2 cooperative enhancement, defined as the percentage increase in the average H-bond strength compared to that in the $H_2O$ dimer. These numbers are reported in parenthesis in Table 3.1. It is fond that all functionals capture the correct trend, i.e., the average H-bond strength increases upon going from dimer to pentamer. In addition, most functionals get the absolute percentage enhancement correct to within 5%. The notable exceptions are BP86, B3P86, and TPSS which for the tetramer and pentamer predict cooperative enhancements that exceed the MP2 values by 10-15%.

**Table 3.2.:** Mean absolute error (MAE) of various DFT functionals from MP2 for five different structural parameters, averaged over the four water clusters examined here. The numbers in bold all have MAE $\leq$0.010 Å for bond lengths and $\leq$0.50° for bond angles. Mean errors (ME) are given in parenthesis. All structures were optimized consistently with MP2 and with each DFT functional with an aug-cc-pVTZ basis set. The order of the functionals is the same as in Table 3.1.

| | $\Delta R_{O\text{-}O}$ (Å) | $\Delta R_{hb}$ (Å) | $\Delta R_{O\text{-}H}$ (Å) | $\Delta\phi$ (°) | $\Delta\theta$ (°) |
|---|---|---|---|---|---|
| X3LYP | **0.002** (-0.002) | **0.003** (-0.003) | **0.001** (0.000) | **0.21** (0.21) | 1.04 (1.04) |
| PBE0 | 0.024 (-0.024) | 0.023 (-0.023) | **0.002** (-0.001) | 0.77 (0.77) | 0.69 (0.69) |
| mPWLYP | 0.012 (0.012) | **0.008** (-0.004) | 0.012 (0.012) | 0.61 (0.47) | 0.51 (0.51) |
| B3P86 | 0.042 (-0.042) | 0.051 (-0.051) | **0.003** (0.001) | 1.00 (1.00) | 0.77 (0.77) |
| PBE1W | 0.011 (0.009) | **0.010** (-0.006) | 0.011 (0.011) | 1.13 (1.13) | **0.13** (0.13) |
| BH&HLYP | **0.006** (-0.003) | 0.015 (0.015) | 0.013 (-0.013) | **0.48** (-0.17) | 1.52 (1.52) |
| PBE | 0.024 (-0.024) | 0.046 (-0.046) | 0.012 (0.012) | 1.43 (1.21) | **0.13** (0.13) |
| B98 | 0.016 (0.016) | 0.015 (0.015) | **0.001** (-0.001) | 0.52 (0.52) | 0.66 (0.66) |
| TPSS | 0.018 (-0.018) | 0.037 (-0.037) | **0.010** (0.010) | 1.28 (1.25) | **0.22** (0.22) |
| B3LYP | **0.009** (0.009) | **0.007** (0.007) | **0.001** (0.001) | **0.31** (0.31) | 0.93 (0.93) |
| PW6B95 | 0.026 (0.026) | 0.029 (0.029) | **0.006** (-0.006) | **0.29** (0.24) | 0.81 (0.81) |
| MPWB1K | **0.006** (0.006) | 0.016 (0.016) | 0.012 (-0.012) | **0.38** (0.31) | 1.09 (1.09) |
| BP86 | 0.028 (-0.028) | 0.051 (-0.051) | 0.014 (0.014) | 1.58 (1.46) | **0.11** (0.11) |
| PW91 | 0.038 (-0.038) | 0.038 (-0.038) | 0.012 (0.012) | 1.44 (1.21) | **0.29** (0.29) |
| XLYP | 0.040 (0.040) | 0.028 (0.028) | 0.011 (0.011) | 0.53 (0.49) | **0.37** (0.37) |
| BLYP | 0.031 (0.031) | 0.015 (0.015) | **0.009** (0.009) | 0.69 (0.64) | **0.37** (0.37) |

### 3.4.3. Geometry

Now aiming to answer the question how good are the structures predicted by each DFT *xc* functional, five key structural parameters of the $H_2O$ clusters that are evaluated here: (i) The distance between adjacent oxygen atoms involved in a H-bond, $R_{O\text{-}O}$; (ii) The length of a H-bond, given by the distance between the donor H and the acceptor O, $R_{O\cdots H} = R_{hb}$ (Fig. 3.1); (iii) The H-bond angle, $\angle(O\cdots H\text{-}O) = \phi$ (Fig. 3.1); (iv) The internal O-H-bond lengths of each water, $R_{O\text{-}H}$; and (v) The internal H-O-H angle of each water, $\angle(H\text{-}O\text{-}H) = \theta$ (Fig. 3.1). In Table 3.2 the mean absolute error (MAE) and mean error (ME) between the MP2 values and those obtained from each functional, averaged over all four clusters, are listed for each of the above parameters. This provides an immediate overview for how the functionals perform. Summarizing the results of this table, X3LYP, BH&HLYP, B3LYP, and MPWB1K perform the best for O-O distances. All those functionals yield results that are essentially identical to MP2, coming within estimated MP2 bond distance error bar of 0.01 Å. B3P86 is the worst functional in terms of O-O distances, with a MAE of 0.04 Å. Largely, these conclusions hold for the related quantity, $R_{hb}$, although now B3P86, BP86, and PBE perform worst with MAE values of $\sim$0.05 Å. In terms of the H-bond angle, $\phi$, X3LYP, B3LYP, PW6B95, MPWB1K, and

BH&HLYP are essentially identical to MP2 coming within estimated MP2 error bar for angles of 0.5° and again PW91, PBE, and BP86 are the worst being ∼1.5° away from MP2. For the internal O-H-bond lengths no functional is worse than ∼0.015 Å and for the internal H-O-H angles, $\theta$, all functionals are within ∼1.5° of MP2.

One specific aspect of the structures of the small cyclic water clusters examined here, that is known from experiment and previous calculations [170, 218] is that the average O-O distances between the $H_2O$ molecules in the clusters shorten as the cluster size increases. This trend is, of course, related to the cooperative enhancement in H-bond strengths discussed already. As can be seen from the plot of computed O-O distances versus cluster size in Fig. (3.3(b)) all functionals correctly capture this effect: the ∼0.2 Å shortening in the O-O bond distances upon going from dimer to pentamer predicted by MP2 is also captured by every DFT functional. To look at this issue more closely and specifically to examine how each functional varies with respect to MP2, the difference between the MP2 and DFT O-O distances for the four clusters are plotted in Fig. (3.3(c)). Positive values in Fig. (3.3(c)) indicate that the DFT O-O bonds are longer than the MP2 ones. To be noted here that the average MP2 O-O distances for the dimer, trimer, tetramer and pentamer are 2.907, 2.787, 2.732, and 2.716 Å, respectively. As indicated already in the previous discussion, X3LYP, B3LYP, BH&HLYP, and MPWB1K perform the best at predicting the correct O-O bond length for each cluster; coming within 0.01 Å of the MP2 values on every occasion. Indeed the consistent closeness of the X3LYP O-O distances to the MP2 ones is remarkable. PBE0 is a little worse than X3LYP for the O-O distances, predicting bonds which are consistently about 0.02-0.03 Å too short. Of the other functionals B3P86 stands out as predicting the shortest O-O distances (always ∼0.04 Å less than MP2) and XLYP and BLYP predict the longest O-O distances, always at least 0.02 Å longer than MP2.

### 3.4.4. Requirement for Large Basis Sets

Here of the functionals tested X3LYP and PBE0 are found to offer exceptional performance for the HBs in small water clusters in their global minimum energy structures. However, a previous benchmark study on the ability of most of the functionals considered here to describe the energetics of HBs between water molecules has arrived at somewhat different conclusions [191]. Specifically, a MAE of 19.5 meV/H-bond has been reported for PBE0, worse than the MAE of 3.6 meV/H-bond obtained here. In addition, MAEs of 5-7 meV/H-bond have been reported with the PW6B95, MPWB1K, and B98 functionals, suggesting improved performance for these functionals over what is found here. In that study the so-called MG3S basis set (identical to 6-311+G(2df,2p) for $H_2O$) was used. By comparing the performance of the above-mentioned functionals with the MG3S and the aug-cc-pV5Z basis sets for the four clusters under consideration here it appears that the incompleteness of the MG3S basis set is the main reason for the small discrepancy. The results, illustrated in the histogram in Fig. (3.4), reveal that the dissociation energies obtained with the MG3S basis set are consistently ∼18 meV (0.42 kcal/mol) per H-bond larger than those obtained with the aug-cc-pV5Z basis set. Thus although PW6B95, MPWB1K, and B98 perform well with the MG3S basis set (all within ±7

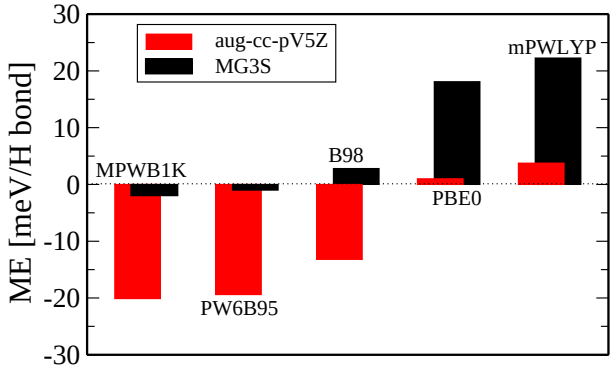


**Figure 3.4.:** Mean error (ME) in the dissociation energies obtained with aug-cc-pV5Z and MG3S basis sets for five selected functionals for the four clusters examined here. Positive values correspond to an average overestimate of the dissociation energy compared to MP2 for the clusters. All errors are measured relative to the reference CBS MP2 values calculated here.

meV/H-bond of MP2 for the clusters considered here), they all exhibit a propensity to underbind when the more complete aug-cc-pV5Z basis set is used. Conversely, PBE0 and one other functional tested, mPWLYP, which predict too strong HBs with the MG3S basis set (MAEs of 18.1 and 22.3 meV/H-bond for the PBE0 and mPWLYP functionals, respectively, for the clusters examined here) actually perform very well with the more complete aug-cc-pV5Z basis set (MAEs of 3.6 and 5.0 meV/H-bond for the PBE0 and mPWLYP functionals, respectively). The small and systematic overbinding due to the incompleteness of the MG3S basis set has also been pointed out by Csonka *et al.* [210].

### 3.4.5. Relevance to Other H-bonded Systems

It is important to know if the results and conclusions arrived at here are of general relevance to $H_2O$ molecules in other environments and to other types of H-bonded systems. Some parallels with DFT simulations of liquid $H_2O$ can be seen. It is generally found, for example, that (when everything else is equivalent) BLYP liquid $H_2O$ is less structured (i.e., the first peak of the O-O radial distribution function (RDF) has a lower maximum) than PBE liquid $H_2O$ [12, 19, 179–181]; consistent with the weaker HBs predicted by BLYP compared to PBE. Similarly, the first simulations of liquid $H_2O$ with hybrid DFT functionals (B3LYP, X3LYP, and PBE0) have recently been reported [19] and the trend in the position of the first peak in the O-O RDF can be interpreted as being consistent with the current observations. Specifically it was found (although the error bars are large because the simulations were short (5 ps)) that the position of the first peak in the O-O RDF moves to shorter separation upon going from B3LYP to X3LYP to PBE0, which is consistent with the small decrease of the O-O distances (Fig. (3.3(b))) and increase in H-bond strengths along this series (Table 3.1). Looking at other H-bonded systems with slightly stronger (for example, $NH_3 \cdots H_2O$) or slightly weaker HBs (for example, $NH_3 \cdots NH_3$) than those considered here it is known, for example, that PBE generally

overestimates these H-bond strengths slightly: PBE overestimates $NH_3 \cdots H_2O$ by ∼30 meV and $NH_3 \cdots NH_3$ by 6 meV [120]. Likewise, BLYP and B3LYP have been shown to underestimate a range of H-bonded systems by 20-30 meV/H-bond [119]. However, the general performance of X3LYP and PBE0 for other H-bonded systems has not been evaluated yet in any great detail with suitably large basis sets. In light of the present results it will be interesting to see how well these functionals perform for other H-bonded systems. Likewise mPWLYP and PBE1W are not widely used. Since they are pure GGAs (without any contribution from HF exchange) they will offer computational savings compared to X3LYP and PBE0, particularly for condensed phase simulations, and would thus be interesting to explore further for other H-bonded systems.

## 3.5. Summary

In summary, MP2 CBS values for the dissociation energies of small $H_2O$ clusters (dimer to pentamer) in their global minimum energy structures were computed. This data has been used to evaluate the performance of 16 DFT functionals. All DFT energies reported here have been obtained with an aug-cc-pV5Z basis set, which for DFT is sufficiently large to enable the true performance of each functional to be assessed, absent from significant basis set incompleteness errors. Among the functionals tested it is found that PBE0 and X3LYP perform best for the energetics of the HBs considered here; always being within 10 meV/H-bond of MP2. In terms of the structures X3LYP offers outstanding performance, predicting structures essentially identical to MP2 for all four clusters. Of the pure GGAs considered mPWLYP and PBE1W perform best. A small but non-negligible difference in the results obtained with PBE and PW91 has been identified, with PBE consistently being 12-14 meV/H-bond closer to MP2 than PW91.

In closing it should be noted that, although X3LYP and PBE0 predict the most accurate H-bond energies, it is important to remember that *all* functionals considered here do reasonably well. If, for example, one's definition of "good" is so-called chemical accuracy (1kcal/mol ≈ 43 meV/H-bond) then it is clear from Fig. (3.3(a)) that all functionals achieve chemical accuracy for all clusters. The problem is, of course, that for bonds as weak as HBs, chemical accuracy is a rather loose criterion since it amounts to around 20-30% of the total bond strength.

# 4. Water Hexamers: The Importance of van der Waals Interactions

## 4.1. Introduction

Having obtained the accurate performance of various DFT *xc* functionals for the equilibrium structures of the water dimer to pentamer, the study is extended to the water hexamers. The water hexamer is extremely interesting and warrants particular attention because it provides a critical test for DFT *xc* functionals. This is mainly because there are four distinct isomers of the water hexamers, which are energetically within 10-20 meV/$H_2O$ of each other. The isomers are known most commonly as the "prism", "cage", "book", and "cyclic" isomers (Fig. (4.1)). Which one has the lowest energy on the Born-Oppenheimer potential energy surface with or without corrections for zero point vibrations or the experimental ground state structure at finite temperature has been a matter of debate for some time [118, 159, 192, 199, 219–225]. This chapter is focussed exclusively on the question of the lowest total energy isomer without zero point corrections, for which a consensus from wave function based methods appears to have emerged recently in favor of the prism isomer as being the lowest energy structure [159, 192, 199, 224, 226]. How many of the widely used *xc* functionals such as PBE, BLYP, and B3LYP perform for the relative energies of these isomers remains unclear, although there are indications that these and other DFT *xc* functionals are likely to encounter problems for the hexamer [162, 178, 227, 228]. Other often cited reasons for being interested particularly in water hexamers are that they represent a transition from cyclic structures favored by smaller water clusters to 3D structures favored by larger water clusters. And, that water hexamers are believed to be important constituents of liquid water and known to be building blocks of various phases of ice [5].

In this chapter the ability of several popular *xc* functionals to describe the energies and structures of the four water hexamers mentioned above is addressed. Comparisons are made with reference data generated here with $2^{nd}$ order Møller-Plesset perturbation theory (MP2) at the complete basis set (CBS) limit. The total energy ordering (i.e., neglecting zero point energies and finite temperature effects) predicted by MP2 and DMC is the same and in the order prism<cage<book<cyclic. However, all popular and widely used *xc* functionals tested fail to predict the correct ordering of the isomers, instead, they opt for either the book or cyclic isomers as the lowest energy ones. This discrepancy is largely attributed to the inability of DFT to correctly capture the van der Waals (vdW) interaction between widely separated molecules in the clusters. By including a empirical $C_6R^{-6}$ correction we are able to explain the origin of the failure of the tested *xc* functionals and recover the correct energetic ordering between the different

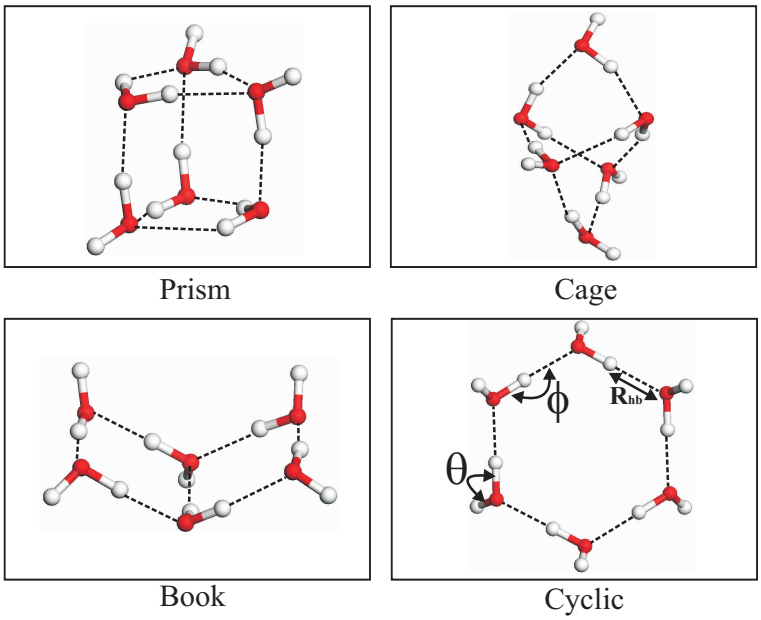


**Figure 4.1.:** Structures of the four isomers of the water hexamer considered here (obtained with MP2 and an aug-cc-pVTZ basis). The dashed lines indicate HBs, with the conventional number of HBs each cluster is assumed to have (prism = 9; cage = 8; book =7; and cyclic = 6). Some of the structural parameters discussed in the text are included alongside the cyclic structure.

conformers.

The remainder of this chapter contains a brief description of the computational details in section 4.2 and details of the DFT and MP2 results in section 4.3. Analysis with many-body decomposition and DFT+vdW dissociation energies are described in the following section 4.3.4 and 4.3.5. Conclusions are summarized in section 4.4.

## 4.2. Computational Details

In order to generate accurate MP2/CBS dissociation energies of the hexamers the same methodology is employed as described in chapter 3.2. To judge the performance of the DFT *xc* functionals a smaller subset of the tested functionals in chapter 3.3 is used here with same computational protocol. Dissociation energies per H-bond of the clusters are calculated as Eq. 5.4. and since the number of HBs is different for each isomer[1] dissociation energies per water are also calculated.

[1]For these hexamers it is invariably assumed that the prism, cage, book, and cyclic isomers have 9, 8, 7, and 6 H-bonds, respectively, [118, 192, 224]. In Fig. 4.1 these conventional H-bond numbers are used. However, it is interesting to note that upon inspection of the optimized MP2 and DFT structures of the four hexamers and employing several standard geometric definitions of HBs between water molecules it is found that the number of HBs counted depends sensitively on which definition is used.

### 4.2.1. van der Waals Correction

It is well known that most popular *xc* functionals generally show unsatisfactory performance for van der Waals (vdW) forces, which inherently arise due to non-local correlations [160, 229, 230]. An accurate and efficient estimation of vdW forces in conjunction with DFT *xc* functionals is not straightforward and is currently a matter of widespread discussion. Some of the approaches which have been popular with a certain degree of success for molecules as well as condensed phases are the following: (i) explicit addition of a pair-wise $C_6R^{-6}$ correction [231–234]; (ii) DFT *xc* functionals explicitly accounting for non-local correlation [235]; (iii) using maximally localized Wannier functions [236]; (iv) modified pseudopotentials [237]; and (v) interaction of the instantaneous dipole moment of the exchange hole [238].

Here the first method is employed, which is fairly simple, however, consistently accurate results have been obtained with the $C_6R^{-6}$ correction and it has a well established physical basis [239]. The $C_6R^{-6}$ correction method was early proposed for correcting HF calculations [240], and specifically applied to DFT by Wu and Yang [231], Grimme [232] and Jurečka *et al.* [233]. With this approach the pairwise vdW interaction ($E_{\text{disp}}$) is calculated by:

$$E_{\text{disp}} = -\sum_{j>i} f_{damp}(R_{ij}, R^0_{ij}) C_{6ij} R^{-6}_{ij} \quad , \tag{4.1}$$

where, $C_{6ij}$ are the dispersion coefficients for an atom pair $ij$, $R_{ij}$ is the inter-atomic distance, $R^0_{ij}$ is the sum of equilibrium vdW distances for the pair, and $f_{damp}$ is a damping function. The damping function is needed to avoid the divergence of the $R^{-6}_{ij}$ term at short distances and reduces the effect of the correction on covalent bonds. As used by many, a Fermi-type function $f_{damp}$ is chosen, which is given as

$$f_{damp}(R_{ij}, R^0_{ij}) = \left(1 + \exp(-d(\frac{R_{ij}}{S_r R^0_{ij}} - 1))\right)^{-1} \quad , \tag{4.2}$$

where $d$ determines the steepness of the damping function (the higher the value of $d$, the closer it is to a step function), and $s_R$ reflects the range of interaction covered by the chosen DFT *xc* functional [233].

The success of this approach solely relies on the choice of the parameters mentioned above and two different sets of parameters are used here. In the first set all the parameters are obtained from empirical fitting to some database. $C_6$ coefficients are taken from the work of Wu and Yang [231], which were empirically fitted to the accurate molecular $C_6$ coefficients. $R^0_{ij}$ values are taken from Bondi's vdW radii [241]. More precisely, for the atom pairs the following radii and vdW coefficients (in a.u.) are used: $R^0_{H-H} = 4.54$, $R^0_{O-O} = 5.74$, $R^0_{O-H} = 5.28$, $C_{6H-H} = 2.78$, $C_{6O-O} = 12.14$, and $C_{6O-H} = 5.67$. The value of $d$ was set to 20 and $s_R$ is 0.80 for BLYP, 1.00 for PBE and 1.03 for PBE0. These values of d and $S_r$ were obtained by fitting to the intermolecular binding energies

of the S22 database[2] at the CBS limit for all DFT *xc* functionals[3] In this case vdW corrected calculations were performed using plane-wave CPMD [242] code with hard pseudopotential of Goedecker *et al.* [150] with an energy cutoff of at least 200 Ry.

The second set of parameters employed is from the scheme by Tkatchenko and Scheffler (hereby denoted as TS) [234]. The major improvement in the TS scheme comes from the fact that $C_{6ij}$ and $R^0_{ij}$ coefficients can be derived self-consistently from DFT electron density. Thus, the $C_6$ coefficients become functionals of the electron density ($n$). This also allows subtle necessary variation in the $C_6[n]$ coefficients depending on the molecular environment without any empirical fitting. The scheme involves three key elements: (i) Hirshfeld partitioning of the electron density to calculate the *relative* polarizability of an atom inside a molecule; (ii) The use of very accurate reference free-atom static dipole polarizabilities and $C_6$ coefficients, calculated with converged wavefunction-based methods; and (iii) Accurate combination rules to derive heteronuclear $C_6$ coefficients from static dipole polarizabilities and $C_6$ coefficients of homonuclear atoms. The scheme, which turns out to be very accurate (5.6% mean absolute relative error on a database of 148 experimental $C_6$ coefficients), is implemented in the FHI-aims code [138]. It is found that this is particularly important for water clusters where H atoms participating in a H-bond can yield different values of $C_6$ and $R_0$ from those not involved in a H-bond (and from the values used in empirical schemes). The only parameter that needs to be fitted though for the choice of DFT xc functionals is $S_r$. The fitting is done again on S22 database [243] and optimized values of $S_r$ turned out to be 0.62, 0.94, and 0.96 for BLYP, PBE, and PBE0 functionals respectively. Calculations with this scheme are performed using the FHI-aims code [138] and NAO basis till *tier3*. Convergence tests of the NAO basis set is described in Appendix B.

Since three different basis sets (Gaussian, plane-waves, and NAO) are used, care has been taken about the convergence of the results using each of basis set and a comparison of the results using the three different basis sets is also illustrated in Appendix C.

## 4.3. Results

First, MP2 reference data are presented and discussed in comparison with CCSD(T) and diffusion Monte Carlo (DMC). Following this the accuracy of the 12 *xc* functionals are evaluated. Later, a many-body decomposition of the total dissociation energies as well as details of the importance of accounting for vdW forces are discussed.

[2] The S22 database contains several H-bonded, vdW bonded and mixed bonded dimer structures. More details can be found in Ref. [233].

[3] Also by fitting to reproduce the MP2 2-body energies of 48 dimers (obtained from four hexamers) starting from BLYP, parameters are scanned over the range $0.8 \leq s_R \leq 1.5$ and $20 \leq d \leq 40$. Interestingly, the set of parameters which yielded the smallest MAE for the 48 dimers are $s_R = 0.82$ and $d = 20$, which are nearly the same as those found from the S22 databse.

**Table 4.1.:** Dissociation energies of the four water hexamers obtained from various electronic structure approaches: MP2/CBS; diffusion quantum Monte Carlo (DMC) (Ref. [158]); CCSD(T)/CBS (Ref. [226]); 12 different DFT exchange-correlation functionals computed, unless indicated otherwise, with an aug-cc-pV5Z basis set; and HF at the CBS limit. The most stable isomer from each method is indicated in bold and the relative energies of the other isomers are given in parenthesis. Mean errors (ME) and mean absolute errors (MAE) in dissociation energies, averaged over the four hexamers in comparison with MP2 are also given. All structures were optimized consistently with MP2, HF and each DFT functional with an aug-cc-pVTZ basis set. DFT *xc* functionals are arranged here with increasing value of MAE from MP2. All values are in meV/$H_2O$ (1kcal/mol = 43.3641 meV).

| Method | Prism | Cage | Book | Cyclic | MAE | ME |
|---|---|---|---|---|---|---|
| MP2 | **332.3** | 331.9 (0.4) | 330.2 (2.1) | 324.1 (8.2) | — | — |
| DMC | **331.9** | 329.5 (2.4) | 327.8 (4.1) | 320.8 (11.1) | — | — |
| CCSD(T) | **337.6** | 336.1 (1.5) | 332.4 (5.2) | 324.4 (13.2) | — | — |
| PBE0 | 322.9 (8.0) | 325.3 (5.7) | **330.9** | 330.8 (0.1) | 5.9 | -2.1 |
| mPWLYP | 323.2 (10.4) | 325.9 (7.7) | **333.6** | 333.3 (0.3) | 6.9 | -0.6 |
| X3LYP | 317.2 (8.8) | 319.2 (6.8) | 325.8 (0.2) | **326.0** | 8.5 | -7.6 |
| PBE1W | 315.2 (6.9) | 314.8 (7.3) | **322.1** | 321.5 (0.6) | 11.3 | -11.3 |
| PBE | 336.1 (9.5) | 339.4 (6.2) | **345.6** | 344.1 (1.5) | 11.7 | 11.7 |
| B98 | 305.3 (7.3) | 306.8 (5.8) | **312.6** | 312.5 (0.1) | 20.4 | -20.4 |
| TPSS | 303.9 (12.8) | 302.8 (13.9) | 313.6 (3.1) | **316.7** | 20.4 | -20.4 |
| PW91 | 351.4 (10.2) | 354.7 (6.9) | **361.6** | 360.3 (1.3) | 27.3 | 27.3 |
| BP86 | 294.9 (13.6) | 297.4 (11.1) | **308.5** | 306.6 (1.9) | 27.8 | -27.8 |
| B3LYP | 294.4 (12.3) | 297.1 (9.6) | 305.1 (1.6) | **306.7** | 28.8 | -28.8 |
| XLYP | 287.9 (10.0) | 286.9 (11.0) | 296.3 (1.6) | **297.9** | 37.4 | -37.4 |
| BLYP | 273.6 (16.2) | 277.4 (12.4) | 287.5 (2.3) | **289.8** | 47.6 | -47.6 |
| HF | 222.9 (12.2) | 224.4 (10.7) | 230.6 (4.5) | **235.1** | 101.4 | -101.4 |

### 4.3.1. Reference Dissociation Energies: MP2

Following the procedure outlined above, MP2 dissociation energies at the CBS limit are obtained for the prism, cage, book, and cyclic hexamers of 332.3, 331.9, 330.2, and 324.1 meV/$H_2O$, respectively (see Table 4.1)[4]. Thus with MP2 the prism is the most stable structure and the energetic ordering of the isomers is prism<cage<book<cyclic. Note that this is consistent with the previous MP2/CBS study of the water hexamer reported by Xantheas *et al.* [192][5] The DMC calculations also have found the prism

[4] It is somewhat difficult to determine the precise "error bar" associated with calculated MP2/CBS estimates. However, as noted before (chapter 3) through comparisons of MP2/CBS and CCSD(T)/CBS, the error [due to MP2 (valence only) treatment of correlation, aug-cc-pVTZ structures, extrapolation to reach the CBS, etc.] is not likely to be more than 5 meV/H-bond.

[5] All the dissociation energies calculated here come within ∼1.3 meV/$H_2O$ of Ref. [192]. These differences are small. Most of it can be attributed to the use of different extrapolation methods. Applying

to be the most stable isomer and predict the same energetic ordering as MP2 [158]. Clearly, the cyclic is the least stable isomer while the prism and the cage isomers appear energetically very close as they only differ by about two standard errors. Moreover, the absolute dissociation energies obtained with MP2 are within 4 meV/$H_2O$ of DMC for all four clusters (Table 4.1). The sequence prism<cage<book<cyclic is also consistent with recent CCSD(T) calculations [159, 199], and the absolute binding energies from CCSD(T) [226] are some 1-6 meV/$H_2O$ larger than MP2/CBS dissociation energies calculated here. Therefore, it is clear that all the explicitly correlated wave function based methods [MP2, DMC, CCSD(T)] predict the same low energy structure – prism – and the same energetic ordering: prism<cage<book<cyclic. With this consensus from different methods now it seems that the question of which isomer is the lowest energy on the Born-Oppenheimer potential energy surface (in the absence of contributions from zero point vibrations) is resolved in favor of the prism, and that suggestions to the contrary are not correct [162]. There remain, of course, minor differences in the relative energetic ordering of some structures on the order of 5 meV/$H_2O$ [notably CCSD(T) predicts particularly unstable book and cyclic structures compared to MP2, with DMC being in between]. Resolving such small remaining differences is beyond the scope of the current study, which instead now focuses on how the various DFT functionals do in describing the energies and structures of these clusters.

### 4.3.2. DFT Dissociation Energies

Considering now the results obtained with the various DFT *xc* functionals, the key questions to be answered are: (i) if the DFT *xc* functionals tested are able to predict the correct energetic ordering of the four hexamer isomers; and (ii) what are the absolute errors in the total dissociation energies for each of the isomers. The answer to the first question is simple. All popular and widely used functionals tested fail to predict the correct minimum energy isomer. Instead of identifying the prism as the minimum energy conformer, all *xc* functionals tested either opt for the *cyclic* or *book* conformers (Table 4.1). This includes the X3LYP and PBE0 functionals, which, in the previous chapter, were identified as the most accurate *xc* functionals of those tested on the global minimum structures of small water clusters. It is somewhat discouraging that most of the *xc* functionals tested despite being immensely popular for liquid water simulations, fail to predict the correct low energy structure for a system as seemingly simple as six water molecules. However, the failure is not entirely unexpected given that according to the wave function methods all four structures are so close in energy (within 10-15 meV/$H_2O$).

With regard to the second issue of how well the functionals perform at predicting the absolute binding energies of the clusters, the best functionals are PBE0, mPWLYP, and

the extrapolation scheme used by Xantheas *et al.* [192] (extrapolating the dissociation energies with a 4, 5 polynomial and taking double-, triple-, quadruple, and pentuple-$\zeta$ values) the dissociation energies obtained by us (Xantheas) are 331.54 (331.45), 331.19 (330.94), 329.59 (329.63), and 324.19 (324.22) meV/$H_2O$ for the prism, cage, book, and cyclic, respectively. Thus when the same extrapolation scheme is used results agree to within 0.3 meV/$H_2O$.

X3LYP, producing mean absolute errors (MAE) averaged over the four clusters of 6, 7, and 9 meV/$H_2O$. PBE and PW91 produce errors of 12 and 28 meV/$H_2O$, respectively. B98 and TPSS both have a MAE of 20 meV/$H_2O$. B3LYP and BLYP under-bind by ∼29 and ∼48 meV/$H_2O$, respectively. All of these conclusions are largely consistent with the previous study on smaller water clusters (chapter 3).

Looking more closely at how the functionals perform for specific clusters, in Fig. 4.2(a) and 4.2(b) the difference between each functional and MP2/CBS ($\Delta D_e^n$) for all four isomers are plotted. Since each cluster nominally has a different number of HBs, and a general interest is also in the description of HBs, in Fig. 4.2(b) the error per H-bond for each of the clusters are plotted. Fig. 4.2 proves to be very illuminating and from it the following key conclusions are extracted: (i) Upon moving from the prism to the cyclic isomer (as plotted in Fig. 4.2), all *xc* functionals display a trend towards increased binding; (ii) Most functionals underbind the prism, with PBE and PW91 being the only exceptions; (iii) As shown before for the dimer to pentamer (chapter 3), here also BLYP performs consistently when the error per H-bond is considered, coming around ∼35 meV/H-bond off MP2. Likewise XLYP yields very similar errors for all four isomers when considered on a per H-bond basis. Later on these conclusions will be discussed further.

Another interesting finding is that the calculations on different water hexamers agree within 0.1 meV/$H_2O$ between the all-electron Gaussian03 and FHI-aims codes and within 1.5 meV/$H_2O$ between Gaussian03 and the pseudopotential plane-wave CPMD code (Table C.1). The latter value is most probably due to the difference in treatment of core electrons, however this difference is still very small for all practical purposes. This level of agreement is also achieved for the smaller clusters (dimer to pentamer) in their equilibrium geometries (Table C.1). This again reinforces that the basis sets employed here are sufficiently large to reflect the true performance of a given *xc* functional, absent of basis set incompleteness errors.

### 4.3.3. Geometry

Let us now consider the quality of the geometrical predictions made by the various *xc* functionals. The five key structural parameters of the $H_2O$ clusters (some of them are shown in Fig. 4.1) evaluate are: (i) The distance between adjacent oxygen atoms involved in a H-bond, $R_{O\text{-}O}$; (ii) The length of a H-bond, given by the distance between the donor H and the acceptor O, $R_{O\cdots H} = R_{hb}$ (Fig. 4.1); (iii) The H-bond angle, $\angle(O\cdots H\text{-}O) = \phi$ (Fig. 4.1); (iv) The internal O-H-bond lengths of each water, $R_{O\text{-}H}$; and (v) The internal H-O-H angle of each water, $\angle(H\text{-}O\text{-}H) = \theta$ (Fig. 4.1).

In Table 4.2, the MAE and ME of each *xc* functional compared to MP2 and averaged over all four clusters are reported. This provides a broad overview of how each functional performs, revealing that for structural predictions X3LYP is the most accurate functional. X3LYP outperforms all other functionals for almost all structural parameters considered with an average error of only 0.02 Å for the bond lengths and 0.5° for the bond angles. Considering the predicted O-O distances, on average, X3LYP, mPWLYP, PBE1W, TPSS, B98, B3LYP, BLYP, and XLYP predict slightly longer (0.008

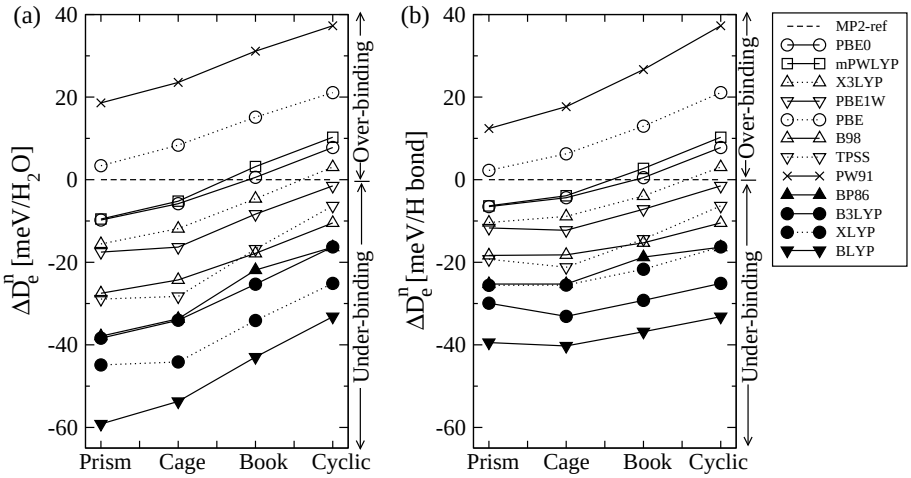


**Figure 4.2.:** Difference in the dissociation energy ($\Delta D_e^n$) in (a) meV/$H_2O$ and (b) meV/H-bond between the various DFT *xc* functionals and MP2. In (b) the generally accepted number of HBs in the prism, cage, book, and cyclic isomers of 9, 8, 7, and 6, respectively, have been used. Positive values correspond to an over-estimation of the dissociation energy by a given DFT *xc* functional. To note that the reference MP2 dissociation energies are at the CBS limit whereas for the DFT *xc* functionals an aug-cc-pV5Z basis set has been employed. Lines are drawn to guide the eye only.

to 0.082 Å) distances, whereas, PBE0, PBE, BP86, and PW91 produce slightly shorter O-O distances (0.017 to 0.034 Å). This conclusion also holds for the related quantity $R_{hb}$. For the O-H-bond length, $R_{O\text{-}H}$, on average all functionals perform reasonably well coming within 0.02 Å. In particular the results for X3LYP, PBE0, B98, and B3LYP are nearly identical to MP2. For the internal H-O-H angle $\theta$, the MAE from all the functionals is within $\sim$1.0°. Finally, for the H-bond angle, $\phi$, X3LYP, B3LYP, PBE0, and mPWLYP perform the best, all coming within 1.0°. For this quantity, however, several functionals exhibit quite large discrepancies. Specifically, XLYP, PBE1W, and TPSS yield average MAEs of 3.7°, 3.9°, and 6.0°, respectively. Going from cyclic to book to cage to prism, the H-bond angles in the clusters become increasingly non-linear (179° for cyclic, $\sim$160° − 170° for book, $\sim$152° − 166° for cage, and $\sim$135° − 168° for prism) and it appears that certain *xc* functionals struggle to reliably describe such non-linear HBs. Indeed closer inspection reveals that the largest errors in $\phi$ are encountered for the prism isomer. In this isomer there are two water molecules that are each involved in donating two hydrogen bonds (the molecules labeled *dd* for double donor in Fig. 4.3), and according to MP2 the HBs these molecules donate are very bent (i.e., values of $\phi$ $\sim$135°). Several of the *xc* functionals fail to describe these very non-linear essentially putative HBs, and for one or both of the waters in the prism sacrifice a single very non-linear H-bond to enable the other to become more linear and hence stronger (Fig. 4.3). TPSS fails for both double donor water molecules and PBE1W and XLYP fail to describe one of them. The limitations of functionals such as those considered here

**Table 4.2.:** Mean absolute error (MAE) of the various DFT functionals from MP2 for five different structural parameters, averaged over the four water hexamers examined here. The numbers in bold all have MAE $\leq$0.010 Å for bond lengths and $\leq$0.50° for bond angles. Mean errors (ME) are given in parenthesis. MP2 and DFT (and HF) structures were optimized consistently with MP2 and with each DFT functional (and HF) with an aug-cc-pVTZ basis set. The DFT+vdW structures were optimized with a numerical atom-centered basis set (FHI-aims code). The order of the DFT *xc* functionals is the same as in Table 4.1.

| | $\Delta R_{O\text{-}O}$ (Å) | $\Delta R_{hb}$ (Å) | $\Delta R_{O\text{-}H}$ (Å) | $\Delta\phi$ (°) | $\Delta\theta$ (°) |
|---|---|---|---|---|---|
| PBE0 | 0.023(-0.017) | 0.028(-0.018) | **0.002**(0.000) | 0.96(-0.01) | 0.69(+0.69) |
| mPWLYP | 0.021(+0.021) | 0.019(+0.008) | 0.013(+0.013) | 0.95(-0.25) | **0.49**(+0.49) |
| X3LYP | **0.009** (+0.008) | 0.012(+0.009) | **0.000**(0.000) | **0.48**(-0.29) | 0.98(+0.98) |
| PBE1W | 0.062(+0.045) | 0.096(+0.051) | 0.011(+0.011) | 3.98(-0.64) | **0.32**(+0.03) |
| PBE | 0.032(-0.019) | 0.055(-0.036) | 0.014(+0.014) | 1.87(+0.12) | **0.24**(+0.18) |
| PBE +vdW | 0.026 (-0.022) | 0.044(-0.039) | 0.012(+0.012) | 1.11(+0.26) | 0.21(+0.03) |
| B98 | 0.025(+0.025) | 0.028(+0.028) | **0.001**(-0.001) | 1.07(-0.20) | 0.66(+0.66) |
| TPSS | 0.094(+0.040) | 0.155(+0.058) | 0.011(+0.011) | 6.03(-0.87) | 0.58(+0.53) |
| PW91 | 0.039(-0.034) | 0.060(-0.051) | 0.014(+0.014) | 1.59(+0.15) | **0.36**(+0.33) |
| BP86 | 0.032(-0.026) | 0.055(-0.046) | 0.016(+0.016) | 1.65(+0.27) | **0.28**(+0.16) |
| B3LYP | 0.019(+0.019) | 0.020(+0.020) | **0.000**(+0.000) | 0.61(-0.28) | 0.89(+0.89) |
| XLYP | 0.092(+0.082) | 0.113(+0.091) | 0.011(+0.011) | 3.73(-0.99) | 0.52(+0.52) |
| BLYP | 0.039(+0.039) | 0.029(+0.028) | 0.012(+0.012) | 1.29(-0.20) | **0.39**(+0.39) |
| BLYP +vdW | 0.030 (-0.026) | 0.052(-0.044) | 0.013(+0.013) | 1.94(0.59) | **0.63**(+0.63) |
| HF | 0.165(+0.165) | 0.200(+0.200) | 0.026(-0.026) | 1.66(-1.39) | 1.62(+1.62) |

in describing non-linear putative HBs in water clusters has also recently been pointed out by Shields and Kirschner [166]. There it was argued that vdW dispersion forces are critical to the binding of such weak H-bond structures. More evidences will be shown below in support of the above statement.

### 4.3.4. Many-body Decomposition of The Dissociation Energies

To identify precisely where the problem with the DFT *xc* functionals lies in correctly describing the energetic ordering of the various isomers, a many-body decomposition of the total dissociation energies of the hexamers is performed. This has involved decomposing the total interaction energy within the clusters into 1-body, 2-body, $\cdots$, 6-body contributions. Such many-body expansions have before proved useful in understanding the binding in H-bonded clusters (including water clusters). A full description of the procedure involved can be found in Refs. [244–247]. Very briefly, the total 1-body en-

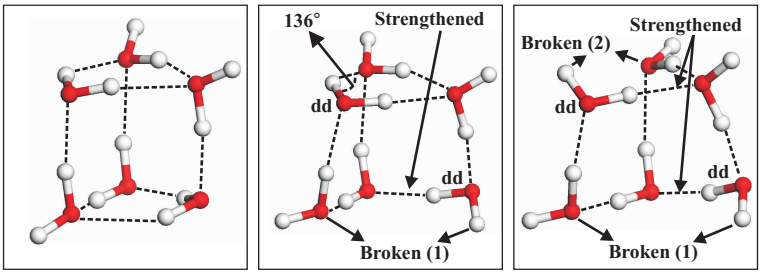


**Figure 4.3.:** Structures of the prism isomer optimized with MP2 and the PBE1W and TPSS *xc* functionals. Dashed lines indicate HBs. For PBE1W one H-bond is broken and for TPSS two HBs are broken, each broken H-bond being associated with a double donor (dd) water molecule. The other HBs which get stronger as a result of the bond breaking are also indicated. A very bent H-bond angle of 136° is also shown in the upper triangle of the PBE1W structure.

ergy is the energy cost incurred upon deforming all six monomers from the equilibrium isolated monomer structure to the structures they assume in a given hexamer. The total 2-body interaction energy is the sum of all possible dimer interactions within the hexamer, i.e., the total energy (gain) to form all possible water dimers within a given hexamer from each of its (deformed) monomers. The total 3-body interaction corresponds to the energy (gain) to form all possible trimer combinations (excluding dimer interactions inside the trimers), and so on for the 4-, 5-, and 6-body interactions. Such a many-body decomposition for the prism and cyclic conformers are performed, since the prism conformer is favored by the wave function approaches and the cyclic conformer is favored by many of the DFT *xc* functionals. The decomposition, the results of which are reported in Table 4.3, has been performed with MP2 (with an aug-cc-pV5Z basis set) and with the X3LYP, PBE0, and BLYP *xc* functionals. To enable an exact comparison between MP2 and the various *xc* functionals, absent of any contributions arising from the slightly different structures obtained with the different approaches, the MP2 geometries are used for all decompositions.

Let us first consider the MP2 reference data. For each cluster a small positive 1-body energy of ∼17 meV/$H_2O$ is observed. The 2-body interaction is attractive (negative) and at –244 meV and –283 meV/$H_2O$ for the cyclic and prism isomers, respectively, comprises by far the largest contribution to the many-body expansion. The 3-body interaction is also large and overall attractive: –84 and –64 meV/$H_2O$ for the cyclic and prism structures, respectively. Indeed because of their magnitude the 2- and 3-body interactions almost decide what the total dissociation energies are. The 4-, 5-, and 6-body terms are all considerably smaller. These results are consistent with those reported by Xantheas *et al.* [245] with a smaller basis set.

Turning attention towards the performance of the DFT *xc* functionals, first the two more accurate *xc* functionals are considered for which the many-body decomposition has been performed (PBE0 and X3LYP). For the 1-, 4-, 5-, and 6-body contributions, reasonably good agreement with MP2 is found. As said before, these terms are small

**Table 4.3.:** Many-body contributions to the total dissociation energies of the cyclic and prism isomers as obtained from MP2, X3LYP, PBE0, BLYP, and BLYP+vdW. For the MP2 many-body decomposition an aug-cc-pV5Z basis set is employed and so the total MP2 dissociation energies differ slightly from the MP2/CBS values given in Table 4.1. Likewise, to avoid complications from the slightly different optimized structures obtained from MP2 and the DFT *xc* functionals, the DFT many-body decompositions are performed on the optimized MP2 structures (with an aug-cc-pV5Z basis set for the DFT energies). Values in the parenthesis are the difference between each functional and the MP2 results. Negative values indicate a gain in energy, i.e., a net attraction when all the n-body interactions of a given class are summed up, and positive values a net repulsion. All values are in meV/$H_2O$.

| | | | **Cyclic** | | |
|---|---|---|---|---|---|
| | MP2 | X3LYP | PBE0 | BLYP | BLYP+vdW |
| 1-body | +16.6 | +12.9 (-3.7) | +16.5 (-0.1) | +2.4 (-14.2) | +2.0 (-14.6) |
| 2-body | -244.2 | -231.2 (+13.0) | -240.8 (+3.4) | -175.8 (+68.4) | -227.8 (+16.4) |
| 3-body | -83.6 | -92.1 (-8.5) | -92.8 (-9.2) | -97.7 (-14.1) | -97.7 (-14.1) |
| 4-body | -16.0 | -13.9 (+2.1) | -8.1 (+7.9) | -14.8 (+1.2) | -14.8 (+1.2) |
| 5-body | +0.5 | -1.7 (-2.2) | -6.4 (-6.9) | -1.9 (-2.4) | -1.9 (-2.4) |
| 6-body | -0.9 | +0.0 (+0.9) | +1.2 (+2.1) | +0.0 (+0.9) | +0.0 (+0.9) |
| Total | -327.6 | -326.0 (+1.6) | -330.4 (-2.8) | -287.8 (+39.8) | -340.2 (-12.6) |
| | | | **Prism** | | |
| | MP2 | X3LYP | PBE0 | BLYP | BLYP+vdW |
| 1-body | +16.7 | +14.4 (-2.3) | +17.3 (+0.6) | +3.4 (-13.3) | +3.2 (-13.5) |
| 2-body | -283.4 | -263.6 (+19.8) | -274.4 (+9.0) | -191.8 (+91.6) | -278.0 (+5.4) |
| 3-body | -63.8 | -61.3 (+2.5) | -59.3 (+4.5) | -79.3 (-15.5) | -79.3 (-15.5) |
| 4-body | -5.2 | -7.6 (-2.4) | -5.2 (0.0) | -2.8 (+2.4) | -2.8 (+2.4) |
| 5-body | -2.6 | +1.4 (+4.0) | -3.7 (-1.1) | +0.1 (+2.7) | +0.1 (+2.7) |
| 6-body | +2.2 | -0.1 (-2.3) | +2.5 (+0.3) | +0.1 (-2.1) | +0.1 (-2.1) |
| Total | -336.1 | -316.8 (+19.3) | -322.8 (+13.3) | -270.3 (+65.8) | -356.7 (-20.6) |

and the difference between MP2 and the two *xc* functionals is typically $\ll$8 meV/$H_2O$. For the (larger) 3-body terms variable performance is observed with overbinding (8-9 meV) for the cyclic isomer and underbinding (3-5 meV) for the prism. It is for the 2-body terms the largest deviations from MP2 is observed with a consistent underbinding for each functional and cluster. Both PBE0 and X3LYP underestimate the 2-body contribution in the prism isomer by 9 and 20 meV/$H_2O$, respectively. And for the cyclic isomer PBE0 and X3LYP underestimate the 2-body contribution by 4 and 13 meV/$H_2O$, respectively. It is interesting that these errors are noticeably larger than the 1-2 meV/$H_2O$ errors obtained with these functionals for the equilibrium water dimer [157]. Thus from the many-body analysis it is observed that *these* xc *functionals yield larger errors when describing the non-equilibrium dimer configurations present in the various water hexamers, compared to the equilibrium water dimer.* Upon inspection of the errors associated with the individual dimer configurations within the hexamers it is found that there is a systematic underbinding for dimers at intermediate separations (O-O distances $\sim$3.0 – 5.0 Å) typical of vdW bonded complexes and also for certain orientations of water molecules held together with very non-linear HBs. There are not enough distinct dimer configurations within the hexamers to allow us to understand the precise dependence of the 2-body error on orientation and H-bond angle. However, the distance dependence of the underbinding is more clear and is something that will be addressed now with a distance dependent vdW correction. Before moving it is noted that the BLYP errors from the many-body analysis are consistently larger compared to PBE0 and X3LYP, consistent with the generally inferior performance of this functional. However, the main conclusion from the many-body analysis that the 2-body terms are underbound (and are more poorly described than the equilibrium dimer) still holds. Recently it was pointed out that many DFT functionals grossly overestimate many-body interactions in vdW systems [248]. However, in the present case the combination of electrostatic and vdW contributions does not allow to clearly discern which part is responsible for the overbinding.

### 4.3.5. DFT+vdW Dissociation Energy

As mentioned earlier the inaccurate description of vdW interaction with standard *xc* functionals are well known. Knowing from the previous section that the 2-body interaction is underestimated with xc functionals here semi-empirical vdW correction is taken in to account as described in section 4.2.1. The dissociation energies of the four hexamers after applying the vdW correction with the PBE, PBE0 and BLYP functionals are shown in Table 4.4. Also the total vdW interaction within each hexamer is reported. One can see that the vdW correction is largest for the prism and cage structures and noticeably less for book and cyclic structures; favoring the prism or cage over the cyclic or the book structure. The new energetic orderings of the hexamers are thus in contrast to all pure DFT functionals, which predict the book or cyclic structures to have the lowest energy (Table 4.1), and in better agreement with the wave function based methods. The energy difference between the most stable and the least stable hexamers is also in reasonably good agreement with MP2 and DMC results (around 10-15 meV). Of the three func-

**Table 4.4.:** Absolute values of vdW interaction energies and vdW corrected total dissociation energies for the four water hexamers for three different *xc* functionals. The DFT structures employed are fully relaxed geometries calculated with the FHI-aims code (the CPMD code gives very similar numbers)For comparison the MP2/CBS results are also displayed. The energies of the most stable isomers are indicated in bold and the relative energies of the other structures with respect to the prism are given in parenthesis. MAE's in total dissociation energies are calculated from the MP2/CBS values averaging over the four hexamers. All numbers are in meV/$H_2O$.

| | **van der Waals interaction energy** | | | | |
|---|---|---|---|---|---|
| Method | Prism | Cage | Book | Cyclic | |
| BLYP+vdW | 93.8 | 90.5 | 75.8 | 60.7 | |
| PBE+vdW | 40.9 | 40.5 | 31.6 | 22.9 | |
| PBE+vdW-TS | 31.9 | 32.2 | 23.7 | 15.8 | |
| PBE0+vdW | 35.2 | 35.4 | 27.4 | 19.4 | |
| | **Total dissociation energy** | | | | |
| Method | Prism | Cage | Book | Cyclic | MAE |
| MP2 | **332.3** | 331.9 (0.4) | 330.2 (2.1) | 324.1 (8.2) | — |
| BLYP+vdW | **359.9** | 359.7 (0.2) | 356.3 (3.6) | 344.8 (15.1) | 25.5 |
| PBE+vdW | 377.8 | **380.1** (-2.3) | 377.8 (0.0) | 367.3 (10.5) | 46.1 |
| PBE+vdW-TS | 369.6 | **372.6 (-3.0)** | 370.6 (-1.0) | 360.7 (8.9) | 38.8 |
| PBE0+vdW | 360.6 | **361.9** (-1.3) | 359.2 (1.4) | 351.4 (9.2) | 28.6 |

tionals to which the correction has been applied, the BLYP+vdW method gives the best agreement with MP2. The MAE in the total dissociation energies for all four hexamers is reduced from 15% to 8%. And, moreover, the correct energetic ordering of the four isomers is recovered, i.e., BLYP+vdW predicts the sequence prism < cage < book < cyclic. The results for BLYP+vdW are encouraging, however, it is important to note that there remains an 8% error (a significant overbinding). In addition, the "success" of BLYP+vdW is achieved at the expense of a smaller $S_r$ parameter which shifts the vdW minima to quite short distances (see Fig. 4.4). Also, the three-body contribution of BLYP, unaffected by the pairwise vdW correction, shows substantial error. Thus, further investigation is required to rule out fortuitous error cancellation for BLYP+vdW. Nonetheless these findings for at least three different functionals support the suggestion that the origin of the incorrect prediction of the energetic ordering of the water hexamers lies in the absence of vdW dispersion forces in the functionals considered.

Results with the parameters obtained from TS scheme are also shown in Table 4.4. As with the empirical correction scheme, the prism and cage structures are favored over book and cyclic structures and it is encouraging that the overestimation in binding energies with PBE+vdW is reduced by 7-8 meV/$H_2O$ for all isomers. This reduction is due to

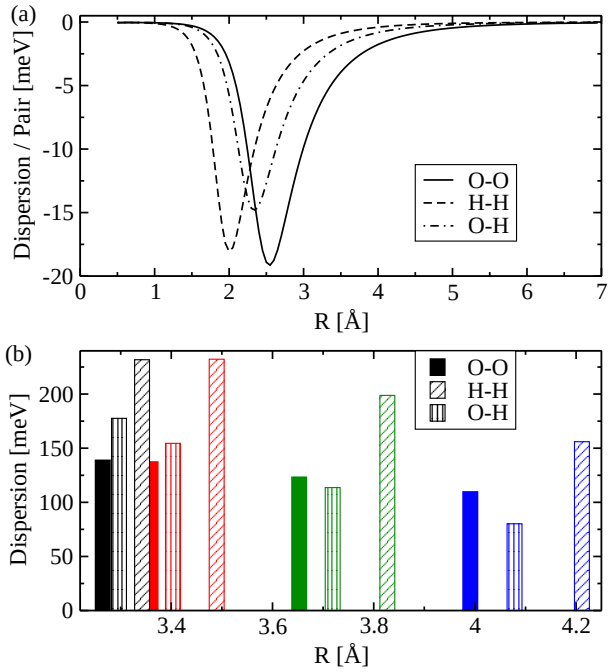


**Figure 4.4.:** (a) Variation in the dispersion contribution with distance from different atom pairs with parameters for BLYP. (b) Inter-molecular dispersion interaction for the four isomers as a function of the average inter-atomic distances of different atom pairs (on BLYP+vdW optimized structures). Here black, red, green, and blue refer to prism, cage, book, and cyclic isomers, respectively.

a larger effective vdW radius of the atoms participating in the HBs. This particular scheme is employed comprehensively in chapter 6.

Having identified a lack of vdW dispersion forces as being at the heart of the incorrect energy ordering of the various water hexamers, a detailed inspection is made to know why the $C_6R^{-6}$ correction scheme applied here works to alter the relative energies of the four isomers. Since the empirical BLYP+vdW scheme recovers the correct energetic ordering for the four hexamers a detailed analysis is carried out for this. First the functional form of the specific empirical dispersion corrections applied in these systems is considered. These are displayed in Fig. 4.4(a) for the three individual types of atom-atom interaction: O–O, O–H, and H–H. Dispersion forces are generally considered to be long range and indeed the tails of all three vdW curves extend to beyond 4 Å. However, the minima of the vdW curves with the specific parameters employed here are located at considerably shorter distances: ∼2.80, ∼2.20, and ∼2.55 Å for the O–O, H–H, and O–H curves, respectively. It is the location of these vdW minima relative to the structures of the various isomers that leads to the revised energetic ordering of the four isomers. In simplest terms the mean inter-molecular distances of the four clusters decreases upon going from cyclic to book to cage to prism and so the magnitude of

the dispersion correction decreases in the order prism to cage to book to cyclic, which ultimately leads to the correct stability sequence prism to cage to book to cyclic. Considering this in more detail in Fig. 4.4(b) the contributions to the total inter-molecular dispersion interaction in each cluster for each type of atomic pair interaction (O–O, H–H, and O–H) are plotted as a function of distance[6]. It can be seen from the histogram that the average inter-molecular O–O, O–H, and H–H distances steadily increase along the sequence prism-cage-book-cyclic and that likewise the dispersion contribution decreases. Further, noted that by simply summing up the contributions from each type of interaction in the hexamers it is found that the majority of the vdW correction comes from H-H interactions (∼44-48%), followed by the O-H (∼22-32%) and then the O-O (∼25-30%) interactions. The H–H interaction dominates simply because there are more of them. For brevity the results of similar analysis performed for the PBE and PBE0 vdW corrections are not shown. However, the general conclusion that the vdW dispersion contribution favors the more compact prism and cage isomers over the less compact book and cyclic isomers because the former are closer to the minima of the vdW curves than the latter also holds for the PBE and PBE0 vdW corrections.

## 4.4. Discussion and Conclusions

Having presented a lot of data obtained with various approaches, in the following the main results are summarized and discussed in a somewhat broader context. To begin, there is the reference data itself, which has been acquired with MP2 and from this it is concluded that the prism is the lowest total energy isomer for six water molecules in the absence of contributions from zero point vibrations. This conclusion agrees with the very recent DMC [158] and CCSD(T) results [158, 226]. There remain, of course, minor differences in the relative energetic ordering of some structures on the order of 5 meV/$H_2O$ [notably CCSD(T) predicts particularly unstable book and cyclic structures compared to MP2, with DMC being in between]. Again stressing that the ordering arrived at here, prism < cage < book < cyclic, is the ordering obtained in the absence of corrections for zero point contributions. It is known that zero point energies will alter the relative energy spacings with indications that the cage becomes the most stable isomer [222–224].

The main part of this chapter is concerned with using the reference data from the wave function based methods to evaluate the performance of several DFT *xc* functionals. A sub-set of the *xc* functionals previously tested for small water clusters [157] was considered. It was found that whilst certain functionals did a reasonable job at predicting the absolute dissociation energies of the various isomers (coming within 10-20 meV/$H_2O$), *none* of the functionals tested predict the correct energetic ordering of the four isomers, nor does any predict the correct lowest energy isomer. All *xc* functionals either predict the book or cyclic isomers to have the largest dissociation energies. There have been

[6]The total intra-molecular O-H and H-H dispersion contributions are 0.6 and $\sim 13 - 17$ meV, respectively. These are small compared to intermolecular contributions and remain almost constant for all the hexamers and for brevity are not shown in Fig. 4.4.

indications before that certain DFT *xc* functionals may not predict the correct lowest energy structure for the water hexamer. BLYP, for example, was long ago shown to favor the cyclic isomer [178]. Likewise X3LYP, B3LYP, and PBE1W have been shown to favor the cyclic structure [159, 161]. Here, it is shown that several other popular *xc* functionals fail to predict the correct lowest energy structure too, yielding results for relative energies that are unreliable and misleading.

Furthermore, by attributing the failure to an improper treatment of vdW forces it seems likely that many other semi-local and hybrid *xc* functionals which do not account for vdW in some way will also fail in this regard. By augmenting the BLYP functional with an empirical pairwise $C_6R^{-6}$ correction the correct energetic ordering of the four hexamers is recovered. Equivalent empirical corrections to other functionals (PBE, PBE0) also improves the ordering somewhat, favoring the prism and cage isomers over the book and cyclic ones. Of course there are other means of incorporating vdW dispersion forces implicitly into DFT *xc* functionals such as the approaches pioneered by Lundqvist and Langreth and Silvestrelli and others [235–238]. Subsequently, two independent works using Lundqvist and Langreth method and wannier function by Silvestrelli also reached to the same conclusion [249, 250]. Indeed on the general point of benchmarking and accessing the performance of existing and new *xc* functionals for the treatment of H-bonded systems, it seems that the water hexamer would be an appropriate test case to add to existing H-bond test sets since it presents a stern challenge for any *xc* functional. Reiterating that it is not suggested that all *xc* functionals which do not account for vdW forces in one way or another are likely to fail to predict the correct energy ordering for the water hexamer. Indeed Truhlar and co-workers have very recently reported that a few empirical hybrid meta-GGA functionals achieve the correct energetic ordering for the hexamers [159]. And, in agreement with Ref. [159] calculations with the M05-2X [251] functional with an aug-cc-pVQZ basis set also find the prism to be the lowest energy structure[7]. This looks like an exciting development but what the precise reason for the success of the functionals tested is remains unclear to us at present.

Finally, this chapter has focused on water clusters. Clusters often exhibit quite different properties from the corresponding bulk substance. However, it does not seem unreasonable to make some speculations about the relevance of the results presented here to DFT simulations of liquid water. As indicated in the introduction, the simulation of liquid water with DFT is by no means free from controversy [12, 17–19, 23, 179–181]. Of the many functionals tested for liquid water, BLYP appears to provide comparatively good agreement with experiment in terms of, e.g., the O-O RDF and diffusion coefficient [17]. However, precise quantitative agreement with experiment for BLYP or, indeed, any *xc* functional remains beyond reach. It seems likely that if an *xc* functional fails to predict the correct energetic ordering of the low energy isomers of the water hexamer then similar errors will exist in describing the many more competing configurations of water

[7] The M05-2X [251] functional with a larger basis set (aug-cc-pVQZ) also find the prism to be the lowest energy structure. Specifically, the dissociation energies are 353.5, 347.9, 339.9, and 333.1 meV/$H_2O$ for prism, cage, book, and cyclic, respectively.

clusters present transiently or otherwise in the liquid. Given that the hybrid *xc* functionals PBE0 and X3LYP also fail for the hexamer, despite otherwise predicting equilibrium H-bond strengths and structures for smaller water clusters in excellent agreement with MP2 it seems likely that these functionals may not offer the promise anticipated for liquid water [157]. Indeed a very recent PBE0 simulation for liquid water, which ran for a reasonably respectable 10 ps, found that the PBE and PBE0 RDFs were essentially indistinguishable [21]. Based on the forgoing results and discussion with unreliable results obtained for the hexamer the lack of a significant improvement in describing the liquid is not entirely unexpected. It can be suggested instead that density-functional methodologies which account for vdW dispersion forces are likely to offer more promise in the quest to improve the description of liquid water. Again very recent MD simulations of liquid water are consistent with this suggestion. Lin *et al.* have reported BLYP simulations for liquid water corrected with a similar $C_6R^{-6}$ correction scheme to the one employed here (but with a different damping function) as well as a separate account for vdW through the use of modified pseudopotentials [24]. These simulations indicate that (at the experimental density and temperatures tested) accounting for vdW forces lowers the peak maximum in the O-O RDF, and in so doing brings the experimental and theoretical RDFs into better agreement. However, others have suggested that dispersion interactions are not very important for liquid water under ambient conditions [252] and so it appears that considerably more work is needed to address this issue.

# 5. Water Clusters Extracted from DFT Liquid Water: The Importance of Monomer Deformations

## 5.1. Introduction

As already mentioned, DFT has been widely used to study liquid water. However, how well DFT with popular exchange-correlation (xc) functionals such as PBE [113] and BLYP [114, 116] performs in describing the structural and dynamic properties of liquid water is a matter of more than a little contention. The debates, which are numerous, have hinged on issues such as the radial distribution functions (RDFs) (in particular the O-O and O-H RDFs), diffusion coefficient, and average number of hydrogen bonds (HBs).

It is now clear that most standard DFT molecular dynamics (MD) simulations with PBE and BLYP predict an overstructured RDF compared to experiment. By overstructured, it is mainly meant that the first peak in the O-O RDF (referred to as $g^{max}_{\mathrm{O-O}}$) is higher than experiment. Consequently the computed diffusion coefficient is too small and the average number of HBs too large. Extended discussions on the magnitude and origin of the overstructuring can be found in, e.g., Refs. [10–32]. In brief, some of the relevant factors include: (i) The intrinsic error associated with a given *xc* functional (including an improper account of van der Waals forces [24, 32, 158]); (ii) The omission of quantum nuclear effects [39, 253–256]; and (iii) The simulation protocol, with relevant factors in this regard being: (a) number of water molecules in the simulation cell [22]; (b) the density of the water within the cell [13–15]; (c) basis set [16, 257]; (d) fictitious electron mass in Car-Parrinello MD simulations [258]; and so on. Since the first DFT MD simulation of liquid water in 1993 [38], important strides have been made to understand how each of the above factors impact upon the computed properties of liquid water. However, simultaneously addressing all issues that could account for the difference between the experimental and theoretical RDFs and diffusion coefficients is not practicable, not to mention the uncertainties that are present in the experimental data itself [8, 259, 260]. Therefore, it has become common to attempt to shed light on the performance of DFT *xc* functionals for treating water by investigating well defined gas phase water clusters for which precise comparison can be made to high level quantum chemistry methods. This approach has been useful and allowed the intrinsic accuracy of many *xc* functionals to be precisely established [119, 120, 153, 157–169], information that may be of relevance to liquid water.

With few exceptions [153, 165–168], previous gas phase benchmark studies of water

clusters have focussed on exploring equilibrium or other stationary point configurations of the gas phase intermolecular potential energy surfaces. However, in the liquid the structures of water clusters and even the water monomers themselves can be considerably different from those of gas phase clusters. For example, the distribution of intramolecular O-H bond lengths in the liquid ranges from ∼0.75 to ∼1.25 Å [8, 260]. Yet in gas phase water clusters such as dimers to hexamers O-H bond lengths deviate by <0.05 Å from the equilibrium water monomer O-H bond length of 0.96 Å [157, 158]. Whether or not the performance of DFT *xc* functionals obtained from gas phase studies on water clusters holds for the 'deformed' structures present in the liquid (referred to throughout this chapter as 'deformed') remains an important open question. Indeed there is already evidence that the benchmark reference data obtained from gas phase clusters does not easily translate to the liquid. For example, BLYP predicts a dissociation energy for the equilibrium gas phase water dimer that is 35 meV too small, yet at a water density of 1 g/cm$^3$ it predicts a $g^{max}_{\mathrm{O-O}}$ that is about 5%-15% too high. Similarly, PBE predicts the dimer dissociation energy to within 10 meV precision, yet yields an even greater $g^{max}_{\mathrm{O-O}}$ than BLYP. Related to this, MD simulations of liquid water have shown that the computed $g^{max}_{\mathrm{O-O}}$ can be considerably reduced if the O-H bonds in the water monomers in the liquid are held rigid at some predefined bond length. Specifically, Allesch *et al.* found that the PBE $g^{max}_{\mathrm{O-O}}$ decreased by ∼10% upon going from fully relaxed water monomers to a liquid with monomer O-H bonds fixed at ∼1 Å [261]. Likewise, Leung *et al.* have shown through a careful and systematic series of simulations that the length of the O-H bonds for rigid water MD simulations directly correlates with $g^{max}_{\mathrm{O-O}}$ [262]: as the intramolecular O-H bonds are allowed to lengthen, $g^{max}_{\mathrm{O-O}}$ increases.

The studies with rigid water and the realization that water monomer and cluster structures in the liquid are likely to differ considerably from gas phase water clusters has prompted to assess the performance of DFT *xc* functionals on water structures more representative of those present in the liquid. This chapter reports herein on the accuracy of three DFT *xc* functionals for various deformed monomers and dimers taken from a PBE simulation of liquid water. Two of the most popular generalized gradient approximation (GGA) *xc* functionals for liquid water simulations (PBE and BLYP) and one of the most accurate hybrid functionals for small water clusters (PBE0 [129]) are assessed here. As a reference, coupled cluster with single and double excitations plus a perturbative correction for connected triples [CCSD(T)] is used with energies extrapolated to the complete basis set limit (CBS). The CCSD(T) reference calculations reveal that 75% of the dimers extracted from within the first coordination shell of the liquid are unbound relative to two equilibrium (gas phase) water monomers. This is mainly due to the large deformation of the monomers inside the liquid compared to the gas phase equilibrium monomer structure. PBE and BLYP consistently underestimate the cost of the monomer deformation, specifically, O-H bond stretching. As a consequence, both PBE and BLYP systematically overbind the deformed dimers extracted from the liquid, by as much as 80 and 43 meV, respectively. These errors are much larger than the usual errors associated with these *xc* functionals for the gas phase equilibrium dimer (chapter 3). In general, the performance of PBE0 is superior to the two GGAs but

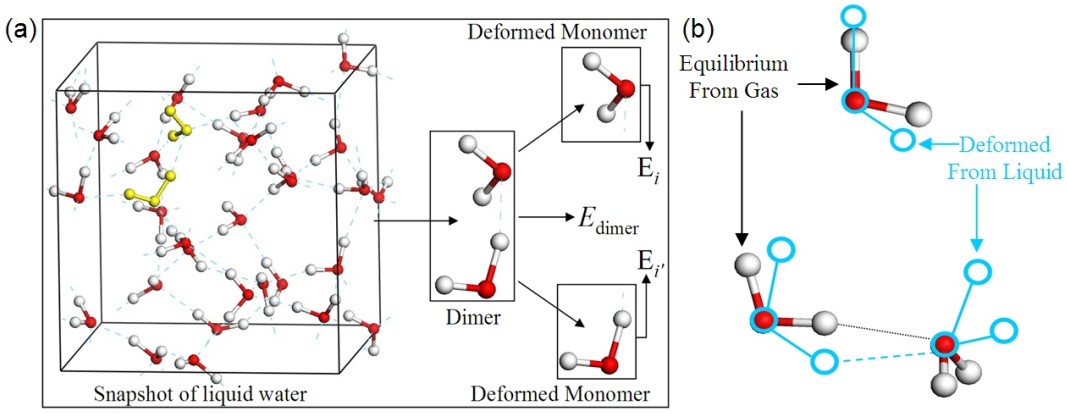


**Figure 5.1.:** (a) From a PBE MD simulation of liquid water, water dimers are extracted (e.g., the highlighted dimer in yellow). Single point energy calculations are then performed with CCSD(T), PBE, BLYP, and PBE0 on the deformed dimers ($E_{\mathrm{dimer}}$) and the constituent deformed monomers ($E_i$, $E_{i'}$). These energies are then used to evaluate the electronic dissociation energy of the dimers (Eq. 5.4) and the associated 1–body (Eq. 5.2) and 2–body (Eq. 5.3) energies. The deformation of the monomers compared to a gas phase equilibrium monomer is also quantified with (Eq. 5.1). (b) A schematic comparison of the structures of gas phase equilibrium monomers and dimers and cartoons of their deformed counterparts from liquid.

noticeable errors are identified for all functionals including PBE0 for the particularly long O-H bonds encountered at the shortest O-O separations. Although this study is restricted to monomers and dimers (and in a sense resembles a highly limited cluster expansion study of the liquid), the results reported here provide a possible explanation for the overstructured RDFs routinely observed in BLYP and PBE simulations of liquid water. The significance of these results to water in other phases and to other associated molecular liquids is also briefly discussed.

## 5.2. Methods, procedures, and definition of parameters

Several methods have been employed to study the water clusters examined here. Described below are some of the relevant computational details, how the water monomers and dimers are selected from the liquid, the definitions of the energetic, and structural parameters used in the subsequent analysis.

### 5.2.1. Liquid water

To generate water monomer and dimer structures representative of those present in liquid water a Born-Oppenheimer molecular dynamics simulation of 32 $D_2O$ molecules in a periodic cubic box of length 9.8528 Å was performed with the CPMD code [242]. The PBE *xc* functional was used along with hard pseudopotentials of Goedecker *et al.* [150] and an associated plane wave energy cut-off of 125 Ry. This simulation was run

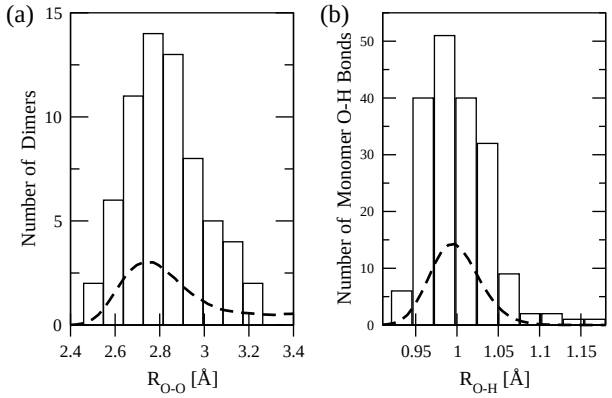


**Figure 5.2.:** (a) Distribution of the number of water dimers selected from the PBE MD simulation of liquid water (plotted as bars) as a function of the O-O separations ($R_{O-O}$) within the dimer. (b) Distribution of the number of O-H bonds for the water monomers selected from the liquid (plotted as bars). The dashed lines represent the corresponding O-O and O-H RDFs from the same PBE liquid water simulation. Only dimers within the first coordination shell of liquid water are considered here.

for 30 ps with an integration time step of 0.5 fs. A Nosé-Hoover chain thermostat[1] was used to maintain a target temperature of 330 K.

Water monomers and dimers were then extracted from the MD simulation. To get an uncorrelated sample of structures, 6-7 dimers were selected each 2 ps over the last 20 ps of the MD trajectory. In total 66 bonded dimers were selected (comprising 92 individual monomers). The criteria followed for selecting dimers were that: (i) they were from within the first coordination shell of the O-O RDF, i.e., all chosen O-O distances ($R_{O-O}$) are $\leq$3.4 Å; and (ii) the distribution of all 66 $R_{O-O}$ of the dimers resembles the O-O RDF for the first coordination shell. Fig. 5.2(a) illustrates that the distribution of dimers selected, which indeed resembles the computed O-O RDF from the MD simulation reasonably well. As an independent check it is found that the distribution in the values of the intra–molecular O-H bond lengths associated with all the selected water molecules is also in reasonably good agreement with the first peak of the computed O-H RDF of liquid water [Fig. 5.2(b)].

### 5.2.2. Clusters

The PBE water monomers and dimers extracted from the liquid water simulation were then examined with a few DFT *xc* functionals and CCSD(T). Throughout this study

[1] A thermostat is required to maintain a target temperature in a canonical (NVT) sampling. It is known that the standard Nosé-Hoover thermostat suffers from non-ergodicity problems for many cases and a chain of thermostats, namely Nosé-Hoover "chain" thermostat [263], assures ergodic sampling of the phase space. This is achieved by coupling (thermostatting) the original thermostat by another thermostat, which is coupled with another and so on. Also a chain of thermostats is more efficient in imposing the desired temperature. Here four such chains of thermostats are employed.

structures collected from the liquid water simulations are used for single point energy calculations with the various methods and no geometries are optimized, unless explicitly stated otherwise. The DFT calculations on the gas phase water monomers and dimers were performed with the GAUSSIAN03 code [200], using large Dunning correlation consistent aug-cc-pV5Z basis sets [264]. It is shown before (section 3.3) that for DFT *xc* functionals such as the ones considered here, this basis set is large enough to get dissociation energies within about 1 meV/$H_2O$ of the CBS limit [157]. Results from three *xc* functionals will be reported, specifically two GGAs that are widely employed in DFT simulations of liquid water (PBE and BLYP), and the hybrid PBE0 functional, which is one of the most accurate functionals in predicting the absolute dissociation energies of small gas phase water clusters (dimer to hexamer) [157, 158].

The CCSD(T) calculations were performed with the NWChem code [201] with localized Gaussian basis sets. Specifically, aug-cc-pVXZ basis sets (X = T, Q, and 5) were used and the resultant energies extrapolated to the complete basis set limit (CBS) with the same standard heuristic schemes as employed by us before [157, 158]. CCSD(T)/CBS is the theoretical 'gold standard' for systems of the size considered here and, in the following, differences between a given *xc* functional and CCSD(T) are referred to as errors with that *xc* functional. In total >600 CCSD(T) calculations have been performed for the reference data presented in this chapter.

### 5.2.3. Definition of Parameters

In order to quantitatively compare the structure of the molecules extracted from the liquid to a gas phase equilibrium monomer a quantity $S_d$, the deformation, is defined as,

$$S_d = \sqrt{\sum_N (\mathbf{R}_N - \mathbf{r}_N)^2} \quad , \tag{5.1}$$

where $N$ is the number of atoms, $\mathbf{R}$ and $\mathbf{r}$ denote the coordinate vectors of deformed and gas phase equilibrium monomer structures, respectively.

Several energy terms will appear repeatedly and it is also useful to define them here. The one-body energy ($E_{1b}$) of a water monomer is calculated as,

$$E_{1b} = E_i - E_{\text{equilibrium}} \quad , \tag{5.2}$$

where $E_{\text{equilibrium}}$ is the energy of the gas phase water monomer at equilibrium and $E_i$ is the energy of a deformed monomer. The two-body energy ($E_{2b}$) of a dimer is defined as:

$$E_{2b} = E_{\text{dimer}} - E_i - E_{i'} \quad , \tag{5.3}$$

where $E_{\text{dimer}}$ is the total energy of the dimer. The electronic dissociation energy ($D_e$) of the dimers is given by,

$$D_e = E_{\text{dimer}} - 2 \times E_{\text{equilibrium}} \quad . \tag{5.4}$$

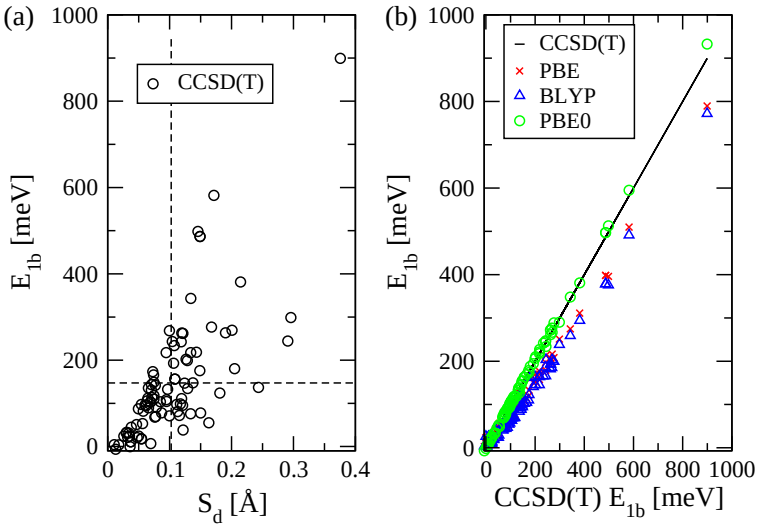


**Figure 5.3.:** (a) CCSD(T) one-body energy ($E_{1b}$) versus deformation ($S_d$) for water monomers taken from PBE liquid water. The horizontal and vertical dashed lines indicate the mean value of $E_{1b}$ and the mean value of the deformation, respectively. (b) Comparison of $E_{1b}$ of PBE, BLYP, and PBE0 with CCSD(T).

Fig. 5.1 schematically illustrates each of the above energetic quantities and the overall procedure used in this study. Since the structures considered here have been taken from a PBE liquid water simulation, $E_{\text{equilibrium}}$ is calculated with a PBE structure[2] The error conceded by the DFT *xc* functionals ($\Delta E$) in comparison to CCSD(T)/CBS is given as,

$$\Delta E = E_{\text{CCSD(T)}} - E_{\text{DFT}} \quad , \tag{5.5}$$

where $E_{\text{CCSD(T)}}$ and $E_{\text{DFT}}$ are energies obtained from CCSD(T)/CBS and DFT, respectively.

## 5.3. Results

Firstly, the water monomers extracted from the liquid are examined, focusing on the cost to go from the gas phase equilibrium monomer structure to the deformed structures present in the liquid. Following this the water dimers are considered. In each case the results of the various DFT *xc* functionals are compared to the CCSD(T)/CBS references.

[2]The choice of a PBE optimized monomer as the equilibrium monomer reference does not influence the general conclusions arrived at here. For example, if a CCSD(T) optimized monomer reference is used, the DFT $E_{1b}$ errors on average differ by no more than 5 meV from those reported.

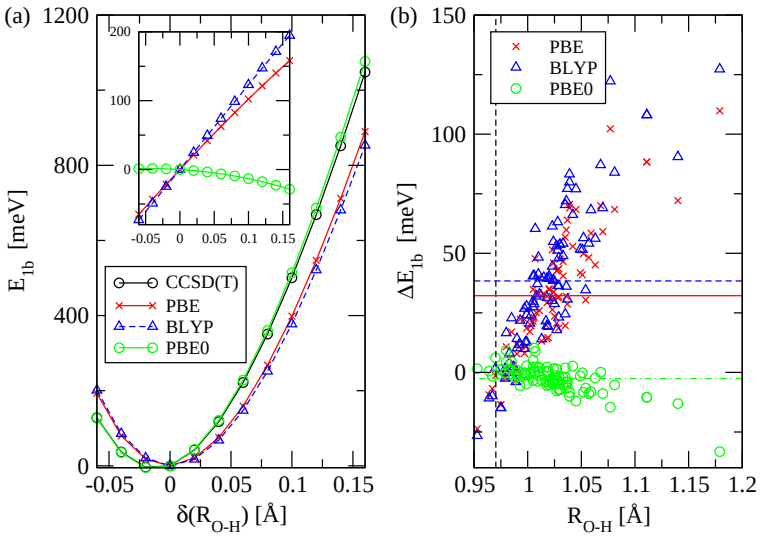


**Figure 5.4.:** (a) Variation in the one-body energy ($E_{1b}$) with the O-H bond lengths of a water monomer calculated with CCSD(T), PBE, BLYP, and PBE0. The inset shows the differences in $E_{1b}$ of the three *xc* functionals compared to CCSD(T). (b) Errors in $E_{1b}$ ($\Delta E_{1b}$) for the deformed monomers selected from liquid water as a function of the longest O-H bond of each monomer. The vertical dashed line indicates the gas phase equilibrium O-H bond length (0.97 Å) of a monomer (optimized with PBE) and the horizontal solid, dashed, and dash-dotted lines represent the average errors of PBE, BLYP, and PBE0, respectively. Here, a positive error of $E_{1b}$ indicates that it is too easy to stretch O-H bonds of the monomers with a given *xc* functional compared to CCSD(T).

### 5.3.1. Monomers

To begin, CCSD(T) was used to establish the relative energies of the monomers taken from the liquid compared to the gas phase equilibrium monomer, i.e., CCSD(T) $E_{1b}$ energies were computed for all 92 monomers. As can be seen from Fig. 5.3(a) these are distributed in a very large range from ∼0 to +900 meV with a mean value of +147 meV. Thus on average the monomers extracted from the liquid are 147 meV less stable than the gas phase equilibrium monomer, a surprisingly large energy. In quantifying the amount of deformation [Eq. (5.1)] for each monomer, as expected, a general increment in $E_{1b}$ is found with the extent of deformation [Fig. 5.3(a)]. The average deformation of the monomers is ∼0.1 Å, which is a measure of how deformed water monomers are in a PBE liquid water structure.

Considering now how the deformation energies computed with PBE, BLYP, and PBE0 compare to CCSD(T). This is shown in Fig. 5.3(b), a parity plot of $E_{1b}$ for the three *xc* functionals compared to CCSD(T). Immediately it can be seen that the performance of the GGAs is markedly different from the hybrid PBE0 functional. Specifically, for PBE and BLYP, $E_{1b}$ is systematically too small compared to CCSD(T). On average the PBE and BLYP deformation energies are 32 and 38 meV, respectively, smaller than

**Table 5.1.:** Computed harmonic vibrational frequencies for a water monomer. $\nu_1$ and $\nu_2$ are the asymmetric and symmetric O-H stretching modes and $\nu_3$ is the H-O-H bending mode. All values are in $cm^{-1}$ and calculated with an aug-cc-pVTZ basis set.

| | $\nu_1$ | $\nu_2$ | $\nu_3$ |
|---|---|---|---|
| CCSD(T) | 3921 | 3812 | 1648 |
| PBE | 3800 | 3696 | 1593 |
| BLYP | 3756 | 3655 | 1596 |
| PBE0 | 3962 | 3856 | 1633 |

that obtained from CCSD(T). The size of the error simply increases with the total CCSD(T) $E_{1b}$ [Fig. 5.3(b)] and for the largest deformations is on the order of 100 meV. Remembering that the monomer deformation is, of course, an endothermic process, smaller values of $E_{1b}$ therefore indicate that *it is too easy to deform monomers to their liquid structures with PBE or BLYP compared to CCSD(T).* In contrast to the GGAs, PBE0 produces $E_{1b}$ in excellent agreement with CCSD(T) with a mean error of only –3 meV. This small negative error reveals that it is marginally too expensive to deform the monomers to their liquid water structure with PBE0 compared to CCSD(T). Since the only difference between PBE and PBE0 is the 25% Hartree-Fock (HF) exchange in the latter, it can be conclude that the inclusion of exact exchange remedies the large error in $E_{1b}$ almost completely. Why this is so will be discussed in the section (5.4).

The monomers extracted from the liquid have both modified bond lengths and H-O-H internal angles. In order to understand in detail where the errors in $E_{1b}$ for the GGAs come from a simple series of tests are carried out, where bond lengths and the internal angle were varied independently. The tests show that the main error in the GGAs comes from the bond stretching. For example Fig. 5.4(a) shows that the symmetric stretching of the O-H bonds of a water monomer costs much less energy with PBE and BLYP compared to CCSD(T). The errors increase almost linearly with the stretching [inset Fig. 5.4(a)] and are as large as ∼200 meV when the O-H bonds are 0.16 Å longer than the gas phase equilibrium bond length of 0.97 Å. A bond stretch of 0.16 Å may sound like a lot but monomers with O-H bonds even as long as 1.18 Å are present in the PBE MD simulation and in experiment and in *ab initio* path integral simulations even longer O-H bonds are observed [39, 260]. As shown for the structures taken from the liquid, PBE0 is in very good agreement with CCSD(T) and even for the longest O-H bond of 1.18 Å comes within 34 meV of CCSD(T). In addition alterations of the H-O-H angle were considered but this makes much less of a contribution to the error in the *xc* functionals than what is found for bond stretching. For example, increasing (decreasing) the bond angle by 15° causes a maximum error of 15 meV (–8 meV) with BLYP and even smaller errors for the two other functionals.

The above tests establish that an inaccurate description of bond stretching is the main origin of the error in $E_{1b}$ for the GGAs. Returning to the structures taken from the

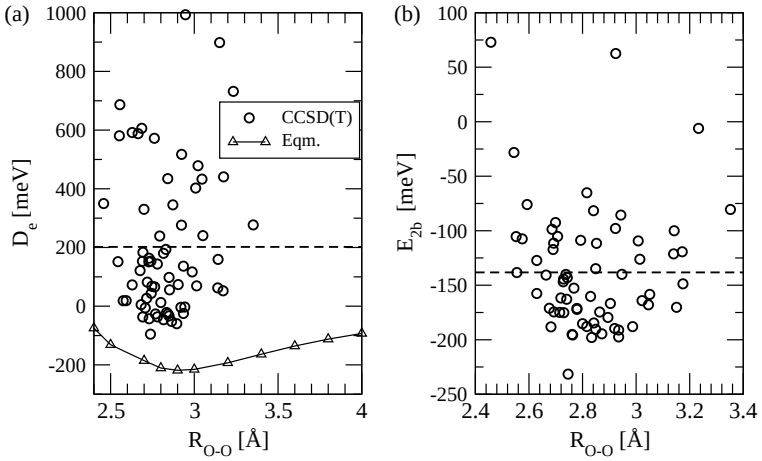


**Figure 5.5.:** (a) CCSD(T) total dissociation energies ($D_e$) of the water dimers taken from the PBE liquid water simulation and the dissociation energy curve for a fully optimized gas phase dimer (Eqm.) as a function of the O-O distance ($R_{O-O}$); (b) CCSD(T) two-body energies ($E_{2b}$) as a function of $R_{O-O}$ for the same dimers. The dashed lines represent the mean values of $D_e$ and $E_{2b}$ in panels (a) and (b), respectively.

liquid, therefore, in Fig. 5.4(b) the $E_{1b}$ error is plotted against the length of the longest O-H bond for each monomer. As with the systematic deformations of the equilibrium monomer, the errors in $E_{1b}$ increase almost linearly with the O-H bond length for the GGAs and for PBE0 they remain very close to zero except at the longest distances. Thus it can be inferred that monomers inside liquid water are energetically too easy to stretch for both PBE and BLYP. Also note that a careful series of tests taking water clusters from a BLYP MD simulation along with subsequent tests with CCSD(T) established that none of the conclusions arrived at here are altered if BLYP structures are used[3].

Another important observation made here is that the discrepancies established here between the three *xc* functionals and CCSD(T) correlate well with the errors in the computed harmonic vibrational frequencies of an isolated water monomer (Table 5.1). Specifically for the two stretching frequencies PBE and BLYP are ∼115 to ∼160 $cm^{-1}$ (∼3-4%) softer than CCSD(T) (Table 5.1), whereas, PBE0 is only ∼45 $cm^{-1}$ (∼1%) harder. This one to one correspondence between error in harmonic vibrational frequencies and $E_{1b}$ may also hold for other *xc* functionals and may therefore provide a cheap diagnostic to estimate in advance how reliably an *xc* functional will be at the determination of $E_{1b}$.

[3]To check if the computed errors in $E_{1b}$ from the *xc* functionals are sensitive to the functional used in the original MD simulation a separate 30 ps BLYP MD simulation was performed. From the BLYP simulation 12 monomers were extracted and average errors in $E_{1b}$ of 23 (PBE), 27 (BLYP), and -0.3 meV (PBE0) obtained, compared to average errors in $E_{1b}$ of 32 (PBE), 38 (BLYP), and -3 meV (PBE0) as obtained from the PBE MD simulation reported.

**Table 5.2.:** Mean values of the one-body, two-body, and dissociation energies of the deformed dimers (selected from the liquid) and the corresponding values for the gas phase equilibrium dimer with CCSD(T), PBE, BLYP, and PBE0. The differences between each DFT *xc* functional and CCSD(T)/CBS are given in parenthesis. Energies are in meV.

| | $D_e$ ($\Delta D_e$) | $E_{1b}$ ($\Delta E_{1b}$) | $E_{2b}$ ($\Delta E_{2b}$) |
|---|---|---|---|
| | | Deformed | |
| CCSD(T) | 201.9 | 339.2 | –137.2 |
| PBE | 121.9 (80.0) | 268.0 (71.2) | –146.1 (8.8) |
| BLYP | 159.3 (42.6) | 254.4 (84.8) | –95.1 (–42.1) |
| PBE0 | 200.7 (1.2) | 346.1 (-6.9) | –145.3 (8.1) |
| | | Gas phase equilibrium | |
| CCSD(T) | –211.6 | 9.7 | –221.4 |
| PBE | –219.9 (8.3) | 3.7 (6.0) | –223.6 (2.2) |
| BLYP | –178.7 (–32.9) | 2.4 (7.3) | –181.1 (–40.3) |
| PBE0 | –213.5 (1.9) | 9.7 (0.0) | –223.2 (1.8) |

### 5.3.2. Dimers

Now moving to the dimers extracted from the liquid, discussing first what CCSD(T) reveals about the stability of the dimers and then considering how well the three functionals perform. In Fig. 5.5(a) the CCSD(T) dissociation energies are plotted as a function of the O-O distance within each dimer. Also reported is the equilibrium (i.e., fully optimized) CCSD(T) dissociation energy curve for a gas phase water dimer. As expected the equilibrium dimer binding energy curve provides a lower bound for the dissociation energies of the deformed dimers, which at each particular value of $R_{O-O}$ exhibit a range of values reflecting the range of dimer structures in the liquid. More importantly, Fig. 5.5(a) provides an overview of the range of dissociation energies for water dimers found inside the first coordination shell of PBE liquid water. The range is large: from –95 to +993 meV, with the mean value being +201 meV. Indeed 75% of the dissociation energies are positive, i.e., 75% of the dimers are unbound compared to two gas phase equilibrium water monomers. Upon decomposing the dissociation energies into the one- and two-body contributions it is found that the average $E_{1b}$ is 339 meV and the average $E_{2b}$ is –137 meV (Table 5.2). Note that the average value of $E_{1b}$ for the dimers is, of course, about twice $E_{1b}$ for the monomers discussed above. Also note that this is a considerably larger $E_{1b}$ than for the gas phase equilibrium water dimer, which is only 10 meV (Table 5.2). The two-body energy gives the binding between the water molecules and 97% of the dimers have an attractive $E_{2b}$ [Fig. 5.5(b)]. The average value of $E_{2b}$ at –137 meV is somewhat smaller than the corresponding value for the gas phase equilibrium dimer of –221 meV. Since the total dissociation energy for the dimers is just

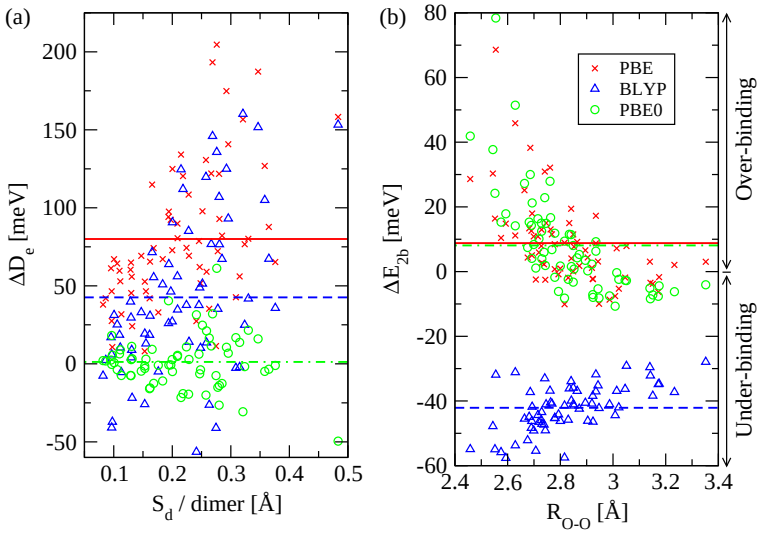


**Figure 5.6.:** (a) Errors in dimer dissociation energy ($\Delta D_e$) as a function of the sum of the deformation of the two monomers within each dimer for PBE, BLYP, and PBE0. (b) Errors in the two-body energy ($\Delta E_{2b}$) from PBE, BLYP, and PBE0 as a function of the O-O distance ($R_{O-O}$) within the dimers. Horizontal solid, dashed, and dash-dotted lines represent the average errors of PBE, BLYP, and PBE0, respectively.

the sum of $E_{1b}$ and $E_{2b}$, it is quite obvious therefore that $E_{1b}$ plays the major role in destabilizing the dimers.

Coming back to the performance of the *xc* functionals, Fig. 5.6(a) reports the error in the dissociation energies for each dimer. It can be seen that overall PBE0 performs very well, yielding an average error of 1 meV. BLYP and PBE, on the other hand, yield quite large average errors of 43 and 80 meV, respectively. This behavior differs significantly from how these two functionals perform for the gas phase equilibrium water dimer, where errors of only –33 and 8 meV are obtained (Table 5.2). Thus a key result is obtained that the performance of the two GGA functionals for the deformed dimer structures is inferior to what it is for the gas phase equilibrium dimer, with both functionals substantially overbinding the dimers taken from the liquid. Table 5.2 reports the key quantities that allow us to understand these results and why they contrast to the equilibrium gas phase dimers. As one might anticipate from section 5.3.1, the key is the one-body deformation energy. In the gas phase equilibrium dimer the absolute value of $E_{1b}$ is small (10 meV) and the resultant errors even smaller (Table 5.2). Thus the performance of a functional for the gas phase equilibrium dimer is dominated by $E_{2b}$, which is accurately described with PBE and PBE0 (8 and 2 meV errors, respectively) and underestimated by some 33 meV with BLYP. However, as it is shown for the structures taken from the liquid, $E_{1b}$ is large [339 meV from CCSD(T)] and the associated errors from the GGA *xc* functionals become significant. Specifically, since both BLYP and PBE predict that the one-body deformation energy is much too small and predict either too weak or about right two-

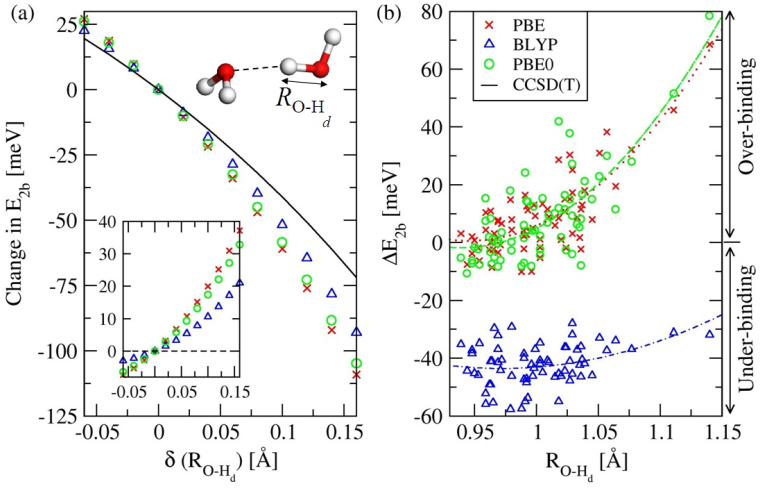


**Figure 5.7.:** (a) Compared to the gas phase equilibrium dimer, the change in the two-body energy ($E_{2b}$) obtained from the systematic variation of the covalent O-H bond of the donor 'H' atom [$\delta(R_{\mathrm{O-H}_d})$] keeping all other atoms fixed. The inset shows the difference ((CCSD(T)–DFT) between the DFT *xc* functionals and CCSD(T). (b) Error in the two-body ($E_{2b}$) energy from DFT compared to CCSD(T) as a function of the $R_{\mathrm{O-H}_d}$, obtained from the dimers from liquid water. Here positive values refer to a stronger two-body interaction. The dashed, dotted, and dash-dotted lines are quadratic fits to the PBE0, PBE, and BLYP data, respectively.

body energies [Fig. 5.6(b)] then the total dissociation energies come out too large. BLYP proves to be more accurate than PBE simply because of more favorable cancelations of errors in $E_{1b}$ and $E_{2b}$ (Table 5.2). Since BLYP is generally considered to produce too weak HBs between water molecules [119, 157, 161, 163] the overbinding observed here is remarkable. The obvious relevance of this finding to liquid water will be discussed below.

A characteristic feature of HBs between water molecules is that the covalent O-H bonds of the donor molecules ($R_{\mathrm{O-H}_d}$) are elongated [2]. The elongation is a result of charge transfer from the acceptor water molecule to the O-H $\sigma^*$ antibonding orbital of the donor molecule [265, 266]. Since it is found that it is too easy to stretch an O-H bond with the GGAs, one can anticipate that this will further influence the strength of the HBs formed and in particular $E_{2b}$. To investigate this, the gas phase equilibrium water dimer is revisited as a test case and systematically stretch the O-H$_d$ bond whilst keeping all other atoms fixed. Fig. 5.7(a) plots the change in $E_{2b}$ as a function of the O-H$_d$ bond length with CCSD(T) and the three *xc* functionals. Clearly all methods predict that as the O-H$_d$ bond increases so too does $E_{2b}$. However, all three *xc* functionals predict too rapid an increase compared to CCSD(T). This is best seen by the inset in Fig. 5.7(a) which displays the error in the change of $E_{2b}$ as a function of $R_{\mathrm{O-H}_d}$ compared to CCSD(T). Likewise, $E_{2b}$ increases slightly too rapidly with the three *xc* functionals for the dimers extracted from the liquid [Fig. 5.7(b)]; this is particularly apparent for PBE and PBE0. Thus in addition to it being too easy to stretch an O-H bond with

BLYP and PBE, for all three *xc* functionals the magnitude of the change in $E_{2b}$ upon stretching is too great, further contributing to the overbinding of dimers with long O-$H_d$ bonds.

## 5.4. Discussion

It is clear from the last section that, despite the $E_{2b}$ errors for the longest O-$H_d$ bonds, the overall performance of PBE0 is superior to that of the GGAs. To understand the origin of the difference between PBE and PBE0 the variation in the exchange and correlation energies was examined upon going from the gas phase equilibrium to the deformed water monomer structures (Table 5.3). The variations in DFT exchange and correlation energies are then compared with the full HF exact exchange and CCSD(T) correlation. It must be noted that the physical interpretation of exchange and correlation differs from DFT (PBE) to CCSD(T) and so use the data reported in Table 5.3 and Fig. 5.8 merely in the hope of obtaining some general qualitative insight. The basic finding from CCSD(T) is that upon going from the gas phase equilibrium to the deformed monomers there is a gain in the (negative) correlation energy and a loss in exchange energy [Fig. 5.8(a),(b)]. Naturally, the absolute change in the exchange energy is far greater than that in the correlation energy. The two DFT *xc* functionals predict a loss in the exchange energy but in contrast to CCSD(T) also a *loss* in the correlation energy, i.e., there is less correlation with PBE in the deformed monomers compared to the equilibrium monomer in the gas phase. Thus, in terms of the correlation energy, PBE/PBE0 predicts qualitatively different behavior from CCSD(T) upon bond stretching. However, the missing correlation in the deformed monomers is compensated for by differences from CCSD(T) in the exchange energy. In PBE0, which predicts exchange energies in better agreement with HF (CCSD(T)) [Fig. 5.8(b)], the missing correlation is compensated by missing exchange so that overall the total energy changes are very similar for PBE0 and CCSD(T). In PBE, however, the lack of correlation is not sufficient to compensate for the larger underprediction of the exchange energy [Fig. 5.8(b)]. Thus it is fond that PBE0 is superior to PBE simply because of a more favorable cancelation of the differences of exchange and correlation from CCSD(T) [Fig. 5.8(c)].

More generally the poor description of covalent O-H bond stretching observed here with PBE and BLYP is likely to apply to many other GGAs. For example, tests with RPBE, mPWLYP, and BP86 (on the 92 monomers taken from the current MD simulation) all produce one-body energies that are 30-40 meV smaller than CCSD(T). Similarly, as with PBE0, the hybrid functionals B3LYP and X3LYP predict rather accurate one-body energies, coming within 10 meV of CCSD(T). Of course the conclusion reached here that HF exact exchange is necessary for the proper description of covalent bond stretching is consistent with what has long been known in the context of covalent bond breaking (and transition state energies) in the gas phase (see, e.g., Refs. [267–271]).

Several previous studies have examined how DFT *xc* functionals perform in treating HBs between water molecules in water clusters [119, 120, 153, 157, 158, 161–168].

**Table 5.3.:** Average differences in the exchange and correlation contributions between the deformed monomers extracted from liquid water and the gas phase equilibrium monomer structure, obtained with CCSD(T), PBE, and PBE0. Note that the exchange contribution of CCSD(T) refers to HF exact exchange. Values in parenthesis are the differences between the two *xc* functionals and CCSD(T). Here positive and negative values indicate energy loss and gain, respectively. All values are in meV.

| | CCSD(T) | PBE | PBE0 |
|---|---|---|---|
| Correlation | –65.5 | +35.2 (–99.7) | +34.5 (–99.0) |
| Exchange | +825.6 | +681.9 (+143.7) | +722.7 (+102.9) |
| Total | 761.1 | 717.1 (+44.0) | 757.2 (+3.9) |

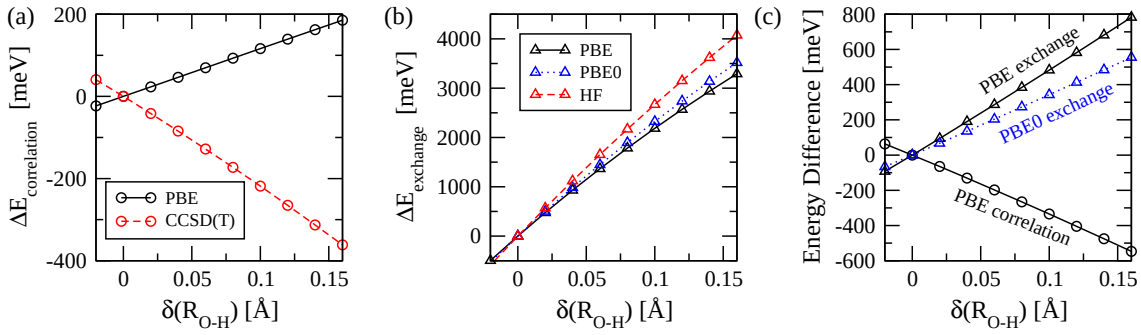


**Figure 5.8.:** Variation in (a) correlation energy ($\Delta E_{\text{correlation}}$) and (b) exchange energy ($\Delta E_{\text{exchange}}$) with O-H bond length for a gas phase water molecule. (c) Variation in the difference of DFT correlation and exchange energies in comparison to the CCSD(T) correlation and HF exact exchange energies, respectively, as a function of the monomer O-H bond length. Positive and negative values refer to energy loss and gain, respectively.

The study made here is somewhat unconventional that examined structures extracted directly from a liquid water simulation instead of exploring equilibrium gas phase structures. This has revealed significant differences in how PBE and BLYP perform for the structures extracted from the liquid compared to the known performance of these functionals for equilibrium gas phase water clusters. Thus it is shown that the behavior of these functionals for, e.g., the gas phase equilibrium water dimer is not a good indicator for how these functionals perform for dimers extracted from the liquid. One must always exercise caution in making connections between interaction energies of gas phase clusters and RDFs for the corresponding liquid phase, particularly in the present circumstances where only one– and two–body terms are considered. Nonetheless, it is plausible that the overbinding observed here for PBE and BLYP, which originates in $E_{1b}$ errors, is connected with the overstructuring of these functionals for liquid water. Indeed, because of the greater error cancelations between the one– and two–body energies calculated with

BLYP, the overbinding of the dimers from the liquid is less for BLYP than for PBE. This may again provide an explanation for why $g^{max}_{\mathrm{O-O}}$ is less in BLYP compared to PBE. This thinking may also explain the low value of $g^{max}_{\mathrm{O-O}}$ reported in MD simulations with the RPBE functional [25, 27]. A computed ∼50 meV underestimation of the $E_{2b}$ for a gas phase equilibrium water dimer suggests that the likely errors in $E_{1b}$ for this non-hybrid GGA will be more than compensated for. In addition, present results are consistent with and help to explain the results from the rigid water MD simulations [261, 262]. First, by fixing O-H bonds at or close to the gas phase monomer equilibrium O-H bond length, the $E_{1b}$ error is eliminated or greatly reduced. Second, the large $E_{2b}$ error associated with the longest O-$H_d$ bonds is also obviated.

Water molecules in other environments such as those in bulk ice or larger gas phase clusters will also possess deformed monomers with elongated bonds. These deformations are smaller than in liquid water but the effect is not negligible. For example, the average deformation of the monomers in a water hexamer is 0.05 Å with PBE optimized geometries and in bulk ice Ih PBE predicts an average deformation of ∼0.06 Å. Based on the approximate relation between $E_{1b}$ error and deformation established in Fig. 5.3, such deformations as encountered in small clusters and ice are likely to lead to errors in $E_{1b}$ of ∼30-40 meV.

Finally, the suggestion that too facile bond stretching may result in an overstructured liquid is likely to be of relevance to other associated liquids apart from water. The relevant experimental and theoretical RDFs of other associated liquids are not as well established as liquid water. However, there are indications of BLYP simulations yielding overstructured RDFs for, e.g., liquid ammonia [272, 273] and methanol [274, 275] despite BLYP underestimating the strength of the corresponding gas phase dimers by ∼45% compared to CCSD(T) [119].

## 5.5. Summary

In summary, from a PBE simulation of liquid water, monomers and bonded dimers (from the first coordination shell of the O-O RDF) were extracted. With CCSD(T) 75% of the dimers were shown to be unbound compared to two gas phase equilibrium water monomers. This is mainly because the structures of the water monomers inside the liquid differ significantly from an equilibrium gas phase monomer. Indeed, with CCSD(T) it is fond that the average monomer extracted from the PBE liquid is about 150 meV less stable than an equilibrium gas phase water monomer. Among the three *xc* functionals tested, the two GGAs (BLYP and PBE) underestimate the energy cost for monomer deformation (i.e., $E_{1b}$) and as a consequence BLYP and PBE predict dissociation energies that are too large by 80 and 43 meV, respectively, compared to CCSD(T). This is inferior to the performance of these functionals for the equilibrium water dimer and other water clusters in the gas phase. Overall PBE0 yields much more accurate dimer dissociation energies, mainly because it is not susceptible to such large bond stretching errors as the GGAs are. However, PBE0 is not free from deficiencies in treating the dimers examined here. Specifically, like the two other functionals, it predicts an increasing error in $E_{2b}$

for the longest O-$H_d$ bonds. Finally, the possible relevance of these results to DFT simulations of liquid water, to water in other environments, and to other associated liquids is discussed. In particular, it is suggested here that the overbinding identified here may provide an explanation for the overstructured RDFs observed in BLYP and PBE simulations of liquid water. However, more work is required to further test this suggestion, with, e.g., larger clusters that give access to higher order terms in the many-body decomposition and/or clusters embedded in an external electrostatic field that mimics the remaining water present in the liquid.

# 6. The Importance of van der Waals Forces in Crystalline Ice

## 6.1. Introduction

Following the observations made in chapter 4 that vdW (dispersion) forces are important to stabilize water hexamers, here the influence of vdW interactions in condensed phase water is investigated. In fact for decades it has been known that the condensed phases of water are held together through a combination of hydrogen bonds (HBs) and vdW forces. Whilst HBs have received widespread attention, relatively little is known about the importance of vdW forces. Partly this is down to the now most popular electronic structure theory (DFT) providing an inadequate description of vdW forces when standard exchange-correlation functionals are used (as discussed in chapter 4). However, improved semi-empirical vdW corrections to DFT [234] and the non-local vdW functional [235] mean that it is now possible to tackle this issue.

Here, simulations on a range of ambient and high pressure phases of ice are reported aiming at understanding the delicate interplay of HBs and vdW forces. It is found that the proportion of the lattice energy coming from vdW forces monotonously increases as the density of the ice phases increases, and as a consequence vdW forces play a crucial role in determining the relative stabilities of the high density phases of ice. In addition, calculations predict that the effective volume of the water molecules is reduced when vdW forces are accounted for. However, the absolute lattice energies are overestimated when dispersion corrections are added.

## 6.2. Methodology

### 6.2.1. Ice Structures

Several phases of ice are studied here, natural ice Ih, the proton ordered version of Ih, i.e., ice XI, and all the high pressure proton ordered phases of ice (Fig. 6.1), i.e., ice II, VIII, IX, XIII, XIV, and XV [276–280]. The unit cells of the ice phases are shown in Fig. 6.2. For proton disordered ice Ih the 12 water unit cell proposed by Hamman [281] is used. In addition independent checks have been done using a 96 water molecule unit cell (taken from Ref. [44]) with PBE and PBE+vdW *xc* functionals The lattice energies obtained from 12 and 96 water molecule unit cells are within 1 meV/$H_2O$) and equilibrium volumes are <0.01 Å$^3$/$H_2O$ for both PBE and PBE+vdW *xc* functionals. So in the following, the reported results of ice Ih are obtained using the 12 water molecule unit cell. In order to obtain the equilibrium lattice parameters with DFT *xc* functionals the primary

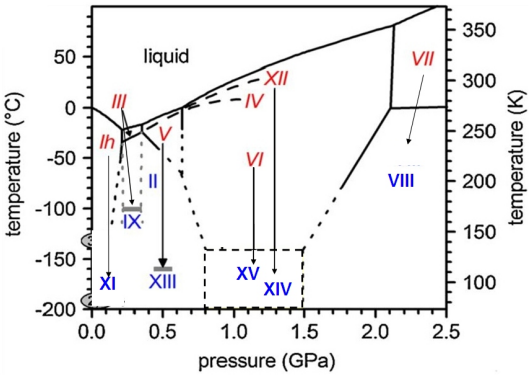


**Figure 6.1.:** Phase diagram of crystalline ice taken from Ref. [276]. Proton disordered phases are shown in red and proton ordered phases in blue. Arrows indicate proton disordered-ordered pairs.

structures are taken from experimental diffraction data and then the lattice parameters are modified isotropically[1] to obtain lattice energies as a function of the effective volume associated with each water molecule. The molecules in each cell were fully optimized and no symmetry constraints were applied. Then the Murnaghan equation of state was employed to obtain the equilibrium volume, lattice energy, and bulk modulus.

Monkhorst-Pack **k** point meshes are used [145] and depending on the unit cell the following **k** point meshes have been chosen: (i) unit cell with 8 water molecules: ice XI ($4 \times 2 \times 2$) and VIII ($3 \times 3 \times 2$); (ii) unit cell with 10 water molecules: ice XV ($3 \times 3 \times 3$); (iii) unit cell with 12 water molecules: ice Ih ($2 \times 2 \times 2$), IX ($2 \times 2 \times 2$), II ($2 \times 2 \times 2$), XIV ($2 \times 2 \times 4$); (iv) unit cell with 28 water molecules: ice XIII ($2 \times 2 \times 2$); and (v) unit cell with 96 water molecules: ice Ih ($1 \times 1 \times 1$). For all of the unit cells the spacing in the **k** point grid in each direction of reciprocal space is within 0.05 $\text{Å}^{-1}$ to 0.08 $\text{Å}^{-1}$. Such fine spacing is sufficient to ensure fully converged results for each of the ice phases considered.

### 6.2.2. Basis Set

All calculations are performed using the all electron full potential FHI-aims code [138], which uses numeric atom-centered orbitals (NAO) as a basis set. The convergence behavior of NAO basis sets with increasing number of basis functions have been carefully tested (see Appendix B) for the binding energy of the gas phase water dimer and the lattice energy of ice Ih. The dissociation energy obtained with a combination of *tier*3 basis for H and *tier*4 basis for O (denoted as $H_{T3}O_{T4}$) is within 1 meV of Gaussian/aug-

[1] Isotropic change refers that the ratios among the lattice parameters are kept fixed and it has been shown before that those ratios are affected negligibly with various *xc* functionals [57]. Also a thorough test has been done here on ice VIII and details are given in Appendix D.

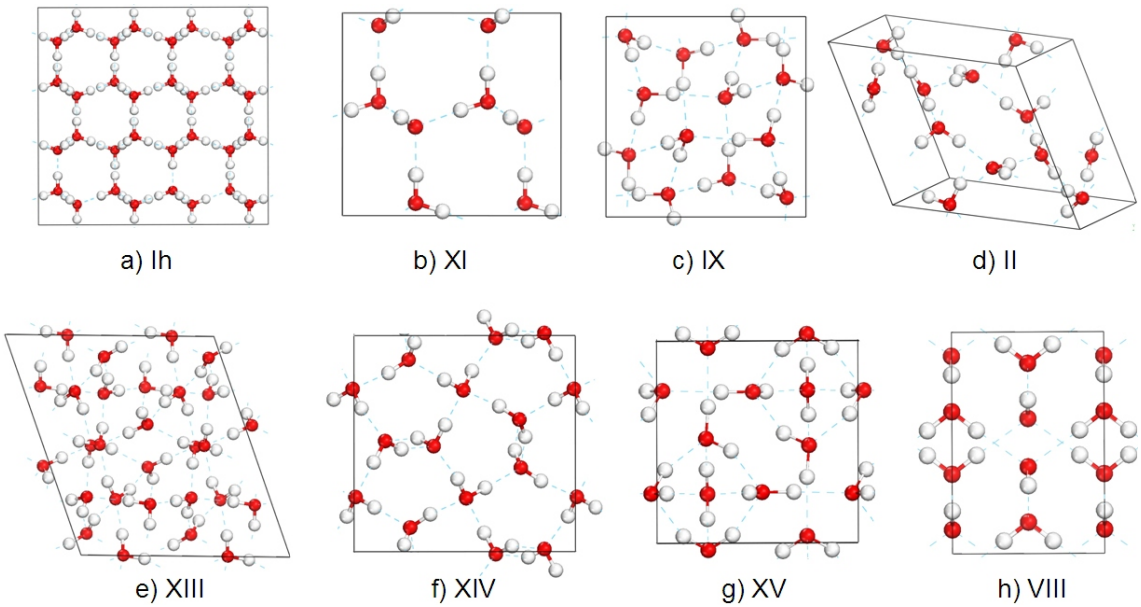


**Figure 6.2.:** Unit cells of all the ice phases studied. Ice Ih with 96 water molecules; ice XIII with 28 water molecules; ice IX, II, and XIV each contain 12 water molecules; and ice XI and VIII each contains 8 water molecules.

cc-pV5Z[2]. For the lattice energies of ice little smaller basis sets like *tier*2 for H and *tier*3 for O (denoted as $H_{T2}O_{T3}$) are reasonably accurate: within 2 meV/$H_2O$ of the energy obtained with $H_{T3}O_{T4}$. Also comparing with a recent study by Feibelman [57] on ice Ih with hard projector augmented wave (PAW) potentials and a 1400 eV plane wave cut off, lattice energy of ice Ih obtained with $H_{T2}O_{T3}$ NAO basis set is within 4 meV/$H_2O$. Thus in this chapter $H_{T2}O_{T3}$ NAO basis has been employed for all the ice calculations.

### 6.2.3. van der Waals Correction

To obtain vdW forces the scheme proposed by Tkatchenko and Scheffler (described in chapter 4) is employed here [234]. For all ice calculations $S_r = 0.94$ for PBE+vdW but a slightly modified value of 0.75 for BLYP+vdW (see Appendix E) are used.

## 6.3. Results

In this section equilibrium lattice energies and effective volume per water molecule are compared for different ice phases with and without corrections for vdW interactions to experimental values.

[2]In chapter 3 it was shown that for all electron DFT calculation with a Gaussian basis set of aug-cc-pV5Z quality the dissociation energy of the water dimer is essentially within 1 meV of the complete basis set limit.

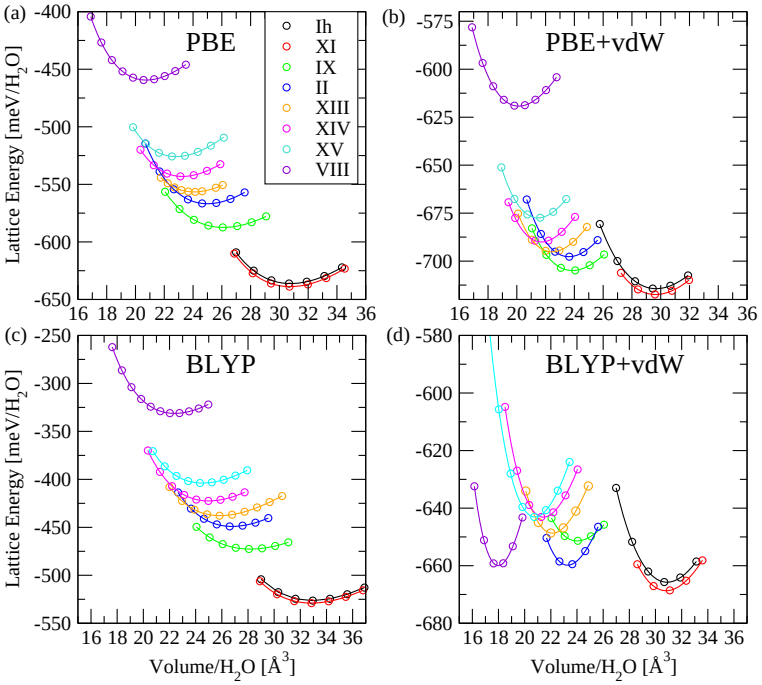


**Figure 6.3.:** Lattice energies of all the ice phases studied here are plotted as a function of volume per water. The Murnaghan equation of state was applied to obtain equilibrium volume and equilibrium lattice energies.

### 6.3.1. Equilibrium volume

To begin with, the choice of all these ice phases provides us with a wide range of densely packed structures from ice Ih to ice VIII. Accurate description of the relative energies and volumes of these phases is a stern test for any electronic structure approach. Fig. 6.3 provides the range of equilibrium volumes per water and the lattice energies for all the ice phases. Table 6.1 summarizes in descending order the experimental values of effective equilibrium volume per water of the ice phases and comparison to the calculated volumes with the DFT *xc* functionals.

Note here that our DFT equilibrium volumes are obtained at zero pressure and the comparisons will be appropriate only when the experimental volumes at zero or ambient pressure are considered. All of the experimental volumes given in Table 6.1 are found near ambient or zero pressure. In particular, this is important for the high pressure phases. For example, the experimental volume per water of ice VIII found at 2.4 GPa is $\sim$18.36 Å$^3$ [278], whereas it is $\sim$10% larger (20.09 Å$^3$) at zero pressure, as reported in Whalley's work [282]. In their corresponding original papers of ice XIII, XIV, and XV lattice parameters are reported at ambient pressure and 80 K [276, 280]. For ice II the volume found at ambient pressure and 4.2 K is taken [283]. For ice IX and VIII volumes reported in the paper by Whalley [282] at $\sim$100 K and zero pressure are chosen here.

**Table 6.1.:** Comparison of calculated equilibrium volumes ($Å^3/H_2O$) of various phases of ice with experiments. Percentage errors with respect to experimental volumes are given in parenthesis. MAE and ME are mean absolute error and mean error over all the ice phases with respect to experimental volume. Here positive and negative signs indicate larger and smaller volumes, respectively, compared to experiment.

| Ice | Expt. | PBE | PBE+vdW | BLYP | BLYP+vdW |
|---|---|---|---|---|---|
| Ih | 32.05 | 30.78 (-3.9) | 29.67 (-7.4) | 32.89 (+2.6) | 30.88 (-3.7) |
| XI | 31.98 | 30.75 (-3.8) | 29.64 (-7.3) | 32.85 (+2.7) | 30.81 (-3.7) |
| IX | 25.67 | 26.11 (+1.7) | 23.86 (-7.1) | 28.17 (+9.7) | 24.02 (-6.4) |
| II | 24.97 | 24.99 (+0.1) | 23.62 (-5.4) | 26.78 (+7.2) | 23.28 (-6.8) |
| XIII | 23.91 | 24.08 (+0.7) | 22.44 (-6.1) | 25.86 (+8.2) | 22.12 (-7.4) |
| XIV | 23.12 | 23.27 (+0.6) | 21.71 (-6.1) | 24.97 (+8.0) | 21.43 (-7.3) |
| XV | 22.53 | 22.82 (+1.3) | 21.47 (-4.7) | 24.52 (+8.8) | 20.79 (-7.7) |
| VIII | 20.09 | 20.74 (+3.2) | 20.13 (+0.2) | 22.38 (+11.4) | 17.98 (-10.5) |
| MAE | | 1.94 | 5.57 | 7.30 | 6.60 |
| ME | | -0.04 | -5.52 | -7.30 | -6.60 |

It is encouraging that both *xc* functionals with and without the vdW correction find the correct trend in the equilibrium volumes for ambient to high pressure phases as observed in the experiments. However, there are significant discrepancies with experiment concerning the absolute values of the volumes. PBE underestimates the equilibrium volume of ice Ih and XI by ∼4% which is known from previous studies (e.g., Ref. [57]) but for most of the high density phases it produces volumes in slightly better agreement with experiment. It is also noticeable that contrary to ice Ih, PBE predicts larger volumes for the high pressure phases, indicating qualitatively different behavior and (unusual for PBE) weaker binding between water molecules. Especially, for ice VIII the PBE volume is 3.2% larger than experiments. On the other hand, BLYP, which is known to predict much weaker HBs, not surprisingly overestimates the volumes largely for all the phases and the performance is particularly bad for the high density phases with the errors in the equilibrium volume being ∼10%.

When vdW interactions are included explicitly with PBE and BLYP, significant reductions in the equilibrium volumes are found for all the ice phases. Going from PBE to PBE+vdW the equilibrium volumes get reduced by 3.6% for ice Ih and XI and ∼3-9% for the high pressure phases. A similar trend is also observed with BLYP+vdW, where the vdW effect is much stronger making a reduction from ∼6% (ice Ih, XI) to as large as ∼20% (ice VIII). This so far clearly indicates that at high pressure the role of vdW interactions is much larger. In comparison to the experimental volumes, the vdW corrected volumes are still much smaller. With PBE+vdW it is 0.2-7.4% and with BLYP+vdW it is 3.7-10.5%. It is also found that upon inclusion of vdW the mean absolute errors

**Table 6.2.:** lattice energies of ice Ih and all proton ordered phases of ice. Relative lattice energies with respect to ice Ih are given in parenthesis. All values are in meV/$H_2O$.

| Ice | Expt. | PBE | PBE+vdW | BLYP | BLYP+vdW |
|---|---|---|---|---|---|
| Ih | 600±10 | 636 (0) | 714 (0) | 526 (0) | 666 |
| XI | | 639 (+3) | 717 (+3) | 529 (+3) | 669 (+3) |
| IX | (-3.5) | 587 (-49) | 705 (-9) | 473 (-53) | 651 (-15) |
| II | (-0.6) | 567 (-69) | 698 (-16) | 449 (-77) | 660 (-6) |
| XIII | | 556 (-80) | 695 (-19) | 438 (-88) | 649 (-17) |
| XIV | | 543 (-93) | 690 (-24) | 422 (-104) | 643 (-23) |
| XV | | 526 (-110) | 678 (-37) | 404 (-122) | 643 (-23) |
| VIII | (-32.8) | 459 (-179) | 619 (-95) | 331 (-195) | 660 (-6) |

(MAE) in the equilibrium volumes do not really improve, in fact for PBE+vdW the volumes get worse than PBE. However, a major improvement is observed with DFT+vdW for the relative stabilities of the high pressure phases, which is reported in the following section.

### 6.3.2. Lattice energy

Table 6.2 summarizes the lattice energies of the ice phases obtained from each of the xc functionals and available experimental results for some of the phases. The experimental lattice energy of ice Ih (600 meV/$H_2O$) is taken from Ref. [284], which was corrected for inter- and intra-molecular vibrational energies, so it can be directly compared with calculated DFT lattice energies, where zero point energy (ZPE) is not included. Also Whalley *et al.* [282] provides the experimental lattice energies of ice IX, II, VIII relative to ice Ih and more importantly energies were extrapolated to absolute zero temperature and pressure. In this case the employed experimental lattice energy value of ice Ih is 491 meV/$H_2O$, which does not have the experimental ZPE removed. But it is still useful to compare the relative energies of those phases (ice IX, II, VIII) since ZPE corrected relative energies will differ by no more than 10 meV/$H_2O$.

Coming to the performance of DFT, PBE yields a 36 meV/$H_2O$ larger lattice energy of ice Ih than the experimental value of 600 meV/$H_2O$ and BLYP yields a lattice energy that is 74 meV/$H_2O$ too small. However, with both PBE and BLYP the high density phases are much more unstable relative to ice Ih than what is observed experimentally. For example, the lattice energy of ice VIII is 179 and 195 meV/$H_2O$ smaller than ice Ih and the experimental value for the same is only ∼33 meV/$H_2O$. A similar trend of much less stability is also observed for ice IX and ice II. Even though absolute lattice energies obtained with PBE and BLYP differ by more than 100 meV/$H_2O$, the relative lattice energies of all high pressure phases (with respect to ice Ih) are similar (within 20 meV/$H_2O$ from two functionals). This indicates that a probable source of the inferior

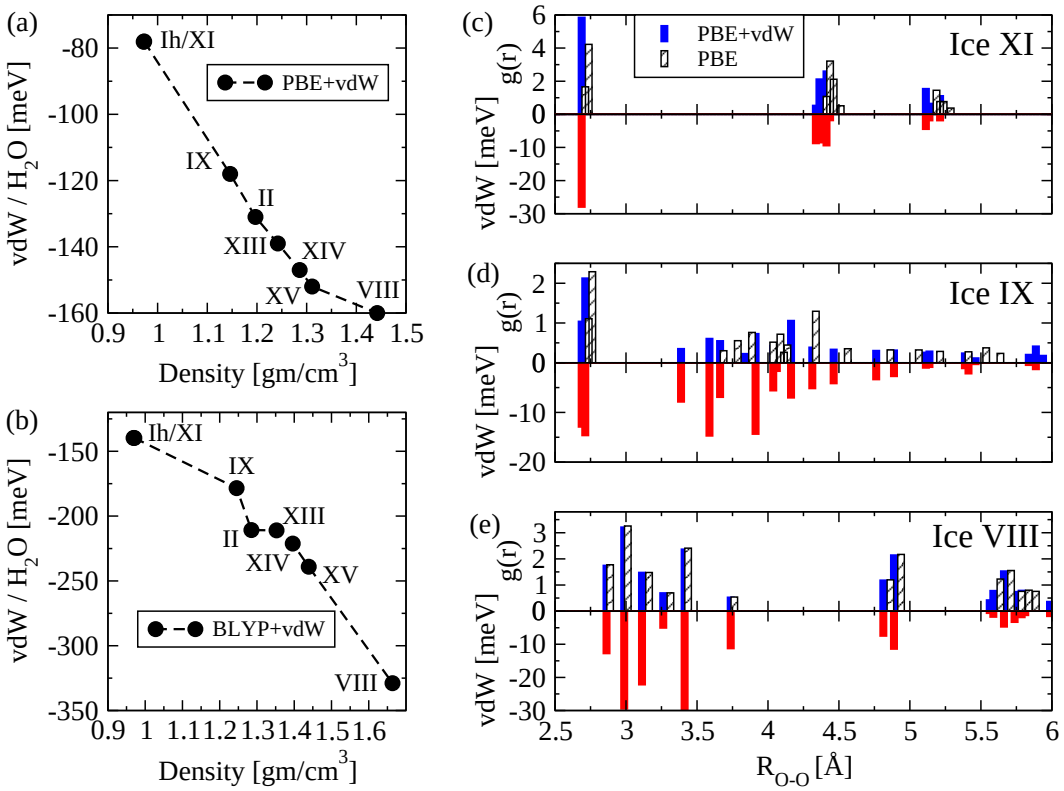


**Figure 6.4.:** Variation in the vdW energy contribution as a function of equilibrium density of various ice phases with (a) PBE+vdW and (b) BLYP+vdW. (c) Upper half is showing the O-O radial distribution functions obtained from PBE and PBE+vdW optimized geometries of ice XI and the lower half provides the corresponding vdW energy contribution from each coordination shell of the PBE+vdW optimized geometry. The same is shown for ice IX in panel (d) and for ice VII in panel (e).

performance in the high density phases is the lack vdW interactions, which is known to be absent from both PBE and BLYP. This would also explain the larger equilibrium volumes observed in the previous section with PBE.

Now with vdW interactions included substantial improvements are observed in the relative lattice energies of the high density phases. In particular, ice VIII is now 95 and 6 meV/$H_2O$ less stable than ice Ih with PBE+vdW and BLYP+vdW, respectively. This is in much better agreement with experiment (33 meV/$H_2O$). Also the relative lattice energies are much improved for ice II and ice XI with both vdW corrected functionals. This indicates that vdW interactions are important in stabilizing the higher density phases. Indeed it is found here that energy contribution from vdW dispersion increase monotonously with increasing density of the ice phases (Fig. 6.4(a) and 6.4(b)). Despite the encouraging results, the absolute values of the lattice energies obtained from both vdW corrected functionals are largely overestimated (Table 6.2).

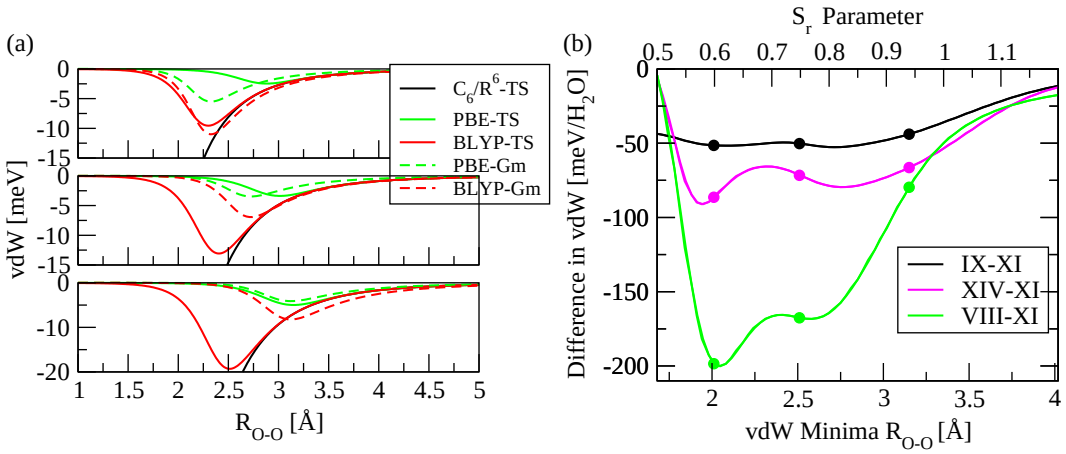


**Figure 6.5.:** (a) vdW energy contributions obtained from H-H, O-H, and O-O atom pairs for ice XI as obtained with the Tkatchenko and Scheffler (TS) scheme and Grimme's parameters (Gm) [232]. (b) Differences in the vdW energy contributions found in high density phases (ice IX, ice XIV, and ice VIII) with respect to low density phase ice XI as a function of the minima in the O-O vdW potential (bottom X axis) and $S_r$ parameter (top X axis)

Further analysis of the ice structures and the trend in the vdW energy contribution from pairwise interaction explains the enhanced stability of the high density phases. In the high density phases (e.g., ice IX and VIII) the water molecules in the second and third coordination shells are much closer than in the low density phases like ice XI. This is illustrated in Fig. 6.4 with the O-O radial distribution function (RDF). The reduction in the effective volume per water with vdW correction is reflected by the shift in the peak positions in the O-O RDF towards shorter O-O separation. In ice each water molecule is connected via HBs with surrounding water molecules sitting inside the first coordination shell (within 3 Å)[3], whereas, the water molecules situated in the second coordination shell and beyond are clearly not H-bonded and the interactions are more vdW like. It can be said that within the first few coordination shells the number of water molecules which interact via vdW is greater in the higher density phases compared to the lower density phases. The vdW dispersion energy contributions from each of the coordination shells are plotted in Fig. 6.4 and it can be seen that the vdW interactions are larger when 2.75 Å $< R_{O-O} <$ 4.5 Å. This is mainly because more water molecules are present in that range in the high density phases than in the low density phases. Also the sum of the vdW dispersion energies within $R_{O-O} <$ 6 Å contributes more than 85% of the total vdW energy contributions obtained from the periodic calculations, thus the major difference in the vdW contribution in low and high density phases come from within 6 Å.

So far it has been shown that accounting for vdW dispersion forces increase the sta-

[3]Ice VIII is an exception, where two non bonded water molecules are present within the first coordination shell. This corresponds to the first smaller peak in the RDF.

**Table 6.3.:** Comparison of calculated $C_6$ coefficients (in Hartree-bohr$^6$) and effective vdW radii (in Å) of H and O atoms in three ice phases. The values are averaged over all the H and O atoms in each of the unit cells. $C_{6OH}$ is calculated using the sum rule suggested in Ref. [234]. Grimme's parameters are taken from Ref. [232], which were empirically fitted to a ceratin database and are used as fixed parameters.

| | | TS | | Grimme |
|---|---|---|---|---|
| Ice | XI | IX | VIII | |
| $C_{6H}$ | 3.3 | 3.6 | 4.1 | 2.8 |
| $C_{6O}$ | 11.4 | 11.6 | 12.1 | 12.1 |
| $C_{6OH}$ | 5.9 | 6.2 | 6.8 | 4.5 |
| $R^0_H$ | 1.46 | 1.49 | 1.52 | 1.11 |
| $R^0_O$ | 1.60 | 1.61 | 1.62 | 1.49 |

bility of the high density phases compared to the low density phases. In addition this is attributed to the presence of more water molecules in the second and third coordination shells at relatively shorter distances of the high density phases. However, the question naturally arises as whether or not the vdW corrections are overestimated and the large difference observed in low and high density phases is an artifact of the nature of the atomic vdW pair potential chosen here. The vdW potential among two atoms largely depends on the functional form of the damping function (Eq. 4.2) and the vdW radii ($R^0_{ij}$) which are scaled (with $S_r$) depending on the choice of *xc* functionals. Fig. 6.5(a) shows the vdW contribution obtained from each of the atom pairs (H-H, O-O, and O-H) in ice XI. The $C_6$ coefficients and vdW radii of H and O calculated from the PBE+vdW equilibrium structures using Hirshfeld analysis (following Ref. [234]) are given in Table 6.3[4]. Due to the much larger scaling of the vdW radii for BLYP ($S_r = 0.75$), the minima in the vdW potentials are shifted towards short range compared to PBE ($S_r = 0.94$). Fig. 6.5(b) shows the difference in the vdW energy contribution in the high density phases to the low density phase ice XI as a function of $S_r$ and the position of the minima in the O-O vdW potential. This tells that for ice IX and ice XIV the relative vdW energies are nearly independent of the shape of the vdW potential, whereas, the stability of ice VIII increases as the vdW correction comes from the shorter range. Thus the stability of ice VIII is to some extent likely to be overestimated with BLYP+vdW. However, in the range $0.6 < S_r < 1.0$ the qualitative trend of more vdW energy at high density is retained.

[4]The $C_6$ coefficients increase while going from the low density phase ice XI to the higher density phases. In particular, the $C_6$ coefficient of H is about 24% larger for ice VIII than that of ice XI. Since the vdW radii also enhances, effectively the vdW potential curves do not change much in ice IX and ice VIII compared to ice XI, thus are not shown for brevity.

## 6.4. Summary

To summarize, several ambient and high pressure phases of crystalline ice have been studied with regular and vdW corrected DFT *xc* functionals. It is observed that the performance of PBE and BLYP functionals deteriorates for the high pressure phases as compared to the ambient pressure phases (ice Ih and ice XI). Both PBE and BLYP produce too unstable high pressure phases (in particular ice VIII) which are too unstable compared to experiment. The relative stabilities of the high density phases are enhanced when vdW interactions are included, producing results that are in better agreement with experiment. The vdW energy contributions are found to increase monotonously with the density of the ice phases. However, the absolute values of the lattice energies and densities of the ice phases are largely overestimated when vdW interactions are included. This study highlights the need for additional work in order to quantitatively understand the importance of vdW dispersion forces in high density ice phases.

# 7. Summary and Perspectives

This thesis has been dedicated to understanding how well present day DFT *xc* functionals can describe HBs among water molecules, what the problems are and possible ways of improvement. This has partly been accomplished by performing series of careful and systematic tests on small gas phase water clusters and crystalline ice.

Effort has been exerted throughout to obtain accurate reference data for the water clusters with explicitly correlated methods, such as, CCSD(T) and MP2. Computational issues such as the basis set incompleteness and basis set superposition errors have been minimized to generate both the reference and the DFT data by employing very large basis sets (e.g., aug-cc-pV5Z) and extrapolations to the complete basis set limit whenever needed. In this way, the "true" performance of the *xc* functionals has been obtained for the HBs between water molecules. The insight arrived at here will also certainly be of relevence to HBs in other systems, e.g., $NH_3$, HF, alcohols, and biomolecules. In addition, all the reference data obtained here can be used to assess the performance of other DFT *xc* functionals not tested here and other electronic structure techniques yet to be developed.

The first series of results was concerned with the global minimum conformers of the water dimer, trimer, tetramer, and pentamer. Among the tested functionals the hybrid PBE0 and X3LYP functionals performed best for the energetics of the HBs; always being within 10 meV/H-bond of MP2 and also they are very accurate for the structural parameters. Of the pure GGAs considered mPWLYP and PBE1W perform the best. All *xc* functionals showed variable performance with increasing cluster size, which means that conclusions drawn from small clusters do not necessarily hold for larger clusters. Having employed functionals from various rungs of "Jacob's ladder" it is clear that the description of HBs is not necessarily improved by riding higher up the ladder.

In the second specific study, similar tests were performed for the water hexamers, where the structure of the lowest energy isomer is controversial. Together with current MP2 data and recent DMC and CCSD(T) calculations, the lowest energy conformer is confirmed to be the prism (in the Born-Oppenheimer potential energy surface). Here it is shown that whilst certain *xc* functionals do a reasonable job at predicting the absolute dissociation energies (coming within 10-20 meV/$H_2O$) of the various isomers of the water hexamers, none of the functionals tested predict the correct energetic ordering of the four isomers, nor does any predict the correct lowest energy isomer. All *xc* functionals either predict the "book" or "cyclic" isomers to have the largest dissociation energies, which is unreliable and misleading. Furthermore, by attributing the failure to an improper treatment of vdW forces it seems likely that many other semi-local and hybrid *xc* functionals which do not account for vdW in some way will also fail in this regard. By augmenting the BLYP functional with semi-empirical pairwise $C_6R^{-6}$ corrections

the correct energetic ordering of the four hexamers is recovered. Equivalent empirical corrections to other functionals (PBE, PBE0) also improves the ordering somewhat, favoring the "prism" and "cage" isomers over the "book" and "cyclic" ones. This clearly implies the importance of vdW forces in holding water molecules together.

Although PBE produces moderately too strong HBs and BLYP gives too weak HBs for the gas phase equilibrium water clusters both yield much too structured liquid water. This has remained without a satisfactory explanation for some time now. To better understand this anomaly, water monomers and bonded dimers were extracted from a PBE simulation of liquid water. It was found that both BLYP and PBE underestimate the energy cost for monomer deformation and as a consequence BLYP and PBE predict dissociation energies that are too large by 80 and 43 meV, respectively, compared to CCSD(T). This is much inferior and contrasting to the performance of these functionals for the equilibrium water dimer and other water clusters in the gas phase. Overall PBE0 yields much more accurate dimer dissociation energies, mainly because it is not susceptible to such large bond stretching errors as the GGAs are. However, PBE0 is not free from deficiencies in treating the dimers examined here. Specifically, like the two other functionals, it predicts an increasing error in dimer interaction energy for the longest O-$H_d$ bonds. The overbinding identified here may provide an explanation for the overstructured RDFs observed in BLYP and PBE simulations of liquid water. Also the suggestion that too facile bond stretching with GGAs may result in an overstructured liquid is likely to be of relevance to other associated liquids apart from water.

Finally, several ambient and high pressure phases of crystalline ice were studied by adding vdW forces to standard *xc* functionals. The results from this study were not entirely satisfactory. On the one hand, it is found that the vdW contribution to the lattice energies increases monotonously with the density of the ice phase and as a result high density phases get more stabilized. This is qualitatively in agreement with the experimental relative lattice energies. On the other hand, the absolute values of the lattice energies are overestimated and also the equilibrium density gets worse in comparison to experiments when vdW interactions are added. Overall there is a lack of reference experimental lattice energies to compare with and other *ab initio* methods. In particular data from something like quantum Monte Carlo would be useful to obtain more accurate lattice energies for benchmark purposes.

On the general point of benchmarking and assessing the performance of existing and new *xc* functionals for the treatment of H-bonded systems, it seems that the water hexamer and clusters extracted from condensed phase would be important test cases to add to existing H-bond test sets. Likewise, various high pressure ice phases should also be included, once, of course, accurate lattice constants and lattice energies have been obtained.

Undoubtedly, from the study on the hexamers presented in this thesis and subsequent studies with Langreth and Lundqvist method [249] the importance of vdW interactions is evident. The problem here though is to simultaneously achieve an accurate ammount of dispersion and accurate absolute lattice energies. So far, neither the vdW correction scheme chosen here nor the methods from Langreth and Lundqvist [249] or Silvestrelli

[250] can get the correct absolute dissociation energies of the hexamers. Again more investigations in this direction is needed although encouraging results have already been obtained by Klimeš *et al.* [285].

Finally, no xc functional tested provides the correct description of HBs in all three phases of water. The quest to find an improved functional such that the reasons for its success or failure can be understood from physical perspectives remains. Nonetheless, as has just been discussed, considerable progress has been made in this thesis. Overall this work suggests that functionals with exact exchange (e.g., PBE0) and schemes that account for dispersion forces (e.g., the Tkatchenko-Scheffler non-empirical correction) offer considerable performance improvements over regular GGAs in simulating hydrogen bonded collections of water molecules. Hopefully, the knowledge earned here will assist in the developments of improved description of HBs with DFT, which will ultimately lead to an accurate *ab initio* phase diagram of water.

# Appendices

# A. Extrapolation Schemes

There are several extrapolation schemes available in the literature and some of them are tested here. Mostly they are developed to be applied with Dunning's correlation consistent basis sets. Some of the methods are briefly describe here:

(i) Feller [202]:

$$E(X) = E_{\mathrm{CBS}} + Ae^{-BX} \quad , \tag{A.1}$$

where, $X$ is the cardinal number in a basis set, i.e., 2 for aug-cc-pVDZ, 3 for aug-cc-pVTZ, 4 for aug-cc-pVQZ, and 5 for aug-cc-pV5Z.

(ii) Halkier and coworkers [144]:

$$E(X) = E_{\mathrm{CBS}} + AX^{-3} \quad . \tag{A.2}$$

(iii) Schwartz [203]: This particular general form was derived from convergence studies of MP2 energies of helium atom:

$$E(X) = E_{CBS} + \frac{A}{(X+d)^m} + \frac{B}{(X+d)^{m+1}} + \frac{C}{(X+d)^{m+2}} \quad ,$$

where, $d$ is angular momentum offset. There are various ways to decide values of $m$ and $d$. Two particular choices are found to provide satisfactory results from the work of Wilson and Dunning [205]: (a) $d = 1$, $m = 4$, $C = 0$ and (b) $d = 0$, $m = 3$, $B = 0$. Using those parameter two equations become:

$$E(X) = E_{\mathrm{CBS}} + \frac{A}{(X+1)^4} + \frac{B}{(X+1)^5} \quad , \tag{A.3}$$

$$E(X) = E_{\mathrm{CBS}} + \frac{A}{X^3} + \frac{C}{X^5} \quad . \tag{A.4}$$

(iv) Truhlar proposed a two point extrapolation scheme [206], which can be employed with X=2 and X=3:

$$E^{\mathrm{HF}}(X) = E^{\mathrm{HF}}_{\mathrm{CBS}} + A^{\mathrm{HF}}X^{-\alpha} \quad ,$$
$$E^{\mathrm{corr}}(X) = E^{\mathrm{corr}}_{\mathrm{CBS}} + A^{\mathrm{corr}}X^{-\beta} \quad .$$

Combination of above two equations leads to,

$$E^{\mathrm{MP2}}_{\mathrm{CBS}} = \frac{3^\alpha}{3^\alpha - 2^\alpha}E_3^{\mathrm{HF}} - \frac{2^\alpha}{3^\alpha - 2^\alpha}E_2^{\mathrm{HF}} + \frac{3^\beta}{3^\beta - 2^\beta}E_3^{\mathrm{corr}} - \frac{2^\beta}{3^\beta - 2^\beta}E_2^{\mathrm{corr}} \quad . \tag{A.5}$$

Suggested values for the parameters are $\alpha = 3.4$ and $\beta = 2.22$.

**Table A.1.:** Difference in the calculated and extrapolated HF ($\Delta E^{\mathrm{HF}}$) and correlation ($\Delta E^{\mathrm{corr}}$) energies with aug-cc-pV6Z basis sets for water monomer and dimer. Energies are given in meV/$H_2O$.

| Extp | Eq. | Monomer | | Dimer | |
|---|---|---|---|---|---|
| | | $\Delta E^{\mathrm{corr}}$ | $\Delta E^{\mathrm{HF}}$ | $\Delta E^{\mathrm{corr}}$ | $\Delta E^{\mathrm{HF}}$ |
| $X$=2,3,4 | A.1 | 38.3 | -11.5 | 39.4 | -12.4 |
| | A.2 | 156 | -21.4 | 154 | -21.3 |
| | A.3 | -16 | -35.6 | -15.7 | -36.4 |
| | A.4 | -6.4 | -39.0 | -6.3 | -39.6 |
| $X$=2,3,4,5 | A.1 | 20.1 | -7.8 | 20.5 | -8.0 |
| | A.2 | 101 | -19.4 | 99.6 | -19.3 |
| | A.3 | -9.4 | -19.9 | -9.4 | -20.1 |
| | A.4 | -5.8 | -23.2 | -5.9 | -23.4 |
| $X$=3,4,5 | A.1 | 7.3 | **-4.9** | 7.1 | **-4.7** |
| | A.2 | 12 | -23.1 | 12.5 | -23.2 |
| | A.3 | -3.9 | -6.6 | -4.1 | -6.3 |
| | A.4 | **-5.3** | -8.5 | **-5.5** | -8.2 |
| $X$=2,3 | A.1 | 248 | 55.0 | -24.4 | 6.9 |
| | A.2 | 264 | 9.9 | 260 | -9.3 |
| $X$=3,4 | A.1 | 86.9 | 3.3 | 22.1 | -7.7 |
| | A.2 | 27.9 | -35.3 | 27.5 | -35.7 |
| $X$=4,5 | A.1 | 21.8 | -3.2 | 9.3 | -5.0 |
| | A.2 | -1.0 | -11.9 | -1.3 | -11.8 |

### Results

To find out the most accurate scheme here a comparison was made between the calculated energy with an aug-cc-pV6Z basis set and the extrapolated value at X=6. Table A.1 provides the differences for the HF and correlation energies for monomer and dimer. Energy differences can be defined as,

$$\Delta E^{HF} = E^{\mathrm{HF}}_{\mathrm{fit}} - E^{\mathrm{HF}}_{\mathrm{computed}} \tag{A.6}$$

$$\Delta E^{\mathrm{corr}} = E^{\mathrm{corr}}_{\mathrm{fit}} - E^{\mathrm{corr}}_{\mathrm{computed}} \tag{A.7}$$

From Table A.1 it is found that for extrapolations of HF and correlation energies, respectively, Eq. (A.1) and Eq. (A.4) are reasonably accurate. Table A.2 shows the extrapolated dissociation energies of the water dimer to tetramer using all the extrapolation equations and the best scheme by combining extrapolation of HF part with Eq. (A.1) and Eq. (A.4) for correlation part. It is observed that if the extrapolation is done using the energies obtained from TZ, QZ, and 5Z quality basis sets then the results are much less sensitive to the extrapolation schemes. In those cases the dissociation

**Table A.2.:** MP2/CBS dissociation energies for water dimer to tetramer obtained from various extrapolation methods for regular and BSSE corrected (BSSEC) values. The dissociation energies taken as the best are highlighted with bold. Energies are given in meV/$H_2O$.

| | | Dimer | | Trimer | | Tetramer |
|---|---|---|---|---|---|---|
| Extp | Eq. | Regular | BSSEC | Regular | BSSEC | Regular |
| $X$=2,3,4 | A.1 | 215.37 | 215.09 | 228.35 | 227.41 | 299.22 |
| | A.2 | 221.07 | 211.87 | 233.37 | 225.08 | 306.58 |
| | A.3 | 216.37 | 217.24 | 229.65 | 229.80 | 299.99 |
| | A.4 | 217.02 | 216.70 | 230.21 | 229.44 | 300.97 |
| | A.1 & A.4 | 217.72 | 216.62 | 231.04 | 229.46 | 302.05 |
| $X$=2,3,4,5 | A.1 | 215.63 | 214.37 | 228.37 | 227.75 | 299.59 |
| | A.2 | 219.61 | 212.82 | 232.09 | 226.24 | 304.65 |
| | A.3 | 215.67 | 215.99 | 228.74 | 229.52 | 299.48 |
| | A.4 | 216.14 | 215.85 | 229.18 | 229.40 | 300.14 |
| | A.1 & A.4 | 216.61 | 215.67 | 229.71 | 229.30 | 300.97 |
| $X$=3,4,5 | A.1 | 216.43 | 213.76 | 228.87 | 228.33 | 300.38 |
| | A.2 | 217.06 | 215.11 | 229.97 | 228.59 | 301.38 |
| | A.3 | 214.62 | 214.11 | 227.36 | 229.11 | 298.72 |
| | A.4 | 214.69 | 214.47 | 227.49 | 229.34 | 298.78 |
| | A.1 & A.4 | **215.87** | 214.76 | **228.58** | 229.54 | **299.96** |
| $X$=2,3 | A.1 | 931.06 | | 1021.4 | | 1576.2 |
| | A.2 | 223.15 | 209.39 | 235.01 | 222.83 | 309.32 |
| | A.5 | 223.03 | 212.96 | 235.69 | 227.32 | 309.89 |
| $X$=3,4 | A.2 | 218.12 | 215.38 | 231.07 | 228.25 | 302.47 |

energies obtained from all the equations (except Eq. (A.5)) are within 3 meV/$H_2O$ of the best estimated values, which arrive from the combination of Eq. (A.1) and Eq. (A.4) (highlighted in Table A.2). Also to be noted that with the two point (DZ and TZ) extrapolation scheme of Truhlar (Eq. (A.5)) binding energies are ∼10 meV/$H_2O$ overestimated than the best estimation but it could be a promising scheme for much larger systems. Moreover, after extrapolation the regular and BSSE corrected dissociation energies are always within 2 meV/$H_2O$ when basis sets of quality TZ or better are employed.

# B. NAO Basis Sets

The numerically optimized radial basis functions (each with $(2l+1)$ angular momentum functions) employed in chapter 6 are summarized in Table B.1. The convergence behavior of the binding energy of the water dimer and lattice energy of ice Ih is displayed in Fig. B.1.

**Table B.1.:** Radial functions selected during the basis optimization for H and O, which are employed as NAO basis sets in FHI-aims code. The first line (*minimal*) summarizes the free-atom radial functions used (noble gas configuration of the core and quantum numbers of the additional valence radial functions). "H($nl$, $z$)" denotes a hydrogen-like basis function for the bare Coulomb potential $z/r$, including its radial and angular momentum quantum numbers, $n$ and $l$. $X^{2+}(nl)$ denotes a $n$, $l$ radial function of a doubly positive free ion of species X.

| | H | O |
|---|---|---|
| *minimal* | 1s | [He] + 2s 2p |
| *tier*1 | H(2s, 2.1) | H(2p, 1.8) |
| | H(2p, 3.5) | H(3d, 7.6) |
| | | H(3s, 6.4) |
| *tier*2 | H(1s, 0.85) | H(4f, 11.6) |
| | H(2p, 3.7) | H(3p, 6.2) |
| | H(2s, 1.2) | H(3d, 5.6) |
| | H(3d, 7.0) | H(5g, 17.6) |
| | | H(1s, 0.75) |
| *tier*3 | H(4 f , 11.2) | $O^{2+}$(2p) |
| | H(3p, 4.8) | H(4f, 10.8) |
| | H(4d, 9.0) | H(4d, 4.7) |
| | H(3s, 3.2) | H(2s, 6.8) |
| | ... | ... |

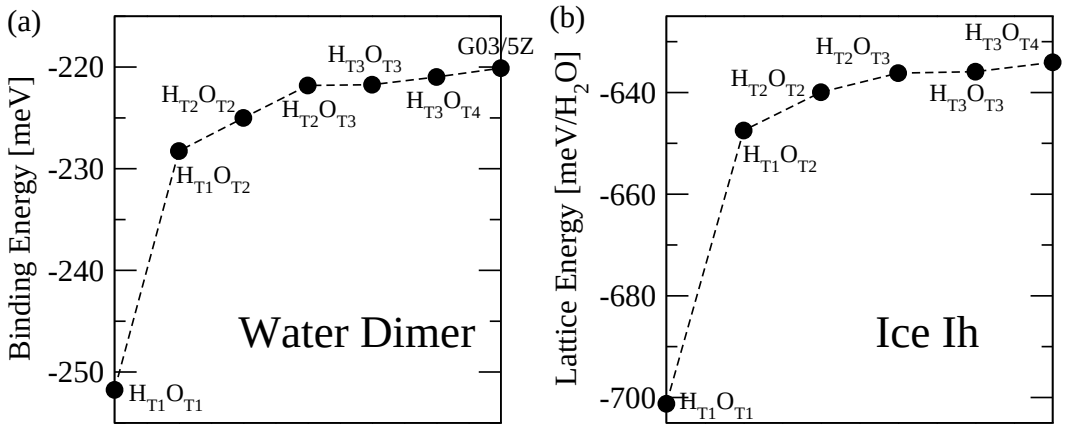


**Figure B.1.:** Convergence behavior of the NAO basis sets with the PBE xc functional (a) for the binding energy of water dimer and (b) for the lattice energy of ice Ih. The result from G03/aug-cc-PV5Z is also shown in panel (a). $T_1$, $T_2$, and $T_3$ refer to *tier1*, *tier2*, and *tier3* basis sets, respectively. $H_{T1}O_{T1}$ refers to NAO basis set for H and O are used up to *tier1* and likewise others.

# C. Comparison of Gaussian, plane-waves, and NAO Basis Sets

To show that the choice of different basis sets does not effect the conclusions obtained in the previous chapters, comparisons of Gaussian, NAO, and plane wave basis sets are presented in Table C.1 for the dissociation energies of several water clusters. Except the values obtained with 70 Ry energy cut off the three other methods produce binding energies within 1 meV/$H_2O$ of each other for all of the clusters. This indicates the basis sets employed in the thesis are close to completeness. In fact with a lower 70 Ry energy cut off the energetic ordering of the water hexamers are found to be different than the other three methods. Given that the 70 Ry is not a small cut off (already larger than the plane wave cut off used in many *ab initio* simulations of liquid water) the sensitivity of the results to basis set completeness observed here may be one source of the differences often observed from one DFT liquid water simulation to the next.

**Table C.1.:** Comparison of the dissociation energies of the four low energy isomers of the water hexamers and the water dimer to pentamer in their global minimum structures calculated with three types of basis sets and BLYP *xc* functional. For Gaussian aug-cc-pV5Z and for NAO *tier3* basis sets are employed. For plane waves GTH pseudopotentials are used [150]. For the hexamers the most stable isomer from each method is indicated in bold and with respect to that the relative energies of the other isomers are given in parenthesis. All values are in meV/$H_2O$.

| | Gaussian | NAO | Plane wave (200 Ry) | Plane wave (70 Ry) |
|---|---|---|---|---|
| Prism | 273.6 (16.2) | 272.1 (17.6) | 272.1 (17.6) | 270.3 (11.3) |
| Cage | 277.4 (12.4) | 277.3 (12.5) | 276.0 (13.7) | 272.5 (9.1) |
| Book | 287.5 (2.3) | 287.4 (2.4) | 286.7 (3.0) | **281.6** (4.5) |
| Cyclic | **289.8** | **289.8** | **289.7** | 279.7 (-1.9) |
| Dimer | 180.7 | 180.6 | 179.3 | |
| Trimer | 191.7 | 191.9 | 190.8 | |
| Tetramer | 264.9 | 265.1 | 263.9 | |
| Pentamer | 281.2 | 281.3 | 280.7 | |

# D. Isotropic Change in Lattice Parameter

For all ice phases to obtain the DFT equilibrium volumes the lattice parameters are varied isotropically from the experimental values. This means that the ratios between $a$, $b$, and $c$ lattice parameters are kept fixed to the ratios obtained in experiments. This constraint is found to be reasonable and will not change any of the conclusions arrived in chapter 6. A recent study of Feibelman [57] has shown that for the hexagonal lattice of ice Ih the $c/a$ ratio differs only by $\sim$0.4%-0.5% from experiment with BLYP and PBE. Also to verify that for other high pressure phases, here specifically ice VIII has been studied with PBE and PBE+vdW. The lattice parameters $a$ and $c$ are changed by $\pm$2% and $\pm$4% starting from PBE and PBE+vdW equilibrium volumes and surrounded the minimum energy point with 24 points. Then calculated data are interpolated using a polynomial fit and the lattice parameters $c$ and $a$ having the lowest energy are located (Fig. D.1). The obtained new $c/a$ ratio is only 0.6%-0.8% smaller than experimental value (see Table D.1). Also the difference in the equilibrium volumes while keeping $c/a$ ratio fixed at the experimental value or varying that is only $\sim$0.04%-0.1% with PBE and PBE+vdW, respectively.

**Table D.1.:** Comparison of calculated equilibrium volumes of ice VIII by keeping $c/a$ ratio fixed at the experimental value and while varying that. Percentage errors with respect to experimental $c/a$ ratio are given in parenthesis. All volumes are in $Å^3/H_2O$ and energies in meV/$H_2O$.

| | Varying c/a | | | | |
|---|---|---|---|---|---|
| | $c$ | $a$ | $c/a$ | Volume/$H_2O$ | Lattice Energy |
| PBE | 7.025 | 4.859 | 1.446 (0.6) | 20.735 | 459.48 |
| PBE+vdW | 6.949 | 4.815 | 1.443 (0.8) | 20.15 | 619.38 |
| Expt. | | | 1.455 | | |
| | Fixed $c/a$ | | | | |
| PBE | 7.056 | 4.849 | 1.455 | 20.744 | 459.44 |
| PBE+vdW | 6.986 | 4.801 | 1.455 | 20.13 | 619.23 |
| Expt. | | | 1.455 | | |

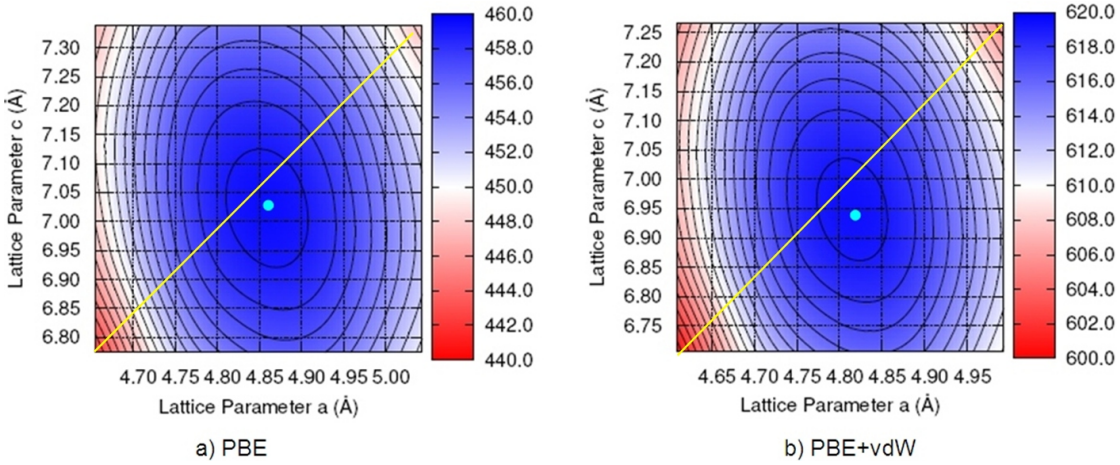


**Figure D.1.:** Contour plot of the polynomial fit to the data calculated in a-c plane for ice VIII. The minimum energy points are indicated with circles. The yellow lines depict the experimental $c/a$ ratio.

# E. Refit of parameter $S_r$ for BLYP+vdW

BLYP produces much weaker bonding for vdW and H-bonded systems than PBE, thus the $S_r$ parameter fitting to the S22 database (from Ref. [243]) turns out to be 0.62 for BLYP and 0.94 for PBE. This tells that with BLYP+vdW we will eventually correct at much shorter inter atomic distances than desired in order to get all the missing interactions. Now applying $S_r = 0.62$ for BLYP+vdW, the dissociation energy of gas phase equilibrium water dimer turns out to be 258 meV, which is about 40 meV larger than MP2 value of 216 meV. This large overestimation also leads to an unphysical situation for ice where we find ice VIII becomes more stable than ice Ih with BLYP+vdW. Looking more closely to the S22 database it is found that BLYP is much inferior for purely vdW bonded system than for H-bonded systems and if the fitting is restricted only to H-bonded systems, the optimized $S_r$ turns out to be 0.72. Since the interaction between water molecules are not purely vdW bonded, $S_r$ parameter is fitted on a larger database including 48 different water dimers (H-bonded and non-bonded) extracted from four low energy isomers of water hexamers along with S22 database. A optimized value of $S_r = 0.75$ is obtained as a result, which produces binding energy of the equilibrium water dimer of 220 meV, very close to MP2. Fig. E.1 shows that $S_r = 0.75$ modifies the damping function simply not to include any vdW interaction within $\sim$2 Å. Henceforth we report all the BLYP+vdW results for ice (chapter 6) using $S_r = 0.75$. For comparison the damping function with $S_r = 0.94$ is also shown, which is used for all calculations with PBE+vdW.

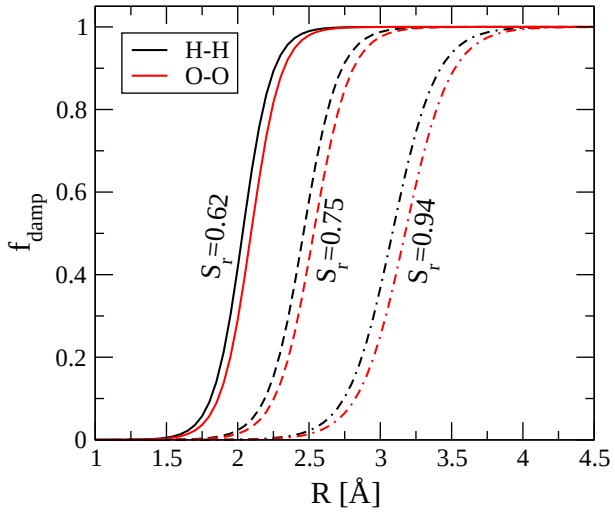


**Figure E.1.:** Damping function defined in Eq. 4.2 is plotted as function of inter atomic distance (R) for three different values of $S_r$.

# Acknowledgements

I am grateful to Prof. Matthias Scheffler for giving me an opportunity to pursue Ph.D. research in his highly motivated group with a great scientific environment. His guidance, discussions, and constant support for attending conferences and making collaborations have been exceptional. I would like to thank Prof. Andreas Knorr for his valuable help and guidance. Also, my very special thanks go to Gaby Tysper, Julia Pach, and Olaf Kostbahn for abundant help in getting me acquainted with FHI and Berlin.

I am extremely fortunate to have Prof. Angelos Michaelides as my research guide (and also mentor). My vocabulary of compliments will not be enough to match the quality of education I have received from him. But in short, I owe my deepest gratitude to Angelos. He has practically groomed me in almost every respect from learning the basics of DFT to writing articles and how to face the audience while presenting scientific results. His constant inspiration and positive outlook have always helped me to overcome the situations when things were not in favor. Without his vigilant guidance this thesis would not be the same as it is now. These three and a half years of working with him has been a great learning and mixed with fun too.

Working in FHI have given me the chance to interact with a variety of people including my colleagues whom I am thankful to. Whenever I have faced problems, I have knocked the doors of Javier Carrasco, Bo Li, Ding Pan, Jörg Meyer, and Joachim Paier, in particular. There were many productive discussions with Martin Fuchs and Alexandre Tkatchenko. I have received instant help whenever needed from the 'ICE' group members in UCL Xiaoliang Hu, Erlend Davidson, Jiri Klimeš, Limin Liu, Brent Walker, Xinzheng Li, Anna Kimmel, Jie Ma, and Changjun Zhang. Special thanks to Javier Carrasco and Franziska Schubert for correcting some part of the thesis earlier and Erik McNellis and Bo Li for providing the artistic LaTeX templates. Also, I have been fortunate to receive Marie Curie fellowship within the EU project network MONET.

Other than discussing science I have had cheerful moments with my colleagues and friends, especially with Javier, Payam, Sudha, Andrea, Sebastain, Juan, Mathis, Matteo, Mariana, Matthias G., Jelena, Sergey, Amudha, all table tennis and football players of FHI, all MONET members, especially Evren, typical *Bengali adda* with Neloy, Shamik, Amrita, Jhuma, and outing with Leonardo, Tim. I thank you all and my other colleagues.

I must not forget few of my old and long-standing pals, especially, Anindya, Sayantan, Shantanu, Jay, Hari, Bidhan, Analu, and Shayeri. Without their timely suggestions and help probably I would not have reached Berlin.

Finally, I am indebted to my beloved parents Barun Santra and Bijoli Santra, my sweet sister Ranita, and few of my close family members who have been beside me in every circumstances for nearly three decades. This thesis is dedicated to them.

# Curriculum Vitae

### Personal Data

| | |
|---|---|
| Name: | Biswajit Santra |
| Date of Birth: | 17.08.1981 |
| Place of Birth: | West Bengal, India |
| Sex: | Male |
| Nationality: | Indian |

### Education

| | | |
|---|---|---|
| 2006–2010 | Ph.D. | Theory Department of Fritz-Haber-Insitut der Max-Planck-Gesellschaft, Berlin, Germany. |
| 2003–2005 | M.Sc. (Physics) | Department of Physics, Unviersity of Pune, Pune, India. |
| 2000–2003 | B.Sc. (Physics) | R. K. M. College Narendrapur, University of Calcutta, Kolkata, India. |

# Publications

1. "On the accuracy of density-functional theory exchange-correlation functionals for H bonds in small water clusters: Benchmarks approaching the complete basis set limit", Biswajit Santra, Angelos Michaelides, and Matthias Scheffler, J. Chem. Phys. **127**, 184104 (2007).

2. "On the accuracy of density-functional theory exchange-correlation functionals for H bonds in small water clusters. II. The water hexamer and van der Waals interactions", Biswajit Santra, Angelos Michaelides, Martin Fuchs, Alexandre Tkachenko, Claudia Filippi, and Matthias Scheffler, J. Chem. Phys. **129**, 194111 (2008).

3. "Coupled cluster benchmarks of water monomers and dimers extracted from density-functional theory liquid water: The importance of monomer deformations", Biswajit Santra, Angelos Michaelides, and Matthias Scheffler, J. Chem. Phys. **131**, 124509 (2009).

# Bibliography


[1] P. Ball, *Life's Matrix: A Biography of Water* (University of California Press, Los Angeles, 2001).

[2] G. A. Jeffrey, *An Introduction to Hydrogen Bonding* (Oxford University Press, Inc., New York, 1997).

[3] G. Gilli and P. Gilli, *The Nature of the Hydrogen Bond* (Oxford University Press, Inc., New York, 2009).

[4] L. Pauling, J. Am. Chem. Soc. **57**, 2680 (1935).

[5] V. F. Petrenko and R. W. Whitworth, *Physics of Ice* (Oxford University Press, Inc., New York, 2003).

[6] S. W. Peterson and H. A. Levy, Acta Crystallographica **10**, 70 (1957).

[7] P. Wernet, D. Nordlund, U. Bergmann, M. Cavalleri, M. Odelius, H. Ogasawara, L. Å. Näslund, T. K. Hirsch, *et al.*, Science **304**, 995 (2004).

[8] A. K. Soper, Chem. Phys. **258**, 121 (2000).

[9] T. Head-Gordon and G. Hura, Chem. Rev. **102**, 2651 (2002).

[10] J. C. Grossman, E. Schwegler, E. W. Draeger, F. Gygi, and G. Galli, J. Chem. Phys. **120**, 300 (2004).

[11] E. Schwegler, J. C. Grossman, F. Gygi, and G. Galli, J. Chem. Phys. **121**, 5400 (2004).

[12] M. V. Fernández-Serra and E. Artacho, J. Chem. Phys. **121**, 11136 (2004).

[13] M. J. McGrath, J. I. Siepmann, I.-F. W. Kuo, C. J. Mundy, J. VandeVondele, J. Hutter, F. Mohamed, and M. Krack, ChemPhysChem **6**, 1894 (2005).

[14] M. J. McGrath, J. I. Siepmann, I.-F. W. Kuo, and C. Mundy, Molec. Phys. **104**, 3619 (2006).

[15] M. J. McGrath, J. I. Siepmann, I.-F. W. Kuo, C. J. Mundy, J. VandeVondele, J. Hutter, F. Mohamed, and M. Krack, J. Phys. Chem. A **110**, 640 (2006).

[16] H.-S. Lee and M. E. Tuckerman, J. Phys. Chem. A **110**, 5549 (2006).

[17] H.-S. Lee and M. E. Tuckerman, J. Chem. Phys. **125**, 154507 (2006).

[18] H.-S. Lee and M. E. Tuckerman, J. Chem. Phys. **126**, 164501 (2007).

[19] T. Todorova, A. P. Seitsonen, J. Hutter, I. W. Kuo, and C. J. Mundy, J. Phys. Chem. B **110**, 3685 (2006).

[20] J. VandeVondele, F. Mohamed, M. Krack, J. Hutter, M. Sprik, and M. Parrinello, J. Chem. Phys. **122**, 014515 (2005).

[21] M. Guidon, F. Schiffmann, J. Hutter, and J. VandeVondele, J. Chem. Phys. **128**, 214104 (2008).

[22] T. D. Kühne, M. Krack, and M. Parrinello, J. Chem. Theory Comput. **5**, 235 (2009).

[23] P. H.-L. Sit and N. Marzari, J. Chem. Phys. **122**, 204510 (2005).

[24] I.-C. Lin, A. P. Seitsonen, M. D. Coutinho-Neto, I. Tavernelli, and U. Rothlisberger, J. Phys. Chem. B **113**, 1127 (2009).

[25] M. V. Fernández-Serra, G. Ferlat, and E. Artacho, Molecular Simualtion **31**, 361 (2005).

[26] D. Asthagiri, L. R. Pratt, and J. D. Kress, Phys. Rev. E **68**, 041505 (2003).

[27] A. E. Mattson and T. R. Mattson, J. Chem. Theory Comput. **5**, 887 (2009).

[28] I.-F. W. Kuo, C. J. Mundy, M. J. McGrath, J. I. Siepmann, J. VandeVondele, M. Sprik, J. Hutter, B. Chen, *et al.*, J. Phys. Chem. B **108**, 12990 (2004).

[29] M. Sprik, J. Hutter, and M. Parrinello, J. Chem. Phys. **105**, 1142 (1996).

[30] P. L. Silvestrelli and M. Parrinello, J. Chem. Phys. **111**, 3572 (1999).

[31] S. Yoo, X. C. Zeng, and S. S. Xantheas, J. Chem. Phys. **130**, 221102 (2009).

[32] J. Schmidt, J. VandeVondele, I.-F. W. Kuo, D. Sebastiani, J. I. Siepmann, J. Hutter, and C. J. Mundy, J. Phys. Chem. B **113**, 11959 (2009).

[33] D. Alfè, M. J. Gillan, and G. D. Price, Nature **405**, 172 (2000).

[34] M. J. Gillan, D. Alfè, J. Brodholt, L. Vocadlo, and G. D. Price, Rep. Prog. Phys. **69**, 2365 (2006).

[35] J. D. Bernal and R. H. Fowler, J. Chem. Phys. **1**, 515 (1933).

[36] J. L. Finney, J. Mol. Liq. **90**, 303 (2001).

[37] B. Guillot, J. Mol. Liq. **101**, 219 (2002).

[38] K. Laasonen, M. Sprik, M. Parrinello, and R. Car, J. Chem. Phys. **99**, 9080 (1993).

[39] J. A. Morrone and R. Car, Phys. Rev. Lett. **101**, 017801 (2008).

[40] C. Lee, D. Vanderbilt, K. Laasonen, R. Car, and M. Parrinello, Phys. Rev. B **47**, 4863 (1993).

[41] D. R. Hamann, Phys. Rev. B **55**, R10157 (1997).

[42] S. J. Singer, J.-L. Kuo, T. K. Hirsch, C. Knight, L. Ojamäe, and M. L. Klein, Phys. Rev. Lett. **94**, 135701 (2005).

[43] E. Schwegler, M. Sharma, F. Gygi, and G. Galli, Proc. Natl. Acad. Sci. U.S.A. **105**, 14779 (2008).

[44] D. Pan, L.-M. Liu, G. A. Tribello, B. Slater, A. Michaelides, and E. Wang, Phys. Rev. Lett. **101**, 155709 (2008).

[45] G. Cicero, J. C. Grossman, E. Schwegler, F. Gygi, and G. Galli, J. Am. Chem. Soc. **130**, 1871 (2008).

[46] L. Liu, M. Krack, and A. Michaelides, J. Am. Chem. Soc. **130**, 8572 (2008).

[47] K. N. Kudin and R. Car, J. Am. Chem. Soc. **130**, 3915 (2008).

[48] F. Schiffmann, J. Hutter, and J. VandeVondele, J. Phys. Condens. Matter **20**(6), 064206 (2008), http://stacks.iop.org/0953-8984/20/064206.

[49] G. Cicero, J. C. Grossman, A. Catellani, and G. Galli, J. Am. Chem. Soc. **127**, 6830 (2005).

[50] L. M. Ramaniah, M. Bernasconi, and M. Parrinello, J. Chem. Phys. **111**, 1587 (1999).

[51] P. J. Feibelman, Science **295**, 99 (2002).

[52] J. Carrasco, A. Michaelides, M. Forster, S. Haq, R. Raval, and A. Hodgson, Nature Mater. **8**, 427 (2009).

[53] S. Schnur and A. Gross, New J. Phys. **11**, 125003 (2009).

[54] A. Hodgson and S. Haq, Surf. Sci. Rep. **64**, 381 (2009).

[55] A. Michaelides, App. Phys. A **85**, 415 (2006).

[56] D. Marx, ChemPhysChem **7**, 1848 (2006).

[57] P. J. Feibelman, Phys. Chem. Chem. Phys. **10**, 4688 (2008).

[58] M. Born and J. R. Oppenheimer, Ann. Phys. **84**, 457 (1927).

[59] J. Behler, B. Delley, S. Lorenz, K. Reuter, and M. Scheffer, Phys. Rev. Lett. **94**, 036104 (2005).

[60] J. Behler, K. Reuter, and M. Scheffer, Phys. Rev. B **77**, 115421 (2008).

[61] A. M. Wodtke, J. C. Tully, and D. J. Auerbach, Int. Rev. Phys. Chem. **23**, 513 (2004).

[62] A. C. Luntz, M. Persson, and G. O. Sitz, J. Chem. Phys. **124**, 091101 (2006).

[63] D. R. Hartree, Proc. Cambridge Phil. Soc. **24**, 89 (1928).

[64] V. Fock, Z. Physik **61**, 126 (1930).

[65] D. P. Taylor, W. P. Hess, and M. I. McCarthy, J. Phys. Chem. B **101**, 7455 (1997).

[66] P. Baranek, G. Pinarello, C. Pisani, and R. Dovesi, Phys. Chem. Chem. Phys. **2**, 3893 (2000).

[67] S. Casassa, A. Ferrar, M. Busso, and C. Pisani, J. Phys. Chem. B **106**, 12978 (2002).

[68] P.-O. Lödin, Adv. Chem. Phys. **2**, 207 (1959).

[69] R. J. Bartlett and M. Musial, Rev. Mod. Phys. **79**, 291 (2007).

[70] C. Møller and M. S. Plesset, Phys. Rev. **46**, 618 (1934).

[71] A. Szabo and N. S. Ostlund, *Modern Quantum Chemistry: Introduction to Advanced Electronic Structure Theory* (Dover Press, USA, 1982).

[72] A. P. Scott and L. Radom, J. Chem. Phys. **100**, 16502 (1996).

[73] P. R. Rablen, J. W. Lockman, and W. L. Jorgensen, J. Phys. Chem. A **102**, 3782 (1998).

[74] L. A. Curtiss, K. Raghavachari, P. C. Redfern, V. Rassolov, and J. A. Pople, J. Chem. Phys. **109**, 7764 (1998).

[75] L. A. Curtiss, P. C. Redfern, K. Raghavachari, and J. A. Pople, J. Chem. Phys. **114**, 108 (2001).

[76] M. L. Leininger, W. D. Allen, H. F. S. III, and C. D. Sherrill, J. Chem. Phys. **112**, 9213 (2000).

[77] J. Čížek, J. Chem. Phys. **45**, 4256 (1966).

[78] J. Čížek and J. Paldus, Int. J. Quant. Chem. **5**, 359 (1971).

[79] P. J. T. Helgaker and J. Olsen, *Molecular Electronic Structure Theory* (Wiley, New York, 2000).

[80] C. D. Sherrill and H. F. I. Schaefer, Adv. Quan. Chem. **34**, 143 (1999).

[81] J. D. Watts, J. Gauss, and R. J. Bartlett, J. Chem. Phys. **98**, 8718 (1993).

[82] S. Hirata, M. Nooijen, I. Grabowski, and R. J. Bartlett, J. Chem. Phys. **114**, 3919 (2001).

[83] W. Klopper, J. G. C. M. van Duijneveldt-van de Rijdt, and F. B. van Duijneveldt, Phys. Chem. Chem. Phys. **2**, 2227 (2000).

[84] E. M. Mas, R. Bukowski, K. Szalewicz, G. C. Groenenboom, P. E. S. Wormer, and A. van der Avoird, J. Chem. Phys. **113**, 6687 (2000).

[85] A. K. Rappe and E. R. Bernstein, J. Phys. Chem. A **104**, 6117 (2000).

[86] Q. Zhang, R. Bell, and T. N. Truong, J. Phys. Chem. **99**, 592 (1995).

[87] R. G. Parr, Ann. Rev. Phys. Chem. **34**, 631 (1983).

[88] T. Ziegler, Chem. Rev. **91**, 651 (1991).

[89] P. Geerlings, F. D. Proft, and W. Langenaeker, Chem. Rev. **103**, 1793 (2003).

[90] R. O. Jones and O. Gunnarsson, Rev. Mod. Phys. **61**, 689 (1989).

[91] R. G. Parr and W. Yang, *Density-Functional Theory of Atoms and Molecules* (Oxford University Press, New York, 1989).

[92] M. R. Dreizler and E. K. U. Gross, *Density Functional Theory : An Approach to the Quantum Many-Body Problem* (Springer, Berlin, 1990).

[93] L. H. Thomas, Proc. Camb. Phil. Soc. **23**, 542 (1927).

[94] E. Fermi, Rend. Accad. Lincei. **6**, 202 (1927).

[95] P. Hohenberg and W. Kohn, Phys. Rev. **136**, B864 (1964).

[96] H. Hellmann, Z. Phys. **85**, 180 (1933).

[97] R. P. Feynman, Phys. Rev. **56**, 340 (1939).

[98] W. Kohn and L. J. Sham, Phys. Rev. **140**, A1133 (1965).

[99] M. R. Dreizler and E. K. U. Gross, *in Density Functional Theory and Its Application to Materials, edited by V. Van Doren* (AIP Press, Melville, New York, 2001).

[100] M. Gell-Mann and K. A. Brueckner, Phys. Rev. **106**, 364 (1957).

[101] D. M. Ceperley and B. J. Alder, Phys. Rev. Lett. **45**, 566 (1980).

[102] J. P. Perdew and A. Zunger, Phys. Rev. B **23**, 5048 (1981).

[103] J. P. Perdew and Y. Wang, Phys. Rev. B **45**, 13244 (1992).

[104] S. J. Vosko, L. Wilk, and M. Nusair, Can. J. Phys. **58**, 1200 (1980).

[105] O. Gunnarsson and B. I. Lundqvist, Phys. Rev. B **13**, 4274 (1976).

[106] O. Gunnarsson, M. Jonson, and B. I. Lundqvist, Sol. Stat. Comm. **24**, 765 (1977).

[107] T. Ziegler, A. Rauk, and E. J. Baerends, Theor. Chim. Acta **43**, 261 (1977).

[108] K. Burke, J. P. Perdew, and M. Ernzerhof, J. Chem. Phys. **109**, 3760 (1998).

[109] V. N. Staroverov, G. E. Scuseria, J. Tao, and J. P. Perdew, Phys. Rev. B **69**, 075102 (2004).

[110] G. I. Csonka *et al.*, Phys. Rev. B **79**, 155107 (2009).

[111] J. Harl, L. Schimka, and G. Kresse, Phys. Rev. B **81**, 115126 (2010).

[112] K. Capelle, Braz. J. Phys. **36**, 1318 (2006).

[113] J. P. Perdew, K. Burke, and M. Ernzerhof, Phys. Rev. Lett. **77**, 3865 (1996).

[114] A. D. Becke, Phys. Rev. A **38**, 3098 (1988).

[115] J. P. Perdew, *in Electronic Structure of Solids '91* (edited by P. Ziesche and H. Eschrig, Akademie Verlag, Berlin, 1991), p. 11.

[116] W. Lee, C. Yang and R. G. Parr, Phys. Rev. B **37**, 785 (1988).

[117] J. P. Perdew, Phys. Rev. B **33**, 8822 (1986).

[118] M. Losada and S. Leutwyler, J. Chem. Phys. **117**, 2003 (2002).

[119] T. Tsuzuki and H. P. Luthi, J. Chem. Phys. **114**, 3949 (2001).

[120] J. Ireta, J. Neugebauer, and M. Scheffler, J. Phys. Chem. A **108**, 5692 (2004).

[121] J. Tao, J. P. Perdew, V. N. Staroverov, and G. E. Scuseria, Phys. Rev. Lett. **91**, 146401 (2003).

[122] V. N. Staroverov, G. E. Scuseria, J. Tao, and J. P. Perdew, J. Chem. Phys. **119**, 12129 (2003).

[123] Y. Zhao and D. G. Truhlar, J. Chem. Theory Comput. **1**, 415 (2005).

[124] Y. Zhao and D. G. Truhlar, J. Phys. Chem. A **109**, 5656 (2005).

[125] A. D. Becke, J. Chem. Phys. **98**, 1372 (1993).

[126] A. D. Becke, J. Chem. Phys. **98**, 5648 (1993).

[127] S. H. Vosko, L. Wilk, and M. Nusair, Can. J. Phys. **58**, 1200 (1980).

[128] P. J. Stephens, F. J. Devlin, C. F. Chabalowski, and M. J. Frisch, J. Phys. Chem. **98**, 11623 (1994).

[129] C. Adamo and V. Barone, J. Chem. Phys. **110**, 6158 (1999).

[130] M. Marsman, J. Paier, A. Stroppa, and G. Kresse, J. Phys. Condens. Matter **20**, 064201 (2008).

[131] J. Heyd, J. E. Peralta, G. E. Scuseria, and R. L. Martin, J. Chem. Phys. **123**, 174101 (2005).

[132] E. N. Brothers, A. F. Izmaylov, J. O. Normand, V. Barone, and G. E. Scuseria, J. Chem. Phys. **129**, 011102 (2008).

[133] Y. Zhao and D. G. Truhlar, J. Phys. Chem. A **108**, 6908 (2004).

[134] D. E. Woon and T. H. Dunning, J. Chem. Phys. **103**, 4572 (1995).

[135] D. E. Woon and T. H. Dunning, J. Chem. Phys. **99**, 1914 (1993).

[136] T. H. Dunning, J. Phys. Chem. A **104**, 9062 (2000).

[137] E. R. Davison and D. Feller, Chem. Rev. **86**, 881 (1986).

[138] V. Blum, R. Gehrke, F. Hanke, P. Havu, V. Havu, X. Ren, K. Reuter, and M. Scheffler, Comp. Phys. Comm. **180**, 2175 (2009).

[139] F. B. van Duijneveldt, J. G. C. M. van Duijneveldt-van de Rijdt, and J. H. van Lenthe, Chem. Rev. **94**, 1873 (1994).

[140] S. F. Boys and F. Bernardi, Mol. Phys. 19 **19**, 553 (1970).

[141] D. G. Truhlar, Chem. Phys . Lett. **294**, 45 (1998).

[142] D. Feller, J. Chem. Phys. **96**, 6104 (1992).

[143] J. M. L. Martin, Chem. Phys . Lett. **259**, 669 (1996).

[144] A. Halkier, T. Helgaker, P. Jørgensen, W. Klopper, H. Koch, J. Olsen, and A. K. Wilson, Chem. Phys. Lett. **286**, 243 (1998).

[145] H. J. Monkhorst and J. D. Pack, Phys. Rev. B **13**, 5188 (1976).

[146] N. Troullier and J. L. Martins, Phys. Rev. B **43**, 1993 (1991).

[147] G. P. Kerker, J. Phys. C **13**, L189 (1980).

[148] D. R. Hamann, M. Schlüter, and C. Chiang, Phys. Rev. Lett. **43**, 1494 (1979).

[149] D. Vanderbilt, Phys. Rev. B **32**, 8412 (1985).

[150] S. Goedecker, M. Teter, and J. Hutter, Phys. Rev. B **54**, 1703 (1996).

[151] D. Vanderbilt, Phys. Rev. B **41**, 7892 (1990).

[152] C. Adamo and V. Barone, J. Chem. Phys. **108**, 664 (1998).

[153] E. E. Dahlke and D. G. Truhlar, J. Phys. Chem. B **109**, 15677 (2005).

[154] Y. Zhang and W. Yang, Phys. Rev. Lett. **80**, 890 (1998).

[155] X. Xu and W. A. Goddard III, Proc. Natl. Acad. Sci. U.S.A. **101**, 2673 (2004).

[156] H. L. Schmider and A. D. Becke, J. Chem. Phys. **108**, 9624 (1998).

[157] B. Santra, A. Michaelides, and M. Scheffler, J. Chem. Phys. **127**, 184104 (2007).

[158] B. Santra, A. Michaelides, M. Fuchs, A. Tkatchenko, C. Filippi, and M. Scheffler, J. Chem. Phys. **129**, 194111 (2008).

[159] E. E. Dahlke, R. M. Olson, H. R. Leverentz, and D. G. Truhlar, J. Phys. Chem. A **112**, 3976 (2008).

[160] Y. Zhao and D. G. Truhlar, J. Chem. Theory Comput. **1**, 415 (2005).

[161] X. Xu and W. A. Goddard III, J. Phys. Chem. A **108**, 2305 (2004).

[162] J. T. Su, X. Xu, and W. A. Goddard III, J. Phys. Chem. A **108**, 10518 (2004).

[163] J. J. Novoa and C. Sosa, J. Chem. Phys. **99**, 15837 (1995).

[164] S. S. Xantheas, J. Chem. Phys. **102**, 4505 (1994).

[165] J. A. Anderson and G. S. Tschumper, J. Phys. Chem. A **110**, 7268 (2006).

[166] G. C. Shields and K. N. Kirschner, Synthesis and Reactivity in Inorganic, Metal-Organic, and Nano-Metal Chemistry **38**, 32 (2008).

[167] A. Csonka, G. I. Ruzsinszky and J. P. Perdew, J. Phys. Chem. B **109**, 21471 (2005).

[168] E. E. Dahlke and D. G. Truhlar, J. Phys. Chem. B **110**, 10595 (2006).

[169] K. Kim and K. D. Jordan, J. Phys. Chem. **98**, 10089 (1994).

[170] K. Liu, J. D. Cruzan, and R. J. Saykally, Science **271**, 929 (1996).

[171] A. Michaelides and K. Morgenstern, Nature Mater. **6**, 597 (2007).

[172] X. L. Hu and A. Michaelides, Surf. Sci. **601**, 5378 (2007).

[173] V. A. Ranea, A. Michaelides, R. Ramírez, P. L. de Andres, J. A. Vergés, and D. A. King, Phys. Rev. Lett. **92**, 136104 (2004).

[174] A. Michaelides and P. Hu, J. Chem. Phys. **114**, 513 (2001).

[175] S. Meng, E. G. Wang, and S. Gao, Phys. Rev. B **69**, 195404 (2004).

[176] A. Michaelides, Farday Discuss. **136**, 287 (2007).

[177] C. Lee, H. Chen, and G. Fitzgerald, J. Chem. Phys. **102**, 1266 (1995).

[178] C. Lee, H. Chen, and G. Fitzgerald, J. Chem. Phys. **101**, 4472 (1994).

[179] H. Lee and M. E. Tuckerman, J. Phys. Chem. A **110**, 5549 (2006).

[180] J. VandeVondele, F. Mohamed, M. Krack, J. Hutter, M. Sprik, and M. Parrinello, J. Chem. Phys. **122**, 014515 (2005).

[181] J. C. Grossman, E. Schwegler, E. W. Draeger, F. Gygi, and G. Galli, J. Chem. Phys. **102**, 1266 (1995).

[182] J. Cerdá, A. Michaelides, M.-L. Bocquet, P. J. Feibelman, T. Mitsui, M. Rose, E. Fomine, and M. Salmeron, Phys. Rev. Lett. **93**, 116101 (2004).

[183] K. Umemoto, R. M. Wentzcovitch, S. Baroni, and S. Gironcoli, Phys. Rev. Lett. **92**, 105502 (2004).

[184] M. de Koning, A. Antonelli, A. J. R. da Silva, and A. Fazzio, Phys. Rev. Lett. **97**, 155501 (2006).

[185] V. A. Ranea, A. Michaelides, R. Ramírez, , P. L. de Andres J. A. Vergés, and D. A. King, Phys. Rev. Lett. **92**, 136104 (2004).

[186] T. Taketsugu and D. J. Wales, Mol. Phys. **100**(17), 2793 (2002).

[187] F. N. Keutsch, J. D. Cruzan, and R. J. Saykally, Chem. Rev. **103**, 2533 (2003).

[188] M. B. Day, K. N. Kirschner, and G. C. Shields, J. Phys. Chem. A **109**, 6773 (2005).

[189] G. S. Tschumper, M. L. Leininger, B. C. Hoffman, E. F. Valeev, H. F. Schaefer III, and M. Quack, J. Chem. Phys. **116**, 690 (2002).

[190] F. Coester and H. Kümmel, Nucl. Phys. **17**, 477 (1960).

[191] E. E. Dahlke and D. G. Truhlar, J. Phys. Chem. B **109**, 15677 (2005).

[192] S. S. Xantheas, C. J. Burnham, and R. J. Harison, J. Chem. Phys. **116**, 1493 (2002).

[193] S. S. Xantheas and E. Aprà, J. Chem. Phys. **120**, 823 (2004).

[194] J. A. Anderson, K. Crager, L. Fedoroff, and G. S. Tschumper, J. Chem. Phys. **121**, 11023 (2004).

[195] H. M. Lee, S. B. Suh, J. Y. Lee, P. Tarakeshwar, and K. S. Kim, J. Chem. Phys. **112**, 9759 (2000).

[196] D. Svozil and P. Jungwirth, J. Phys. Chem. A **110**, 9194 (2006).

[197] I. M. B. Nielsen, E. T. Seidl, and C. L. Janssen, J. Chem. Phys. **110**, 9435 (1999).

[198] L. A. Curtiss, D. J. Frurip, and M. Blander, J. Chem. Phys. **71**, 2703 (1979).

[199] R. M. Olson, J. L. Bentz, R. A. Kendall, M. W. Schmidt, and M. S. Gordon, J. Chem. Theory Comput. **3**, 1312 (2007).

[200] M. J. Frisch *et al.*, Gaussian 03, Revision C.02, Gaussian, Inc., Wallingford CT, 2004.

[201] E. J. Bylaska *et al.*, "NWChem, A Computational Chemistry Package for Parallel Computers, Version 5.0" (2006), Pacific Northwest National Laboratory, Richland, Washington 99352-0999, USA.

[202] D. Feller, J. Chem. Phys. **98**, 7059 (1993).

[203] C. Schwartz, Phys. Rev. **126**, 1015 (1962).

[204] W. Kutzelnigg and J. D. Morgan III, J. Chem. Phys. **96**, 4484 (1992).

[205] A. K. Wilson and T. H. Dunning Jr., J. Chem. Phys. **106**, 8718 (1997).

[206] D. G. Truhlar, Chem. Phys. Lett. **294**, 45 (1998).

[207] A. Halkier, W. Klopper, T. Helgaker, P. Jørgensen, and P. R. Taylor, J. Chem. Phys. **111**, 9157 (1999).

[208] P. J. Feibelman, Science **295**, 99 (2002).

[209] A. Michaelides, A. Alavi, and D. A. King, Phys. Rev. B **69**, 113404 (2004).

[210] A. Csonka, G. I. Ruzsinszky and J. P. Perdew, J. Phys. Chem. B **109**, 21471 (2005).

[211] V. N. Staroverov, G. E. Scuseria, J. Tao, and J. P. Perdew, J. Chem. Phys. **119**, 12129 (2003).

[212] A. D. Becke, J. Chem. Phys. **104**, 1040 (1995).

[213] W. A. Bingel, Theoret. Chim. Acta (Berl.) **8**, 54 (1967).

[214] T. Kato, Commun. Pure Appl. Math. **10**, 151 (1957).

[215] A. E. Mattsson, R. Armiento, P. A. Schultz, and T. R. Mattsson, Phys. Rev. B **73**, 195123 (2006).

[216] S. S. Xantheas, Chem. Phys. **258**, 225 (2000).

[217] J. Ireta, J. Neugebauer, M. Scheffler, A. Rojo, and M. Galván, J. Phys. Chem. B **107**, 1432 (2003).

[218] J. K. Gregory and D. C. Clary, J. Phys. Chem. **100**, 18014 (1996).

[219] C. J. Tsai and K. D. Jordan, Chem. Phys. Lett. **213**, 181 (1993).

[220] K. Kim, K. D. Jordan, and T. S. Zwier, J. Am. Chem. Soc. **116**, 11568 (1994).

[221] K. Liu, M. G. Brown, R. J. Saykally, J. K. Gregory, and D. C. Clary, Nature **381**, 501 (1996).

[222] J. K. Gregory and D. C. Clary, J. Phys. Chem. **100**, 18014 (1996).

[223] J. K. Gregory and D. C. Clary, J. Phys. Chem. A **101**, 6813 (1997).

[224] J. Kim and K. S. Kim, J. Chem. Phys. **109**, 5886 (1998).

[225] K. Nauta and R. E. Miller, Science **287**, 293 (2000).

[226] D. M. Bates and G. S. Tschumper, J. Phys. Chem. A **113**, 3555 (2009).

[227] K. Laasonen, M. Parrinello, R. Car, C. Lee, and D. Vanderbilt, Chem. Phys. Lett. **207**, 208 (1993).

[228] D. A. Estrin, L. Paglieri, G. Corongiu, and E. Clementi, J. Phys. Chem. **100**, 8701 (1996).

[229] S. Kristyán and P. Pulay, Chem. Phys. Lett. **229**, 175 (1994).

[230] J. M. Pérez-Jordá and A. D. Becke, Chem. Phys. Lett. **233**, 134 (1995).

[231] Q. Wu and W. Yang, J. Chem. Phys. **116**, 515 (2002).

[232] S. Grimme, J. Comput. Chem. **25**, 1463 (2004).

[233] P. Jurečka, J. Černý, P. Hobza, and D. R. Salahub, J. Comput. Chem. **28**, 555 (2007).

[234] A. Tkatchenko and M. Scheffler, Phys. Rev. Lett. **102**, 073005 (2009).

[235] M. Dion, H. Rydberg, E. Schröder, D. C. Langreth, and B. I. Lundqvist, Phys. Rev. Lett. **92**, 246401 (2004).

[236] P. L. Silvestrelli, Phys. Rev. Lett. **100**, 053002 (2008).

[237] O. Anatole von Lilienfeld, I. Tavernelli, U. Rothlisberger, and D. Sebastiani, Phys. Rev. Lett. **93**, 153004 (2004).

[238] A. D. Becke and E. R. Johnson, J. Chem. Phys. **122**, 154104 (2005).

[239] I. G. Kaplan, *Intermolecular Interactions: Physical Picture, Computational Methods and Model Potentials* (John Wiley & Sons Ltd, Chichester, 2006).

[240] R. Ahlrichs, R. Penco, and G. Scoles, Chem. Phys. **19**, 119 (1977).

[241] A. J. Bondi, J. Phys. Chem. **68**, 441 (1964).

[242] J. Hutter *et al.*, *computer code* CPMD, version 3.11; Copyright IBM Corp. 1990-2006, Copyright für Festkörperforschung Stuttgart, Germany, 1997-2001, http://www.cpmd.org/.

[243] P. Jurečka, J. Šponer, J. Černý, and P. Hobza, Phys. Chem. Chem. Phys. **8**, 1985 (2006).

[244] S. S. Xantheas, J. Chem. Phys. **100**, 7523 (1994).

[245] S. S. Xantheas, Chem. Phys. **258**, 225 (2000).

[246] J. M. Pedulla, F. Vila, and K. D. Jordan, J. Chem. Phys. **105**, 11091 (1996).

[247] M. Quack, J. Stohner, and M. A. Suhm, J. Mol. Struct. **599**, 381 (2001).

[248] A. Tkatchenko and O. A. von Lilienfeld, Phys. Rev. B **78**, 045116 (2008).

[249] A. K. Kelkkanen, B. I. Lundqvist, and J. K. Nørskov, J. Chem. Phys. **131**, 046102 (2009).

[250] P. L. Silvestrelli, Chem. Phys. Lett. **475**, 285 (2009).

[251] Y. Zhao, N. E. Schultz, and D. G. Truhlar, J. Chem. Theory Comput. **2**, 364 (2006).

[252] O. Akin-Ojo, Y. Song, and F. Wang, J. Chem. Phys. **129**, 064108 (2008).

[253] B. Chen, I. Ivanov, M. L. Klein, and M. Parrinello, Phys. Rev. Lett. **91**, 215503 (2003).

[254] G. S. Fanourgakis, G. K. Schenter, and S. S. Xantheas, J. Chem. Phys. **125**, 141102 (2006).

[255] F. Paesani, S. Luchi, and G. A. Voth, J. Chem. Phys. **127**, 074506 (2007).

[256] C. J. Burnham, D. J. Anick, P. K. Mankoo, and G. F. Reiter, J. Chem. Phys. **128**, 154519 (2008).

[257] S. B. Rempe, T. R. Mattson, and K. Leung, Phys. Chem. Chem. Phys. **10**, 4685 (2008).

[258] R. Car and M. Parrinello, Phys. Rev. Lett. **55**, 2471 (1985).

[259] T. Head-Gordon and M. E. Johnson, Proc. Nat. Acad. Sci. U.S.A **103**, 7973 (2006).

[260] A. K. Soper, J. Phys. Condens. Matter **19**, 335206 (2007).

[261] M. Allesch, E. Schwegler, F. Gygi, and G. Galli, J. Chem. Phys. **120**, 5192 (2004).

[262] K. Leung and S. B. Rempe, Phys. Chem. Chem. Phys. **8**, 2153 (2006).

[263] G. J. Martyna, M. L. Klein, and M. Tuckerman, J. Chem. Phys. **97**, 2635 (1992).

[264] R. A. Kendall, T. H. Dunning, Jr., and R. J. Harrison, J. Chem. Phys. **96**, 6796 (1992); T. H. Dunning, Jr., D. Woon, and K. A. Peterson (unpublished).

[265] K. Müller-Dethlefs and P. Hobza, Chem. Rev. **100**, 143 (2000).

[266] R. Z. Khailiullin, A. T. Bell, and M. Head-Gordon, Chem. Eur. J. **15**, 851 (2009).

[267] J. Baker, J. Andzelm, M. Muir, and P. R. Taylor, Chem. Phys. Lett. **237**, 53 (1995).

[268] J. L. Durant, Chem. Phys. Lett. **256**, 595 (1996).

[269] B. J. Lynch, P. L. Fast, M. Harris, and D. G. Truhlar, J. Phys. Chem. A **104**, 4811 (2000).

[270] Y. Zhao, N. González-García, and D. G. Truhlar, J. Phys. Chem. A **109**, 2012 (2005).

[271] B. G. Janesko and G. E. Scuseria, J. Chem. Phys. **128**, 244112 (2008).

[272] M. Diraison and G. J. Martyna, J. Chem. Phys. **111**, 1096 (1999).

[273] A. D. Boese, A. Chandra, J. M. L. Martin, and D. Marx, J. Chem. Phys. **119**, 5965 (2003).

[274] M. Pagliai, G. Cardini, R. Righini, and V. Schettino, J. Chem. Phys. **119**, 6655 (2003).

[275] J.-W. Handgraaf, E. J. Meijer, and M.-P. Gaigeot, J. Chem. Phys. **121**, 10111 (2004).

[276] C. G. Salzmann, P. G. Radaelli, E. Mayer, and J. L. Finney, Phys. Rev. Lett. **103**, 105701 (2009).

[277] C. Lobban, J. L. Finney, and W. F. Kuhs, J. Chem. Phys. **117**, 3928 (2002).

[278] W. F. Kuhs *et al.*, J. Chem. Phys. **81**, 3612 (1984).

[279] J. D. Londono, W. F. Kuhs, and J. L. Finney, J. Chem. Phys. **98**, 4878 (1993).

[280] C. G. Salzmann *et al.*, Science **311**, 1758 (2006).

[281] D. R. Hamann, Phys. Rev. B **55**, R10157 (1997).

[282] E. Whalley, J. Chem. Phys. **81**, 4087 (1984).

[283] A. D. Fortes, I. G. Wood, M. Alfredsson, L. Vočadlo, and K. S. Knight, J. Appl. Cryst. **38**, 612 (2005).

[284] E. Whalley, *in Physics and Chemistry of Ice*, edited by E. Whalley, S. J. Jones, and L. W. Gold.

[285] J. Klimeš, D. R. Bowler, and A. Michaelides, J. Phys. Condens. Matter **22**, 022201 (2010).